The Dissertation Committee for Etienne González Domínguez Certifies that this is the approved version of the following dissertation:

GEOSYNTHETIC ENCASED COLUMNS FOR SOFT SOIL IMPROVEMENT MODELLING WITH LAPONITE

Committee:

_____
Jorge G. Zornberg, Supervisor

_____
Ellen Rathje

_____
Robert Gilbert

_____
Michael Pyrcz

GEOSYNTHETIC ENCASED COLUMNS FOR SOFT SOIL IMPROVEMENT MODELLING WITH LAPONITE

by

Etienne González Domínguez

Dissertation

Presented to the Faculty of the Graduate School of

The University of Texas at Austin

in Partial Fulfillment

of the Requirements

for the Degree of

Doctor of Philosophy

The University of Texas at Austin

May 2024

Dedication

To my parents.

Acknowledgments

This investigation presented in this dissertation is the culmination of a synergy that wouldn't be possible without the contribution in different aspects from family, friends, and colleagues.

I am grateful to my advisor Prof. Jorge G. Zornberg, for his mentorship and rigorous formation to think, learn, criticize, analyze, and produce knowledge. My appreciation to my committee members Prof. Ellen Rathje, Prof. Robert Gilbert and Prof. Michael Pyrcz.

I would like to recognize and express my appreciation to my fellow colleagues that became my friends during this journey. Their invaluable aid is reflected in this work: Abed Al Mikati, Dawie Marx and Gino Sicha. To all my research group, thank you for the insights and fruitful discussions in the laboratory.

I would like to acknowledge Huesker Synthetic GmbH for their financial funding of this investigation. Huesker's resources allowed me to dive and explore freely the potential of geosynthetics.

My deepest gratitude to my family, without them I wouldn't have achieved this project, their love and support was my everyday motivation. My parents Mercedes and Juan Manuel; and my beloved sisters, Stéphanie and Fabiola.

I am fully grateful to Ana Elena for her unconditional support and being understanding and patient with me during this journey.

Abstract

GEOSYNTHETIC ENCASED COLUMNS FOR SOFT SOIL IMPROVEMENT MODELLING WITH LAPONITE

Publication No. _____

Etienne González Domínguez, Ph.D.
The University of Texas at Austin, 2024

Supervisor: Jorge G. Zornberg

Geosynthetic encased columns (GECs) have been effectively used as a ground improvement technique for soft soils, particularly for those in which the undrained shear strength is so low (e.g. below 15 kPa) that stone columns are not feasible. They involve sand/gravel columns encapsulated using high-tensile strength geotextile. This research, utilizing transparent clay and physical modeling, aims to: (1) evaluate the effect of key design parameters on GEC performance, including the encasement stiffness, column diameter, column infill density, and overburden pressure; (2) understand the failure mechanisms and detailed tensile strength mobilization of the encasement; and (3) investigate the behavior of the interface between the GEC and the surrounding soil during load mobilization.

Despite the growing interest in GECs for ground improvement, there are still knowledge gaps in understanding the complex interactions between the encasement, column

infill material, and surrounding soil. While previous research has demonstrated the performance improvement achieved by adding a geosynthetic encasement to stone columns, the internal behavior of GECs has been largely based on assumptions due to the inability to directly observe the variation in their response.

To address this limitation, the first component of this research focused on the development of a transparent unit cell chamber using laponite clay to visualize GEC deformations under undrained conditions. This experimental component revealed that laponite effectively simulated soft clay behavior, with the innovative setup developed in this study allowing measurement through direct visualization of key performance variables of the encasement (e.g., vertical and encasement radial column strains, column volume changes), as well as relevant performance variables of the surrounding soil (e.g., extent and uniformity of shear bands). The testing methodology demonstrated repeatability, providing valuable insight into GEC deformation pattern and failure modes as well as enabling the generation of reliable data for analysis and modeling.

The second component of this study focused on the influence of various parameters on GEC performance. The results showed that GEC performance depends on its encasement tensile strength mobilization. Non-uniform encasement radial strains developed along the column, and various failure modes were identified, including encasement tensile breakage and bulging. The encasement developed hoop stresses, which were quantified by the linear-elastic material behavior relationship between the characterized stiffness of the encasement and the measured radial deformations of the GEC column. The ultimate tensile strength of the encasement properties and column geometry were found to govern the failure mode, but the encasement secant stiffness proved to have an impact on load capacity, with mobilized hoop stresses enhancing GEC performance compared to encasements with lower secant stiffness.

The third component examined the interface shear behavior between GEC and laponite clay using digital image correlation (DIC). Pullout tests were found to reliably assess interface behavior. The results revealed that, despite the low shear strength of the laponite, interface shear may provide a non-negligible contribution to the overall column capacity, particularly by mobilizing load transfer under comparatively low strains. The interface shear strength was found to vary along the length of the column, with the uniformity of the interface shear being dependent on the stiffness of the encasement; higher encasement stiffness resulted in more uniform and higher interface shear developed along the column. The development of shear bands within the clay could be visualized along the interface with the GEC, with the encasement stiffness being identified as a key parameter in their development. Non-uniform mobilization of interface shear strength, shear band evolution, and encasement stiffness were identified a relevant factors for optimizing GEC load transfer.

In summary, this research provides valuable insight into GEC behavior in soft soils using an innovative transparent soil modeling approach. The experimental framework enables the visualization and quantification of column deformations, failure mechanisms, and interface shear behavior. The findings advance the understanding of GEC-reinforced foundation soil structures, with a primary focus on encasement strength mobilization and soil interface behavior. Key findings that may affect the design of GECs in the future include the importance of considering the non-uniform mobilization of tensile strength along the encasement and its impact on the failure mode and load capacity of the GEC, the significant contribution of interface shear strength to the overall column capacity, particularly under low strain conditions, and the role of encasement stiffness in the uniformity of interface shear mobilization, as well as the identification of encasement stiffness as a relevant parameter in optimizing GEC load transfer and controlling the development of shear bands at the soil-GEC interface.

Table of contents

List of tables

List of figures

Chapter 2

Chapter 3

Chapter 4

List of Symbols

τ	Shear stress	[kPa]
γ'_s	submerged unit weight of soft soil	[kN/m^3]
γ'_c	column fill material submerged unit weight	[kN/m^3]
ϕ'_s	soft soil effective friction angle	[°]
$\sigma_{v,c}$	vertical applied stress	[kPa]
$\sigma_{h,g}$	horizontal stress supported by geosynthetic	[kPa]
$\Delta\sigma_{h,c}$	increase in horizontal stress on the column infill	[kPa]
$\Delta\sigma_{h,g}$	increase in geosynthetic confinement stress	[kPa]
$\Delta\sigma_{h,s}$	increase in horizontal stress of soil	[kPa]
$\Delta\sigma_{v,c}$	increase in vertical stress of the column infill	[kPa]
$\Delta\sigma_{v,s}$	increase in vertical stress of the surrounding soil	[kPa]
σ_0	in-situ vertical stress	[kPa]
γ_s	total unit weight of soil	[kN/m^3]
Δr_c	column infill radial deformation	[m]
Δ_{rg}	encasement radial deformation	[m]
γ_w	specific unit weight of water	[kN/m^3]
A_c	cross sectional area of the column	[m^2]
a_E	area replacement ratio	[-]
A_E	column influence area	[m^2]
B	width of adjacent piles	[m]
c'	effective cohesion	[kPa]
d_c	diameter of the column	[m]
d_e	diameter of the influence area	[m]
e_0	initial void ratio	[-]
E_c	elastic modulus of column infill	[kPa]
$E_{oed,s}$	constrained modulus of soft soil	[kPa]
E_s	elastic modulus of soil	[kPa]
$E_{u,s}$	undrained elastic modulus of soil	[kPa]
F_{all}	geosynthetic allowable tensile force	[kN/m]
F_R	hoop force developed in geosynthetic encasement	[kN/m]
G_s	specific gravity of the soil	[-]
h_0	initial column height	[m]
H_{emb}	embankment height	[m]
H_s	soft soil layer thickness	[m]
$J_{5\%}$	geosynthetic secant stiffness at ε_a=5%	[kN/m]
K_0	coefficient of at-rest lateral earth pressures	[-]
K_0*	modified coefficient of at-rest lateral earth pressures	[-]
K_a	coefficient of active earth pressures	[-]
K_p	coefficient of passive earth pressures	[-]

n	stress concentration factor	[-]
n_g	Poisson's ratio of the geosynthetic	[-]
p^*	effective vertical stress in middle of soft soil layer	[kPa]
p_{ref}	reference effective vertical stress	[kPa]
q	vertical applied load	[kN/m^2]
R	radius of the influence area	[m]
r_c	column's radius	[m]
r_g	original encasement radius	[m]
s	column center to center spacing	[m]
S	column settlement	[m]
S_u	undrained shear strength	[kPa]
T	geosynthetic tensile force	[kN/m]
t	time	[day]
U	degree of consolidation	[-]
w_L	liquid limit	[%]
w_n	natural water content	[%]
w_p	plastic limit	[%]
z	depth	[m]
Δu	excess pore water pressure	[kPa]
$\delta_{frontal}$	Pullout frontal displacement	[m]
$\varepsilon_{r,g}$	radial strain in geotextile encasement	[%]
ϕ_c	friction angle of column infill	[^{o}]
γ_{sat}	saturated unit weight of soil	[kN/m^3]
υ	Poisson's ratio	[-]
ψ_c	dilatancy angle of column infill	[^{o}]

Chapter 1: Introduction

1.1.- RESEARCH MOTIVATION

The rapid urbanization and growing demand for infrastructure worldwide have led to a decrease in land availability, posing increasingly feasibility challenges for geotechnical engineers in the ground improvement of critical soils, particularly very soft soils. Improving the mechanical properties of these soils is often necessary and can be achieved using various methods found in practice and literature. However, for critical soil conditions such as very soft clays (e.g., with undrained shear strength $S_u < 25$ kPa), the available options for improvement are limited due to their high compressibility and very low shear strength.

Despite the challenges, a ground improvement technology that has been increasingly used in recent years is geosynthetic encased columns (GECs). This technology involves constructing a granular column (sand, gravel, or stone) wrapped with a cylindrical geotextile encasement that possesses high tensile strength and low creep properties. GECs are commonly employed as a foundation system to support embankments constructed on soft clay deposits. However, predicting the GEC mechanical response, particularly the radial deformation of the geotextile encasement and the column settlement, remains a challenge. Further research is needed to bridge the gap between laboratory and numerical studies and the design methods used in practice.

Physical modelling constitutes a promising approach to investigate the behavior of GECs. Over the last decade, several researchers (Murugesan & Rajagopal, 2009a, 2009c; Gniel & Bouazza, 2009; Ali et al., 2012; Y.K, 2012; Ghazavi & Nazari Afshar, 2013; Ali et al., 2014; Nazari Afshar & Ghazavi, 2014; Miranda & Da Costa, 2016; Mohapatra et al., 2016; Hong et

al., 2016; Miranda et al., 2017; Cengiz & Güler, 2018a; Najjar et al., 2018; Cengiz & Güler, 2018b; Alkhorshid et al., 2019, 2021; X. Zhang et al., 2021) have studied the influence of various parameters on the response of GEC systems. These parameters include the encasement secant stiffness ($J_{5\%}$), column diameter (Ø), column length (L), column material properties (e.g., friction angle ϕ), and the spatial distribution of columns within a group. As a result of this research, fundamental observations have been established, narrowing down the optimal application range for GECs. The recommended ranges for key design parameters are as follows:

- Column diameter (Ø): 0.60-1.0 m
- Column length (L): 10-20 m
- Area replacement ratio (a_E): 15-25%
- Column infill material friction angle (ϕ): 30-40°
- Soft soil undrained shear strength (Su): < 30 kPa
- Applied vertical stress (σ_v): 100-150 kPa
- Encasement stiffness ($J_{5\%}$): 1500-3000 kN/m

These ranges provide valuable guidance for the design and implementation of GECs in soft soil conditions, ensuring optimal performance and cost-effectiveness.

Previous physical modeling studies, many of which did not follow rigorous scaling laws, have primarily focused on the improvement in bearing capacity and settlement reduction provided by GECs. However, these studies have not placed sufficient emphasis on understanding the mechanical performance of the geosynthetic encasement, which is the core element of the GEC system. Field observations have shown that a common failure mode of GECs involves bulging of the upper portion of the column, typically extending to a depth of

about three times the column diameter. This observed behavior contradicts the assumptions made in various design methods, which consider different bulging lengths depending on multiple parameters and conditions (Najjar, 2013; Hong et al., 2016). Consequently, understanding the deformation and stress transfer mechanisms within the geosynthetic encasement is crucial for accurately predicting the behavior of GECs at both serviceability and ultimate limit states, and for improving current GEC design methods.

Much of the research on GECs to date has been conducted using the concept of a unit cell, which represents a single column and its tributary surrounding soil, assuming that the behavior of this unit cell is representative of the entire GEC system. Two widely used analytical design methods, proposed by Raithel & Kempfert (2000) and Pulko et al. (2011), are based on the unit cell approach. The main difference between these two methods lies in the assumptions made regarding the mechanical behavior of the soil column: Raithel & Kempfert (2000) consider an elastic behavior, while Pulko et al. (2011) adopt an elastoplastic behavior. Both methods provide upper and lower bounds for the tensile strain profile along the geosynthetic encasement.

To evaluate the accuracy of these analytical solutions, continuous data on the radial strain development along the length of the GEC is required. However, current physical modeling techniques have limitations in obtaining such data. Local strain sensors can only measure radial deformations at discrete points during testing, while obtaining the complete strain profile requires the exhumation of the column. This process may introduce disturbances to the column, making it difficult to analyze the entire process of column behavior during loading. Consequently, there is a need for improved experimental techniques that can provide continuous, non-destructive measurements of radial strain along the GEC length, enabling a more comprehensive validation of analytical and numerical models.

An evaluation of the current state of the art on GECs reveals several questions that remain to be answered about the performance of geosynthetic encased granular columns installed in soft soils.

1. Under rigid loading conditions (e.g., embankments), what is the level of improvement in the overall bearing capacity when GECs are installed in very soft clays? How do variations in GEC geometry and geosynthetic material properties influence this improvement, and what are the implications for design methodologies?

2. How do the stresses measured at the top and bottom of the GEC compare with predictions from analytical design methods that assume a rigid loading plate?

3. How do tensile stresses develop within the geosynthetic encasement along the depth of the GEC, and what are the most appropriate tools and methodologies for evaluating these stresses?

4. How does the presence of GECs influence the behavior of the surrounding soft clay, particularly in terms of the development of shear bands during loading? What are the most effective ways to assess the interaction between the GECs and the surrounding soil as the system approaches failure?

Addressing these questions will provide valuable insights into the fundamental behavior of GECs in soft soils, enabling the development of more accurate and reliable design methods for these ground improvement systems.

1.2.- RESEARCH OBJECTIVES

GEC physical models tested in previous investigations have been limited to models that often involve unrealistic scaling considerations (Ghazavi & Nazari Afshar, 2013; Murugesan & Rajagopal, 2009a). The experimental investigation conducted in this study focuses on the evaluation of a single GEC behavior under 1-g and undrained conditions. To achieve this goal, a new GEC experimental setup has been developed in this research, scaled to realistic prototype values in terms of geometry, material properties and applied loads. The following objectives were sought in the research:

- Develop a new experimental setup suitable for use of laponite as a transparent clay surrogate to investigate the behavior of geosynthetic encased columns (GECs) under simulated field conditions. Establish the repeatability of the experimental setup based on the non-intrusive, continuous monitoring of GEC behavior and soil response. The new experimental setup should also facilitate the understanding of GEC performance and soil-structure interaction mechanisms through direct visualization and quantification of strains and load transfer

- Investigate the influence of key GEC design parameters, including the geosynthetic encasement stiffness (J), column fill material relative density (RD), applied vertical stress (σv), and column diameter ($\emptyset$). Establish the relevance of these parameters in assessing the overall performance of GECs and their failure mechanisms. By identifying the key factors governing GEC behavior, this study aims to provide insights into optimizing GEC design for improved load capacity, settlement reduction, and overall stability.

- Quantify the load transfer mechanisms within GECs, including the contribution of interface shear between the GEC and surrounding soil, using both instrumentation and digital image correlation (DIC) techniques. This will elucidate the complex load transfer and soil-structure interaction mechanisms in GECs, generating valuable data for the future development of more accurate analytical and numerical models.

- Characterize the evolution of soil deformation fields, strain localization patterns, and shear band development around GECs under axial loading using advanced image analysis techniques. Providing insight into the spatial distribution of soil deformations and shear strains surrounding GECs, contributing to a better understanding of the soil-structure interaction.

Overall, this research aims to bridge the gap between experimental observations and understanding of GEC behavior, ultimately leading to improved design methodologies and more reliable performance predictions for GEC-reinforced foundation soils in practice.

1.3.- SCOPE OF DISSERTATION

The dissertation is structured into three self-contained research topics, with each component involving specific aspects of the GEC behavior that can be drawn from physical models involving transparent clay surrogates.

Chapter 2 focuses on the design and development of a transparent unit cell chamber using laponite as a clay surrogate to model GEC behavior. The scope of this research component includes optimizing the laponite mixture and preparation method to achieve the desired undrained soft clay properties and transparency. Digital image correlation (DIC) techniques are employed to analyze the encasement radial strain profiles along the length of the column, providing a continuous measurement of the lateral deformation of the GEC. The experimental setup developed in this research component aims to collect comprehensive data, including: load-settlement response curves, encasement radial strain profiles along the length of the column, geosynthetic encasement tensile stresses, measured column axial strains, stress ratios, which represent the proportion of the applied load carried by the GEC relative to the surrounding soil, volumetric strains within the column infill material, soil displacement vectors in the surrounding soft soil mass and identification of failure modes.

By gathering this extensive dataset, the transparent unit cell chamber enables a thorough investigation of GEC behavior and provides valuable insights into the complex interactions between the geosynthetic encasement, column fill material, and surrounding soft soil. Chapter 3 includes the results of a parametric study conducted using the transparent unit cell chamber to investigate GEC performance and failure modes under various testing conditions. The scope of this research component involves varying parameters such as geosynthetic encasement stiffness, column infill relative density, overburden pressure, and column diameter. The impact of these parameters on the GEC bearing capacity, stress transfer,

and geosynthetic encasement strain mobilization is analyzed. The chapter focuses on single GEC behavior and its mechanism of failure, aiming to provide insights into the factors influencing GEC performance.

Chapter 4 investigates the interface shear behavior between an end-bearing GEC and the surrounding transparent laponite clay. The scope of this research component includes utilizing instrumentation to measure the contribution of interface shear to the bearing capacity of the GEC. Embedded markers and digital image correlation (DIC) techniques are adopted to track soil displacement fields during loading. The chapter also includes an analysis of the development of interface shear stresses along the GEC and the spatial extent of the shear influence zone. The focus is on achieving high-resolution measurements of the shear stresses developed during GEC-soil interaction under simulated field conditions, contributing to a better understanding of load transfer mechanisms in GEC-reinforced foundation soils.

Chapter 5 includes the overall conclusions of this investigation, recommendations for the design and analysis of GECs based on the findings of this study, followed by suggestions for future research directions in the field of GEC-reinforced foundation soils.

Chapter 2: Experimental Setup to Model Geosynthetic Encased Columns Using a Transparent Clay Surrogate

ABSTRACT

Geosynthetic encased columns (GECs) have proven to be an effective ground improvement technique for increasing bearing capacity and reducing settlements in soft soils. While previous laboratory studies have investigated various aspects of GEC behavior, the use of a transparent soil surrogate, such as laponite, allows for a better understanding of column behavior under loading. This study focuses on utilizing an optimized laponite mix as a transparent soft clay surrogate to model GEC behavior in a newly constructed Transparent Unit Cell Chamber. The experimental setup and methodology, which include advanced imaging techniques and reliable instrumentation, enable direct and continuous observation of GEC behavior under undrained conditions. Typical results obtained from testing a baseline GEC model demonstrate the effectiveness of the approach, providing detailed insights into the load-settlement response, column deformations (including encasement vertical displacements, encasement radial strains, and column infill volumetric strains), and soil-column interaction through Digital Image Correlation (DIC) analysis. The consistent testing protocols yield repeatable results, providing confidence in the observed mechanisms and quantified responses. The findings from this study contribute to a more comprehensive understanding of GEC behavior and soil-column interaction, which can inform the development of more accurate and efficient design methods for GEC-reinforced foundation soils and structures. The use of laponite as a transparent soil analog opens up new possibilities for in-depth experimental research on GECs, enabling the measurement of key parameters along the column length and providing valuable data for improving the accuracy of design methods.

2.1.- INTRODUCTION

Geosynthetic encased columns (GECs) have been shown to provide a very effective ground improvement technique to increase the bearing capacity and reduce settlements in projects involving particularly soft soils. The applications of GECs have included supporting flexible structures such as road embankments, oil storage tanks, and silos. These columns typically comprise a core of sand or gravel, enveloped within a cylindrical geotextile with high tensile strength and low creep characteristics. The fundamental role of GECs is to maintain the integrity of stone columns that would not be stable without encasement, allowing an efficiently transfer of structural loads to deep soil layers.

The geosynthetic encasement has been the focus of previous laboratory testing involving physical modeling. Specific aspects investigated by researchers have included the influence of the encasement on bearing capacity and settlement improvement compared to ordinary stone columns (Ali et al., 2012; di Prisco, 2006; Ghazavi & Nazari Afshar, 2013; Gniel & Bouazza, 2009; Murugesan & Rajagopal, 2009b; Nazari Afshar & Ghazavi, 2014; Hong et al., 2016; Miranda et al., 2017; Chen et al., 2018; Alkhorshid et al., 2019), shear loading behavior and resistance against lateral displacements (Chen et al., 2015; Mohapatra et al., 2016; Murugesan & Rajagopal, 2009d; X. Zhang et al., 2021), the influence of column infill relative density (Miranda & Da Costa, 2016), the response of GECs under cyclic and seismic loads (Kempfert et al., 1999; di Prisco & Galli, 2011; Cengiz & Güler, 2018a, 2018b), their performance as floating columns (Ali et al., 2012; Dash & Bora, 2013), and the impact of partial encasement (Gniel & Bouazza, 2009; Ali et al., 2012; Dash & Bora, 2013). The outcomes of these studies consistently demonstrated the improved performance of GECs over ordinary columns (OC), revealing enhancements in bearing capacity and settlement reduction across various approaches.

However, the behavior of GECs themselves, independent of the surrounding soil matrix, has received limited attention. To address this, the use of a transparent soil as a clay surrogate would allow for a better understanding of column behavior under loading. In some physical modeling studies, researchers have used an approach where columns are filled with Plaster of Paris, which is later exhumated to measure encasement radial deformations (Ali et al., 2012; Alkhorshid et al., 2019, 2021; Dash & Bora, 2013; Ghazavi & Nazari Afshar, 2013, 2013; Hong et al., 2016). This technique only allows for observation at the final stage after exhumation, potentially introducing sample disturbance. In contrast, transparent soil enables continuous, high-resolution viewing and strain measurement throughout the test, permitting uninterrupted analysis of the column's progression under loading.

While the exhumation method has been used to examine the ultimate failure stage, typically characterized by a bulging failure mode observed near the upper 2-3 column diameters (Najjar, 2013), conflicting observations in previous studies reveal variable bulging lengths influenced by factors such as L/D ratios, encasement strength, soil materials, loading types, and boundary conditions (Hong et al., 2016). These inconsistencies highlight the need for a more comprehensive understanding of GEC behavior under various conditions, which can be facilitated by the use of transparent soil in physical modeling studies.

A relatively recent geotechnical modeling approach involving the use of transparent synthetic soils has been successfully used (Iskander et al., 2002). These materials offer a physical and mechanical properties suitable for simulating the behavior of clay, sand, or gravel. Additionally, they introduced consistent modeling techniques for observing and quantifying deformations in geotechnical systems, primarily through Digital Image Correlation (DIC) techniques (Sadek et al., 2003). Among these transparent soils, laponite, a type of soft clay

surrogate, demonstrated notable potential advantages for researching soft clay behavior (Almikati et al., 2023a; Pierozan et al., 2022a).

While previous studies investigating the use of laponite as a transparent soil surrogate have significantly advanced our understanding of this material, challenges arise when the physical models require cells with comparatively large volumes. Large laponite models may experience reduced transparency at greater distance from the object of study, raising concerns regarding visualization and image analysis quality, in addition to logistical difficulties during preparation. As a result, large laponite models require careful consideration and a well-designed preparation methodology to preserve transparency without compromising the desired geotechnical properties.

Considering the challenges posed by the limited understanding of GEC behavior and the opportunities provided by transparent soil modeling, this research focuses on utilizing laponite as a transparent soft clay surrogate to model GEC behavior. The objectives of this study include designing an optimized laponite mix, developing laboratory techniques and tools to leverage the advantages of laponite, and obtaining qualitative and quantitative results. By using laponite and advanced image analysis techniques, this study facilitates direct and continuous observation during testing without the need for intrusive processes. A key aspect of the approach involves the design of a newly constructed Transparent Unit Cell Chamber with well-defined assumptions and boundary conditions.

In addition to the characteristics of the new testing setup, this paper illustrates typical datasets generated from GEC evaluation, including load pressure-displacement curves, encasement radial strain profiles across the entire column at various loading stages, back-calculated encasement tensile stresses, column axial strains, column volumetric strain, soil

displacement field vectors, and observations of potential failure modes. A discussion about the validation and limitations of the transparent unit cell chamber method for modeling GEC behavior is also provided.

This research represents a pioneering effort to leverage laponite as a transparent soil surrogate for modeling GEC behavior. By addressing crucial knowledge gaps in GEC, we aim to contribute to a more effective experimental evaluation technique.

2.2.- BACKGROUND INFORMATION

2.2.1.- GEOSYNTHETIC ENCASED COLUMN

The use of GECs allows the construction of stone columns by adding confinement to the column infill material in projects where confining support is inadequately provided by surrounding weak, soft soils. Extensive research has been conducted on single stone columns throughout the years, as summarized in Najjar (2013). The behavior of single stone columns has been shown to match the behavior of column groups in terms of effectiveness, as confirmed by results from numerical analysis, laboratory tests, and field measurements (Ambily & Gandhi, 2007; White et al., 2007; Black et al., 2011; Stuedlein & Holtz, 2012). Similarly, for GECs, which are a more recent technology, a few research studies have also confirmed the validity of studying single columns (Ali et al., 2012; Castro, 2017).

The unit cell concept is commonly used in the design and analysis of stone columns and GECs. It is defined as the cross-sectional slice cylinder of soil materials within the tributary area of a single column. This approach assumes that the behavior of a single column can accurately represent the internal behavior of an element within a large group of columns when they are loaded simultaneously. By studying a single column using the unit cell concept, researchers and designers can gain insights into the performance of the entire column group.

Experimental GEC research to date, conducted under the unit cell approach on single columns, and the current design methods adhere to this rationale of using a single column to understand its behavior within a column group. **Table 2.1** summarizes the GEC experimental studies reported in the literature. Each reference includes (1) the type of test, (2) the scaling, if reported, (3) the geometry of the GEC, (4) the soft soil properties, and (5) the encasement secant stiffness. Despite the fact that each of these references selected different hypotheses and

experimental boundary conditions, the unit cell approach was consistently adopted, highlighting its widespread acceptance in the study and design of GECs.

Because of the effectiveness of studying a single column and its compatibility to use unit cells as an approach for their analysis, the transparent unit cell chamber was also adopted in the experimental setup developed for this study. However, some limitations in the geometry and material properties selection in the experimental setup should be considered to properly interpret the outcomes of this investigation.

2.2.2.- LAPONITE A TRANSPARENT SOFT CLAY SURROGATE

Transparent soils have been used in fundamental research for geotechnical physical models, offering strong potential for field applications. Specifically, laponite has been shown to emulate the behavior of a soft clay geomechanically. In addition, its transparency allows for non-intrusive and continuous measurement of deformations within the material itself through the introduction of colored markers that can be installed across a plane of interest.

The physical and geotechnical properties of laponite have been extensively studied (Bonn et al., 2002; Cummins, 2007; Wallace & Rutherford, 2015; Zhang et al., 2020; Pierozan et al., 2022b; Almikati et al., 2023b). Laponite is a thixotropic non-Newtonian colloidal material that exhibits properties between a gel and a soft glass (Bonn et al., 1999, 2002). The transparent properties of laponite largely depend on its concentration, rheological additive dosage, and aging time (Pierozan et al., 2022b). The geotechnical properties of laponite are consistent with those of soft clays loaded under undrained conditions (Wallace & Rutherford, 2015). Fundamental tests, such as Atterberg limits, consolidation, and undrained shear strength (Chini et al., 2015; Wallace & Rutherford, 2015; Ads et al., 2020; Almikati et al., 2023b), as well as complex assessments of thermal transfer in soft soils (Black & Tatari, 2015), have been

conducted using laponite, providing informative and visual responses that contribute to a better understanding of soil behavior.

The use of laponite has allowed direct, non-intrusive, and continuous measurement of deformation patterns for a variety of geotechnical structures (Bonn et al., 2002; Cummins, 2007; Wallace & Rutherford, 2015; Zhang et al., 2020). However, to obtain such data, it is necessary to use markers placed in the cross-sectional plane of interest during the construction of the physical model. Depending on the nature of these markers, they may require specific conditions to be visualized and captured. For instance, Timiron nano particles (10-60 mm) illuminated with a laser frame were used by Ni et al. (2010) to create a plane with a speckle pattern that could be tracked while using amorphous silica and mineral oil. Some other transparent soils, due to their texture and shape, can provide the required speckle pattern by themselves with the help of a laser frame (Sang et al., 2019; Yuan et al., 2019). Small laponite models (less than 5 liters in volume) were studied with this latest approach for the visualization of shearing failure (Chini et al., 2015; Wallace & Rutherford, 2015). However, when working with laponite, the major limitation of the laser technique is the penetration depth and the large diffraction of the laser beam crossing the layer of laponite mixed with nano markers such as Timiron. As a result, there is a considerable loss in image quality when the model becomes large in volume, making it challenging to obtain clear and accurate deformation measurements throughout the entire model.

Experimental models using transparent soils have typically used containers with volumes ranging from 1 to 2 liters and penetration depths ranging from 100 to 200 mm. These models were specifically tailored to study the soft clay itself by analyzing a customized plane strain region, using markers for detection through laser beams or direct observation. These

markers were tracked using DIC techniques to generate vector field displacements and subsequently derive the strains generated.

Table 2.1.- Summary of relevant GEC experimental studies published

Reference	Type of test	#Column	Scale	Ø [m]	H [m]	Soft Soil	S_u [kPa]	Column soil	Friction angle [°]	Encasement $J_{5\%}$ [kN/m]
(Kempfert et al., 1999)	Uniaxial Monotonic & cyclic	Single	1:1, 1:6.5, 1:11.5, 1:13	0.067	1.30	Peat	8.5			800
(di Prisco, 2006)	Uniaxial	Group	-	0.04	0.40	Sand	**ϕ=32°	Sand	32-42	22.5-625
(Murugesan & Rajagopal, 2009b, 2009d)	Uniaxial & shear	Single / Group	-	0.05-0.10	0.20-0.60	Clay	2.5	Granite chips	41.5	15.0
(Gniel & Bouazza, 2009)	Uniaxial	Single	-	0.051	0.293-0.317	Kaolinite	5	Sand	35	4.8
(di Prisco & Galli, 2011)	Uniaxial Monotonic and cyclic	Single	-	0.040	0.40	Sand	**ϕ=36°	Sand	36-42	18-80
(Dash & Bora, 2013)	Uniaxial	Single	1:7	0.10	0.10-0.70	Clay	5	Crushed Stone	48	2.9
(Ghazavi & Nazari Afshar, 2013; Nazari Afshar & Ghazavi, 2014)	Uniaxial	Single/ Group	1:10	0.06-0.10	0.30-0.50	Clay	15-30	Crushed Stone	46	16-35
(Ali et al., 2014)	Uniaxial	Single/ Group	-	0.03	0.30	Kaolinite	6.8	Stone chips	38/45	890-3250
(Miranda & Da Costa, 2016)	Triaxial	Single	-	0.10	0.20	-	-	Gravel	28-35	620
(Miranda, 2014; Miranda et al., 2017)	Rowe-Barden oedometric cell	Single	1:10	0.0847	0.146	Kaolinite	3	Gravel	39-47	620
(Chen et al., 2015)	Centrifuge	Group	1:25	0.032	0.40	Kaolinite	1	Silica sand	36.7	4.0
(Mohapatra et al., 2016)	Direct shear test	Single/ Group	-	0.05-0.10	0.14	sand	**ϕ=36°	Aggregate	36	1.7-153
(Hong et al., 2016)	Uniaxial	Single	1:10	0.050	0.25	Clay	1.36	Sand	36-38	4-15
(Chen et al., 2018)	Triaxial	Single	-	0.30	0.60	-	-	Gravel	43-45	254-438
(Cengiz & Güler, 2018a, 2018b)	Dynamic & Uniaxial	Single	1:6.25	0.13	1.35	Kaolinite	4.6-8.1	Sand/ Gravel	37-44	400-1000
(Alkhorshid et al., 2019, 2021)	Uniaxial	Single	1:4	0.15	1.0	Slurry	3-5	Sand/ Gravel/ RCDW	41-42	53-120
(X. Zhang et al., 2021)	Centrifuge	Group	1:25	0.032	0.40	Kaolinite	0	Silicon Sand	43.4	135.0

2.3.- CONSIDERATIONS IN THE DESIGN OF A NEW TRANSPARENT UNIT CELL CHAMBER

The focus of this study is to model specific aspects of the behavior of GECs rather than attempting to replicate the entire natural process. Attention will be given to certain key parameters that influence GEC performance, rather than providing a comprehensive review of all factors involved. The test setup adopted in this study allows for the evaluation of distinct stages during the loading of a GEC, including a stage indicative of failure. However, it will not replicate the chronological progression of a prototype GEC system. One limitation of the study is the inability to reproduce the soil consolidation process in the physical model using laponite. This is because laponite has an extremely low consolidation rate according to Almikati et al. (2023a) with a coefficient of consolidation c_v between 0.01 and 0.03 m^2/yr, making it technically challenging to simulate the time-dependent consolidation process for laboratory testing.

Consequently, this study aims to evaluate specific conditions or stages, such as the reasons leading to system failure, rather than reproducing the entire loading process of a prototype GEC. While a complete replication of the GEC loading process is beyond the scope of this study, valuable insights can still be collected from examining specific stages during GEC loading. By focusing on specific stages and conditions, the test setup allows for the isolation of key factors influencing GEC behavior, while avoiding the influence of uncontrollable factors such as the clay's compressibility parameters. This approach makes the study fundamentally important in understanding the mechanisms governing GEC performance, even though it may not provide a comprehensive representation of all aspects of GEC behavior in the field.

2.3.1.- UNIT CELL APPROACH

The design of the setup chamber adheres strictly to the unit cell approach, which represents the composite cylinder volume of the soft soil corresponding to the cross-sectional area of a single column and the column itself being entirely loaded. In this setup, the load is applied separately to two sections: the tributary area of the surrounding soil is loaded with a constant dead weight acting as an overburden, while the column head is loaded with a displacement-controlled stiff plate. This experimental setup differentiates itself from other testing arrangements by strictly adhering to the unit cell boundary conditions criterion. In contrast, testing chambers in other studies are often larger than the assumed tributary area of the column, and the loading is only applied either to the diameter of the column or to an assigned tributary area, leaving a gap of unloaded soil.

2.3.2.- UNDRAINED CONDITIONS OF LAPONITE

Laponite transparent optical properties allow measurement of deformation patterns directly, non-intrusively and continuously (Bonn et al., 2002; Cummins, 2007; Wallace & Rutherford, 2015; Y. Zhang et al., 2020; Pierozan et al., 2022b). However, laponite will be tested under essentially undrained conditions, so it may be considered incompressible for practical purposes . Almitaki et al. (2023) reported a coefficient of consolidation c_v of 0.007 m^2/yr at 48 kPa for a mixture of 11% concentration of laponite and 0.41% of SPP, meaning that no settlements are expected from laponite alone during a reasonable testing time. This is true as the laponite mixture is saturated maintaining its volume inside the transparent unit cell chamber during loading. For this reason, the technical method designed consists of imposing settlements to the column and letting the laponite move freely around the column by only imposing a constant overburden load. As result, during the displacement-controlled testing the column will settle while the laponite moves upwards as the column

compresses vertically and expands radially. Since the volume of the system is encapsulated in the transparent unit cell chamber and the only compressible material is the sand inside the column, then a continuous tracking of the volume change of the column is obtained.

2.3.3.- DIGITAL IMAGE CORRELATION

An important characteristic of transparent soils is the ability to capture visually the continuous response of the soil tested (Iskander, 2010; Iskander et al., 2015). However, to obtain such data it is needed to recur to markers previously placed in the cross-section plane of interest and depending on their nature they may need of specific conditions to be visualized and captured.

Therefore, the model developed, consisting of a large cylindrical cell with a volume of 17 liters of laponite needed to implement a marker system that wouldn't interfere with the column visualization. For this reason, the technique developed did not recur the use of Timiron micro seeding particles and a laser frame, instead tailored black markers made of glass beads with a diameter of 1.5 mm that were spread creating a speckle pattern on a cross sectional plane during the construction of the sample. The markers can be observed at direct sight, however, for optimal digital image correlation, special lightning was also applied to enhance the quality of the image captured coupled with a tailored camera setup. Details are provided in the experimental procedure section 2.5.

2.3.4.- SCALING LAWS

Multiple researchers (Ghazavi & Nazari Afshar, 2013; Nazari Afshar & Ghazavi, 2014; Hong et al., 2016; Ghazavi et al., 2018; Cengiz & Güler, 2018b; Alkhorshid, 2017; Alkhorshid et al., 2019) have reported using 1-g model scaling factors, presented in **Table**

2.2, to experimentally study GECs. The scaling factors include $J_{5\%}$, the secant stiffness of the encasement; T_{ult}, the ultimate tensile strength of the encasement; Su, the undrained shear strength of the soil; ⌀, the diameter of the column; σ, the overburden of the soil; and ε_{rg}, the encasement radial strain. Additionally, typical prototype values based on reported case histories (Alexiew & Raithel, 2015) are also presented, with a scale of λ=10 used in this investigation to provide an idea of experimental magnitudes.

Table 2.2.- 1g GEC Scaling factors, with λ=10

Parameter	Unit	Scaling factor	Typical Prototype Value	Model Value
$J_{5\%}$	$\left[\frac{kN}{m}\right]$	λ^2	2000 – 5000	20 – 50
T_{ult}	$\left[\frac{kN}{m}\right]$	λ^2	100 – 600	10 –60
S_u	$[kPa]$	λ	<25	0.5 – 2
∅	$[m]$	λ	0.6 – 1.2	0.06 – 0.12
σ	$[kPa]$	λ	80 – 150	8 – 15
ε_{r_g}	$[-]$	1	0.01 – 0.05	0.01 – 0.05

From the 1-g scaling factors, the secant stiffness and ultimate tensile strength of the encasement should be reduced by a factor of λ^2, becoming one of the main difficulties in finding a commercially available matching material. Regarding the stresses σ applied to the soil and column, they are reduced by a factor of λ, which is technically convenient for laboratory testing. The undrained shear strength S_u of a clay soil should also be reduced by the same factor λ. However, this is difficult when using the same soft clay material, leading investigations to use kaolinite mixes with S_u below 5 kPa. In contrast, laponite can achieve S_u values between 1-2 kPa, perfectly matching prototype values of 15-20 kPa for a model scale with a scaling factor λ of 10. However, the shearing properties of the column filling material, corresponding to a friction angle between 35°- 40°, cannot be technically

downscaled and must be considered in analyzing the results, given they deviate from true reduced-scale conditions.

2.3.5.- CELL CHAMBER

The unit cell chamber in **Figure 2.1** is based on the conceptual design considerations presented, physically it consists of three elements: first the main body cylinder acrylic wall 1/8 inches (3.175 mm) thick, 8 inches (203.2 mm) diameter and 2 ft (609.6 mm) height that holds the core volume of laponite and the installed GEC model, second is the ring overburden plate made of acrylic consisting of a rigid ring shaped plate covering the foot-print of the laponite, the ring plate apply a constant overburden pressure to the tributary area of the column with a dead weight on top and it is free to move vertically, third is the core column plate, a closed-cylinder shaped plate fitting perfectly inside the inner circle of the ring plate, avoiding any leakage of laponite between the two plates when both are moving. The core plate moves in downward direction when the displacement-controlled load is applied.

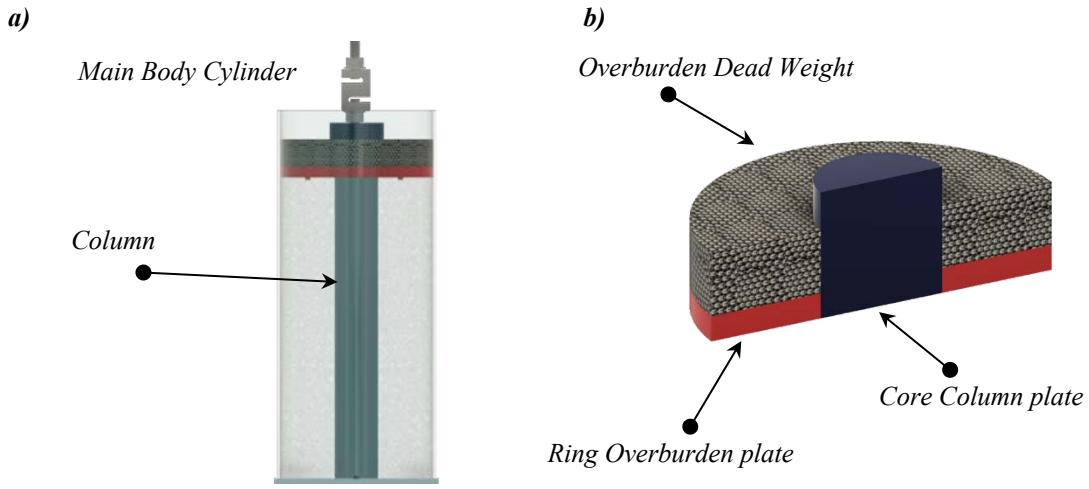

Figure 2.1.- Transparent Unit Cell Chamber: a) Unit cell chamber, b) Schematic configuration of the loading plate

To summarize, the unit cell conception approach, combined with the assumed loading conditions, was adapted to match the properties of laponite (undrained condition with no volume change). **Figure 2.2** presents the model development stages required to reach the design stage, starting from the prototype conditions. The subscripts "p" and "m" denote the prototype and model conditions, respectively. The sequence of variables in each stage is as follows: the vertical stress on the soil (σ_s), the vertical stress on the column (σ_c), the vertical displacement of the column (δ_c), and the undrained shear strength of the soil (Su). The stages are defined as follows:

- Initial Stage: In this stage, the initial vertical stresses on the soil ($\sigma_{sm,d}$), which remains constant during the entire test, and the column ($\sigma_{cm,0}$) of the model, and the initial vertical stresses on the soil ($\sigma_{sp,0}$) and the column ($\sigma_{cp,0}$) of the prototype are all uniform. The undrained shear strength of the soil in the prototype is (Su_0) and the undrained shear strength of the soil in the model is (Su_d).

- Loading Stage: During the loading stage, the vertical stress on the column in the prototype ($\sigma_{cp,L}$) becomes greater than the vertical stress on the soil ($\sigma_{sp,L}$). Similarly, in the model, the vertical stress on the column ($\sigma_{cm,L}$) becomes greater than the vertical stress on the soil ($\sigma_{sm,d}$). The column undergoes a vertical displacement ($\delta_{c,L}$) in the prototype due to consolidation of the soil and in the model due to the axial compression of the column.

- Design Stage: At the design stage, the vertical stress on the column in the prototype ($\sigma_{cp,d}$) is greater than both the vertical stress on the column in the loading stage ($\sigma_{cp,L}$) and the vertical stress on the soil ($\sigma_{sp,d}$). The same trend is observed in the model, where the vertical stress on the column ($\sigma_{cm,d}$) is greater than both the

vertical stress on the column in the loading stage ($\sigma_{cm,L}$) and the vertical stress on the soil ($\sigma_{sm,d}$). The column experiences further vertical displacement ($\delta_{c,d}$) in both the prototype and the model, with the displacement in the prototype being attributed to consolidation and the displacement in the model being due to the axial compression of the column. In the prototype, the undrained shear strength of the soil at the design stage (Su_d) is greater than the undrained shear strength of the soil at the loading stage (Su_L) and the undrained shear strength of the soil at the initial stage (Su_0). In contrast, the undrained shear strength of the soil in the model remains constant throughout all stages due to the undrained conditions of the laponite.

Although the stress history in the model differs from that in the prototype due to the inability to consolidate laponite, the analysis focuses on the "Design Stage," where the stress concentration ratio (stress on top of the GEC over stress applied on top of the surrounding soft soil) and the achieved axial strain in the model represent prototype conditions. As the column compresses, the laponite moves upward relative to the column, but the control volume remains the cylindrical volume below the column top. Laponite outside this volume is excluded from the analysis, and its weight is negligible compared to the applied overburden pressure. The primary goal of the model is to reproduce the "Design Stage" rather than the entire prototype stress history, thus overcoming the limitations posed by the inability to consolidate laponite in the adopted testing methodology.

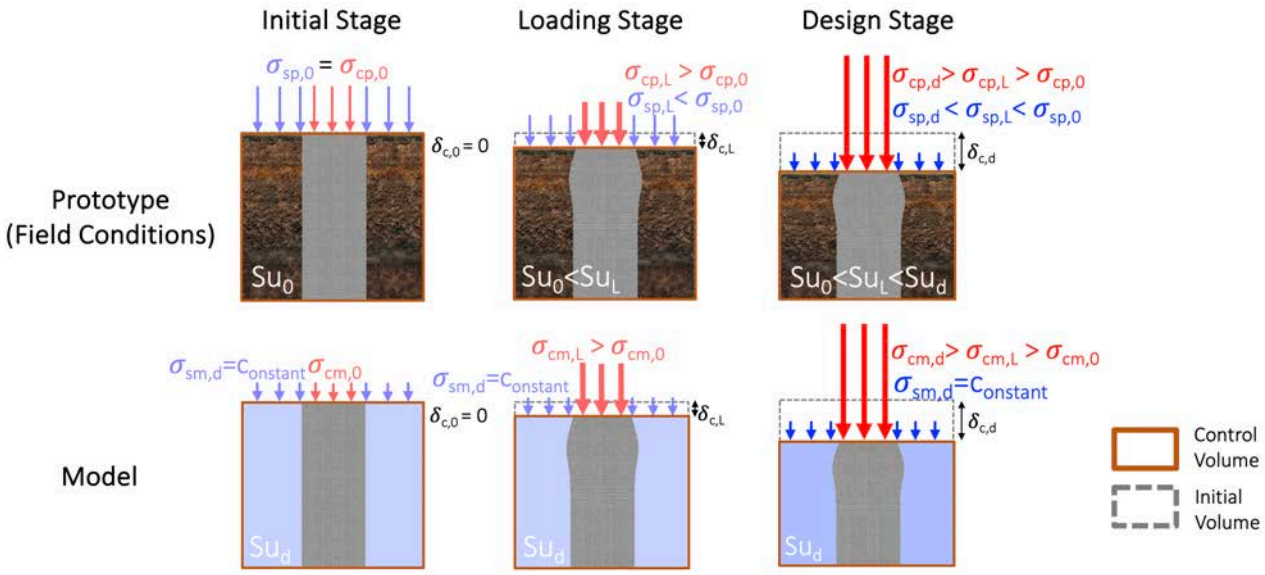

Figure 2.2.- Stages indicating the sequence of loading in Prototype and Model GECs

2.3.6.- EQUIPMENT, SENSORS, AND IMAGE ACQUISITION SYSTEM

The loading frame consists of a modified HM-3000 Humboldt (9000 kgf capacity) actuator that holds the transparent unit cell chamber and the image acquisition system (cameras and lighting). The actuator which was calibrated previously to the testing program can provide a constant displacement rate of 1 mm/min.

The test collects measurements of the load applied as result of the reaction between the core column plate and the column through a load cell of 2,270 kgf capacity (Interface SSM-AJ-5000). The ring overburden plate at the same time is equipped with two miniature pressure sensors of 500 kPa capacity (Tokyo Measurements PDA) previously calibrated in laponite, several tests were made confirming consistency and repeatability of measurements, sensors are equally distant from the center of the column to measure the pressure at the top of the laponite. At the column bearing base an additional pressure sensor of 500 kPa capacity (Tokyo Measurements PDB) was installed to measure the load

transferred to bottom. A calibrated LVDT (Omega LD620-150), with a range of 150 mm, measuring the displacement of the ring overburden plate is also implemented. All the readings were recorded through a data logger system (DataQ Instruments DI-718B).

The image acquisition system holds on two high-resolution camera bodies (Canon EOS 5DSR DSLR) of 50 megapixels equipped with a 50 mm prime lens (Sigma 50mm F1.4 ART DG HSM) and a 24-70 mm lens (Canon 24-70mm Ultrasonic) respectively , the cameras were fixed to the loading frame through a rigid arm at a distance of 1.05 m which is the optimal focal distance given the dimensions of the model.

2.4.- MATERIALS AND PROPERTIES

2.4.1.- LAPONITE MIXING AND PROPERTIES

The laponite mix employed is the result of an exhaustive investigation that optimized geotechnical and optical characteristics. The selected mixture dosage consisted of laponite-RD from BYK Additives and Instruments, Sodium Pyrophosphate Decahydrate (SPP) as additive produced by Acros Organics and distilled water. The following resulting mix dosage obeyed to optimal values of the undrained shear strength, the aging time and the transparency needed for the GEC model. The laponite mixes analyzed followed an adapted method of Pierozan et al. (2022) and the gravimetric concentration dosage was calculated as follows:

$$c_{lap} = \frac{m_{lap}}{m_w + m_{SPP} + m_{lap}} \cdot 100 \qquad \textit{Eq. 2-1}$$

$$c_{SPP} = \frac{m_{SPP}}{m_w + m_{SPP} + m_{lap}} \cdot 100 \qquad \textit{Eq. 2-2}$$

where: c_{lap} is the laponite content in %, c_{SPP} is the rheological additive dosage in %, m_w is the total mass of water in g, m_{SPP} is the mass of SPP in g , and m_{lap} is the mass of laponite-RD in g

Laponite Undrained Shear Strength

The undrained shear strength S_u is primarily the most important property in the selection of the material to represent the soft soil in an experimental model. Laponite mix undrained shear strength is known to be very low from mixes containing less than 15% of

laponite-RD concentration. (Ads et al., 2020; Almikati et al., 2023b) measured values no more than 2 kPa regardless of the additive concentration employed, with a median value close to 1 kPa. For this reason, seven laponite mixes with different concentration of laponite-RD were tested to find the concentration that would provide a S_u above 1 kPa between 14 to 28 days of aging, needed for the GEC model. From ***Figure 2.3***, only mixes above 10% of laponite-RD reached 1 kPa at least at 14 days of aging. However, besides the strength of the transparent soft soil, the transmittance of the material defines the optimal visualization properties.

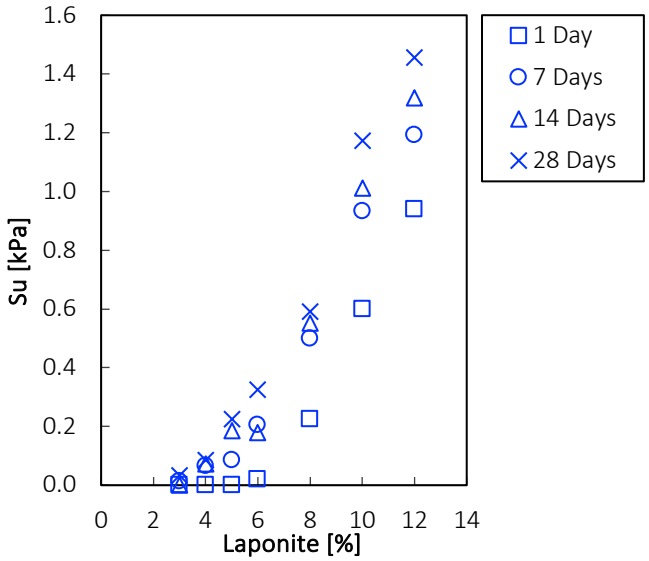

Figure 2.3.- Laponite mix Su vs % Concentration from Almikati et al. (2023)

The extensive use of 17 liters of laponite to fill the transparent unit cell chamber points out the relevance to assess the undrained shear strength of such large volume at different depths inside the sample. For this reason, a tailored vane shear was built with a stepper motor rotating at a rate of 1°/min, a torque gauge of 7 Ncm capacity and a shaft of 600 mm long coupled with a vane blade of 15.24 mm in diameter and 30.48 mm of height, presented in

Figure 2.4.- High resolution vane shear setup and typical results: a) Vane shear Test Setup, b) Undrained shear strength measurements mix L10-S0.78 at 28 days aging

a further details about the investigation of the laponite undrained shear strength are investigated in **SECTION 4.3.1**. Measurements were performed in at the center of a cylinder of 200 mm of diameter and 600 mm height in steps of 50 mm of incremental depth. Variability of S_u along the depth after 28 days of aging was measured following the ASTM D4648/D4648M-13 guideline. The typical undrained shear strength measurements for a mix of 10 % Lapointe-RD and 0.78% SPP concentration (L10-S0.78) are presented in

Figure 2.4.- High resolution vane shear setup and typical results: a) Vane shear Test Setup, b) Undrained shear strength measurements mix L10-S0.78 at 28 days aging

b showing a softening behavior with the peak values varying from 1-1.4 kPa from 5 to 500 mm depth. Similar observations from S_u variation with depth were reported by (Ads et al., 2020) but limited to 100 mm and using a ball penetrometer.

a) ***b)***

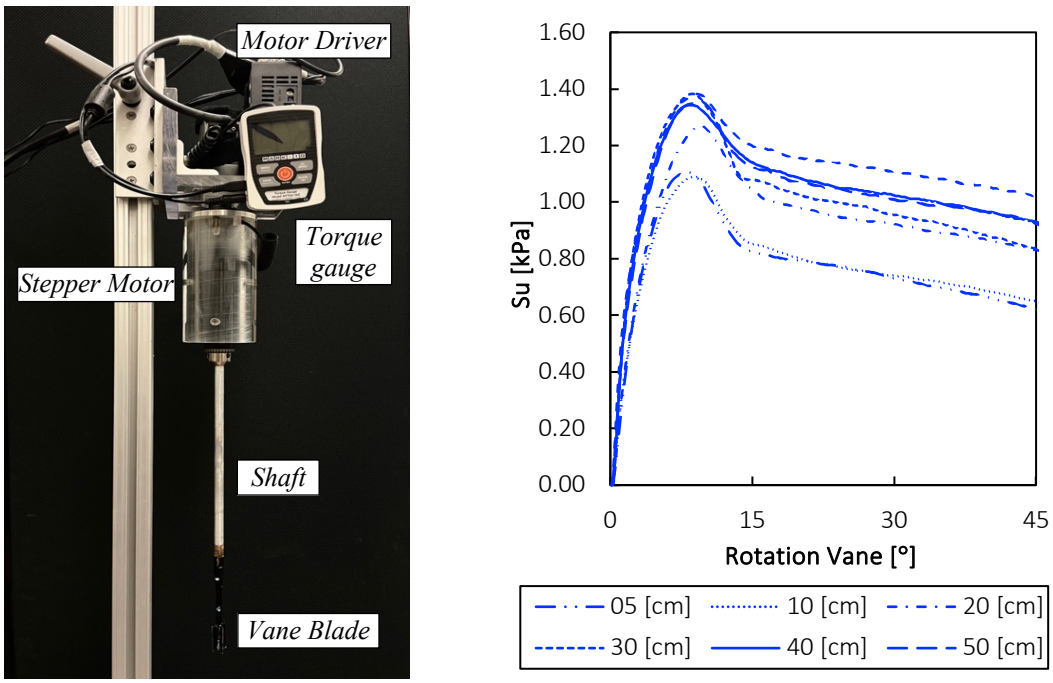

Figure 2.4.- High resolution vane shear setup and typical results: a) Vane shear Test Setup, b) Undrained shear strength measurements mix L10-S0.78 at 28 days aging

Laponite Transparency

The transparency of the laponite mix, is assessed by its transmittance after 28 days of aging. The transmittance (T) is a transparency index defined as the ratio index between the intensity of an incident laser beam that impacts the laponite layer evaluated (I_f) over the intensity of the transmitted laser beam across a void layer (I_0), meaning that a value of 1 represents a full transparent media as shown in **Eq. 2-3**.

$$T = \frac{I_f}{I_0} \qquad \textit{Eq. 2-3}$$

From **Figure 2.5**, multiple dosages of laponite mixture were evaluated at their S_u at 50 mm depth and their transmittance in a 300 mm depth layer of laponite with aid of a

laser power meter model FieldMaxII-Coherent . Among the samples evaluated, the mix of 10% laponite-RD and 0.78% SPP concentration presented the highest undrained shear strength without compromising its transmittance, being the optimal mix design among the broad range of mixes evaluated obeying our needs.

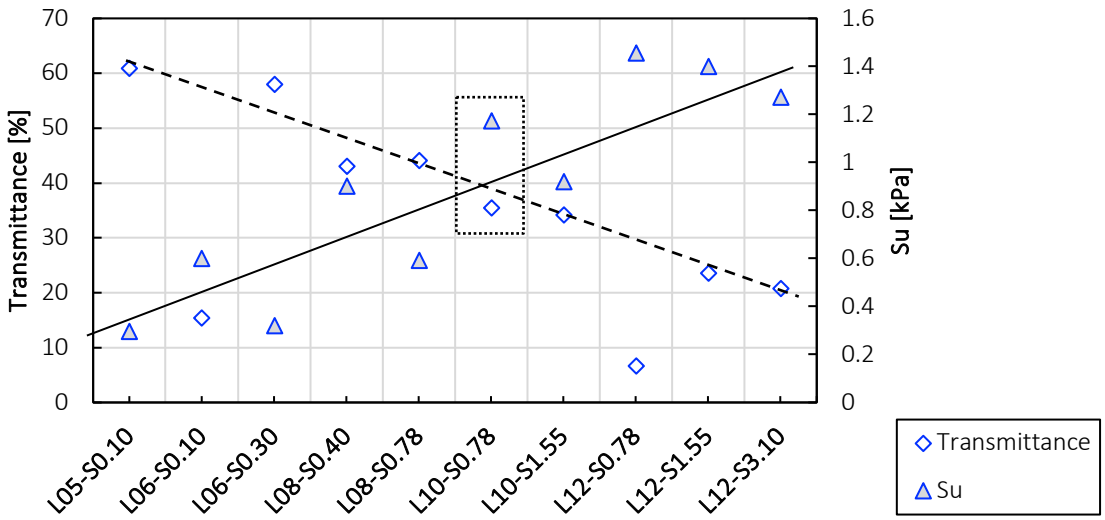

Figure 2.5.- Laponite Su and Transmittance for mixes investigated at 14 days aging

The developed model consists of a large cylindrical cell with a volume of 17 liters of laponite. Optimizing the transparency quality and implementing a marker system that does not interfere with column visualization were key considerations in the design process. For this reason, the technique chosen did not rely on seeding particles such as Timiron and a laser frame, which have been used by certain authors in previous studies (Ni et al., 2010). Instead, tailored black glass beads with an average diameter of 1.5 mm were spread, creating a speckle pattern on a cross-sectional plane during the construction of the sample. The markers can be observed directly through a 150 mm layer of the designed laponite mix; however, for optimal digital image correlation, special lighting was implemented to enhance the quality of the captured images.

2.4.2.- MONTEREY SAND

The column infill material employed is Monterey sand No. 30, it is a clean uniformly graded sand. The sand particle size distribution has a uniform distribution with particle sizes smaller than 0.762 mm and is composed of medium to fine, and subangular to sub-rounded particles. The mean particle size D_{50} is 0.44 mm and the coefficient of uniformity C_u, and the coefficient of curvature C_c, are determined as 1.6 and 1.0, respectively.

Three relative densities RD of 65%, 85% and 95% with effective friction angles φ' between 36° and 40 °were employed with a void ratio e_{max} of 0.78, e_{min} of 0.56, a dry unit weight γ_d measured as 15.91 kN/m^3, and a specific gravity G_s of 2.6 g/cm^3. Main characteristics of Monterey sand No. 30 are summarized in **Table 2.3**.

Table 2.3.- Characteristics Monterey Sand No. 30 (SP)

Parameter		Value
D_{50} [mm]		0.7
C_u [-]		1.8
C_c [-]		1.1
G_S [-]		2.65
$\gamma_{d,max}$ [kN/m^3]		15.91
e_{min} [-]		0.76
e_{max} [-]		0.56
RD 65%	φ' [º]	36.4
RD 85%	φ' [º]	38.5
RD 95%	φ' [º]	40.1

2.4.3.- GEOTEXTILE ENCASEMENT

In the GEC experimental research, the model scaling factors are important to generalize the quantitative model outcome to the prototype. For this reason, the material property that mostly explains the constitutive response of the GEC is the encasement secant stiffness $J_{5\%}$ (kN/m), evaluated as the modulus resulting from the tensile force per unit width at 5% of strain and assuming an elastic regime.

Four polyester geotextiles were selected to produce the encasements, GTX08 non-woven with a $J_{5\%}$ of 08 kN/m, GTX11 non-woven with a $J_{5\%}$ of 11 kN/m, GTX34 woven with a $J_{5\%}$ of 34 kN/m, and GTX70 woven a with a $J_{5\%}$ of 70 kN/m, representing a low, medium, and high stiffness geotextile respectively. The strength characteristics were obtained from wide tensile tests, conducted following the ASTM D4595-17 standard, results in **Figure 2.6** show the four tensile plots for each material used. All encasements were seamed through a 10 mm overlap longitudinal joint with a flexible adhesive made specifically for polyester fabric. Tensile strength tests of the joints were also performed for the three materials and plotted in **Figure 2.6,** results show that seamed and un-seamed fabrics present a same tensile strength path, confirming the suitability of the joint procedure

for the test. Finally, in **Table 2.4** summary of the geosynthetic encasement properties is provided.

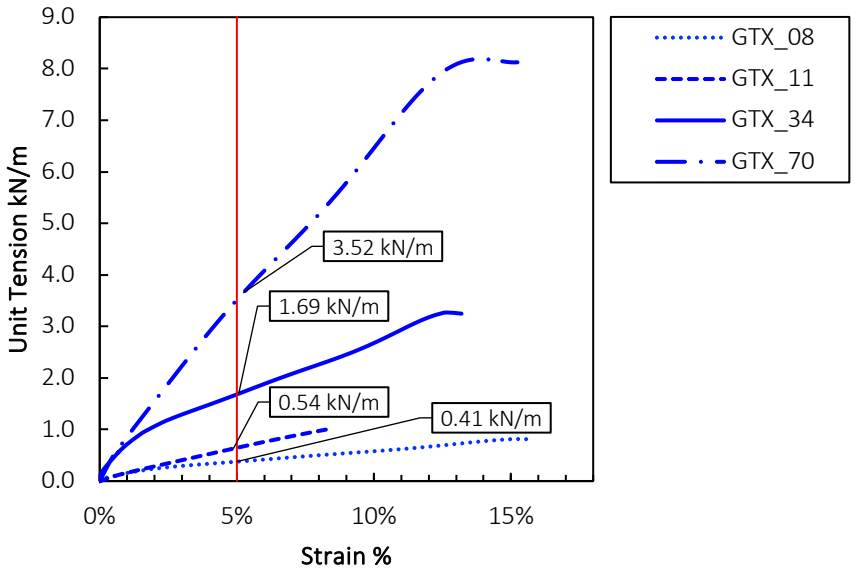

Figure 2.6.- Wide tensile test results from geosynthetics encasements selected

Table 2.4.- Mechanical properties of geosynthetic encasements

Parameter	GTX08	GTX11	GTX34	GTX70
Ultimate Tensile strength [kN/m]	0.81	1.01	3.25	8.12
Secant Tensile stiffness 5% [kN/m]	08	11	34	70
Rupture strain [%]	15.8	8.4	13.2	15.1

2.5.- METHODOLOGY OF TRANSPARENT CHAMBER TESTING

2.5.1.- CONSTRUCTION OF LAPONITE CELL

The proper preparation of the mixture is crucial as the precision involved in selecting the proportions of materials. Furthermore, to meet the practical requirements of the GEC model, each batch was meticulously prepared to yield 100 liters, thereby facilitating the simultaneous creation of five samples. A constant temperature of 21°C was maintained during the entire testing schedule.

Vigorous mixing was obtained by using a polyethylene drum of 30 gallon, and an industrial mixer of 2 HP and 1750 RPM capacity with a coupled 7 in axial impeller, 4-bladed. Such equipment allowed to mix at a speed of 550 RPM producing a stable vortex to properly hydrate the laponite and assure repeatability at every batch. The mix starts first by adding the water, then the SPP was added and mixed for 10 minutes, subsequently the laponite-RD is added all at once and mixed for 20 minutes. This step is important since a slow pouring process of laponite will lead to the creation of multiple lumps and heterogeny mix, even with high mixing speed the lumps would not break and dissolve; instead, air bubbles will be created. Once the laponite mix is finished, the workability of the liquid mix last up to 3 hours, after that period the laponite gelation process is advanced and any bubble created during the pouring may not reach the surface.

For this investigation a two-step process was implemented to create a cross sectional plane equipped with black glass bed markers within the cylindrical transparent unit cell chamber. Complementing the step-by-step process is shown in ***Figure 2.7***. It is important to mention that for steps 2 and 5 when pouring large volumes of laponite, early gelation must be prevented, therefore the use of a water pump of max 1/10 HP is

recommended. This tool facilitates largely the task and any bubble created during the process will quickly reach the surface. Additionally, the lids used were sealed with vacuum grease from the inside and generous rapid dry silicone glue at the contours.

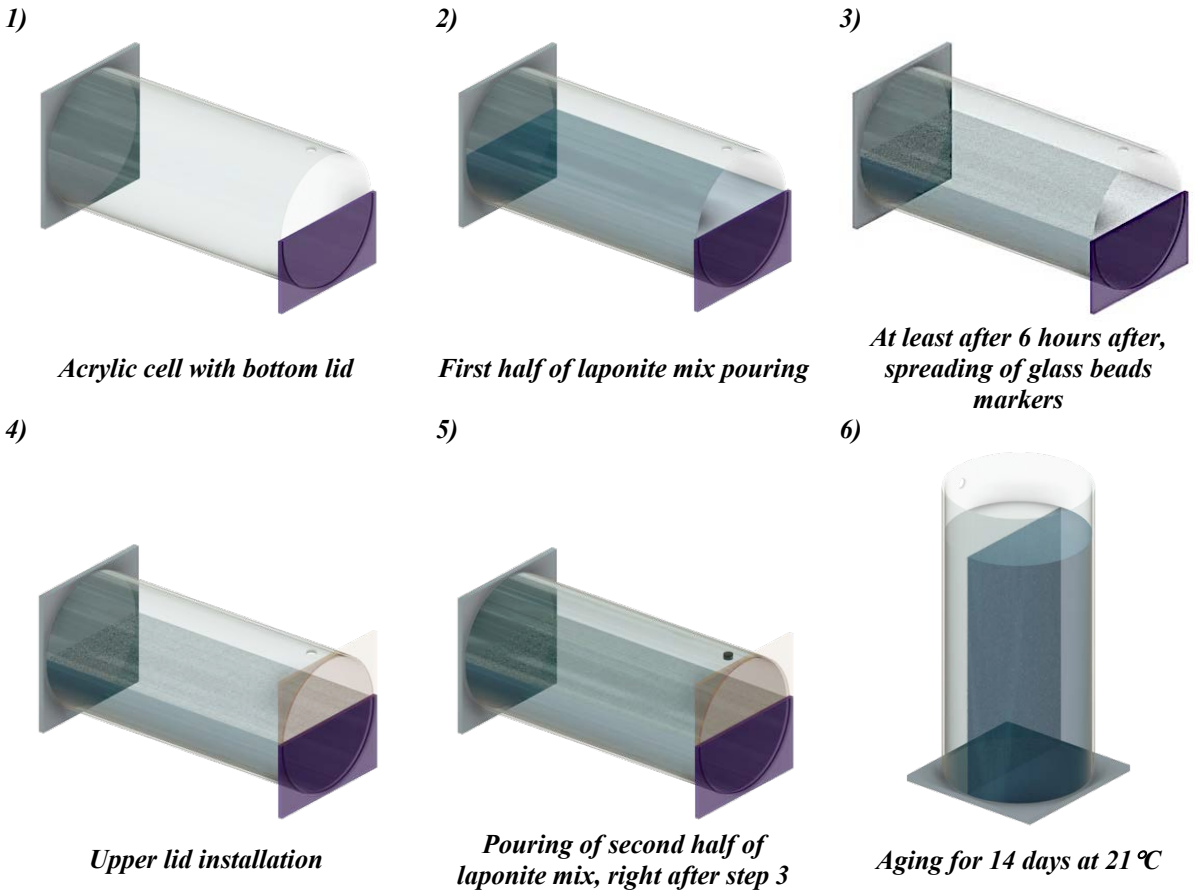

Figure 2.7.- Laponite Unit Cell Chamber construction process, part 1 of 2

To prepare the markers plane in step 3, black markers were spread with the help of a thin acrylic tube with 10 mm inner diameter and 800 mm long with drilled holes of 2 mm along one edge, emulating a saltshaker. This method allowed to obtain a proper speckle pattern shown in **Figure 2.8**. To successfully achieve this step, it should be done at least 6 hours after pouring the laponite, since the samples by that time accumulated a decent

strength and gelation for the markers not to sink. Finally, samples were aged in a controlled temperature room at 21°C for 14 days reaching a S_u of 1 kPa ± 0.1 kPa at 50 mm depth measured at the center of the cell.

a) ***b)***

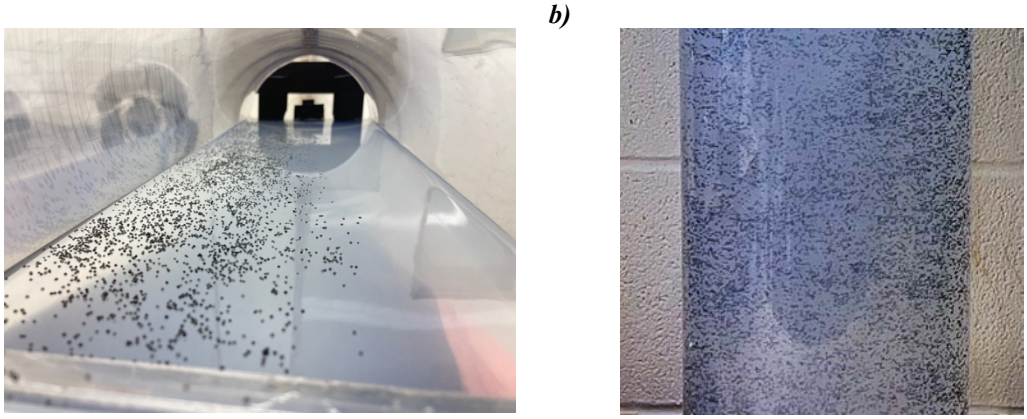

Figure 2.8.- Glass beads in GEC model with laponite, a) Glass beads plane view during markers spreading and b) Glass beads plane front view from finished sample cell

2.5.2.- COLUMN INSTALLATION

After 14 days of aging time, the column installation shown in **Figure 2.9** begins by removing the upper lids. The top 100 mm of laponite are then removed as it served only for the laponite cell construction. After that, a guidance plate is placed as presented in step 7, and a casing is driven through the entire sample until reaching the footprint of the column bearing base. then the interior is completely cleaned from the laponite with the help of a long spoon. The bottom sensor, in step 8, is installed and wired through a reservation for this purpose. In step 8, the encasement is introduced inside the casing and then the Monterey sand is poured and compacted by layers with thickness of 50 mm to target the relative density using a stick vibrator with a frequency of 60 Hz. Once the column filled, the casing is carefully removed resulting in step 9. In step 10, the ring overburden loading

plate with the assigned dead weight on top and the core column plate are positioned with the pressure sensors previously installed and wired.

The column then is placed in the load-control frame as displayed in **Figure 2.10**, the LVDT is also positioned, and the core loading plate is coupled to the actuator. The loading was done solely to the core column using a displacement-controlled actuator with a rate of 1 mm/min.

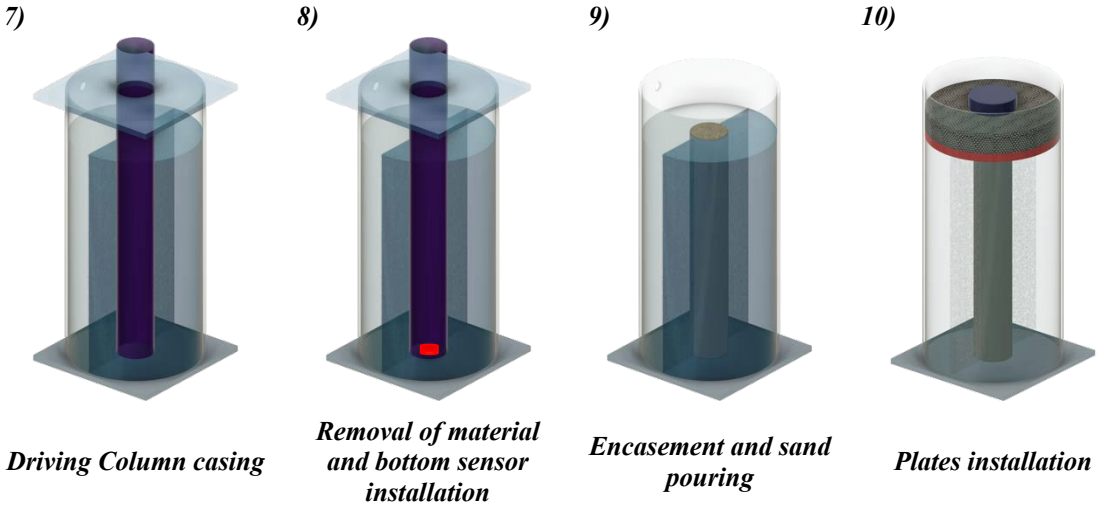

Figure 2.9.- GEC Installation procedure, part 2 of 2

2.5.3.- CAMERA SETUP & CONFIGURATION

For the consistency between all tests, the cameras were programmed to collect images at every 30 seconds. The optimal focal distance between the camera and the column was 1.04 m using the 50 mm prime lens and a 24-70mm lens. The camera properties were fixed at a focal length of 50 mm, an aperture of F/2, shutter speed of 1/100 th seconds, ISO of 100, auto white balance, and no flash. The 50 mm camera targeted the entire unit cell chamber, specifically focusing the cross-sectional plane of markers, and the 24-70mm camera focused only the upper third of the cell.

To achieve repeatable testing conditions, the tests were performed in a dark room with special LED lamps to illuminate white beams across all the sample, helping in obtaining the best quality pictures for image processing.

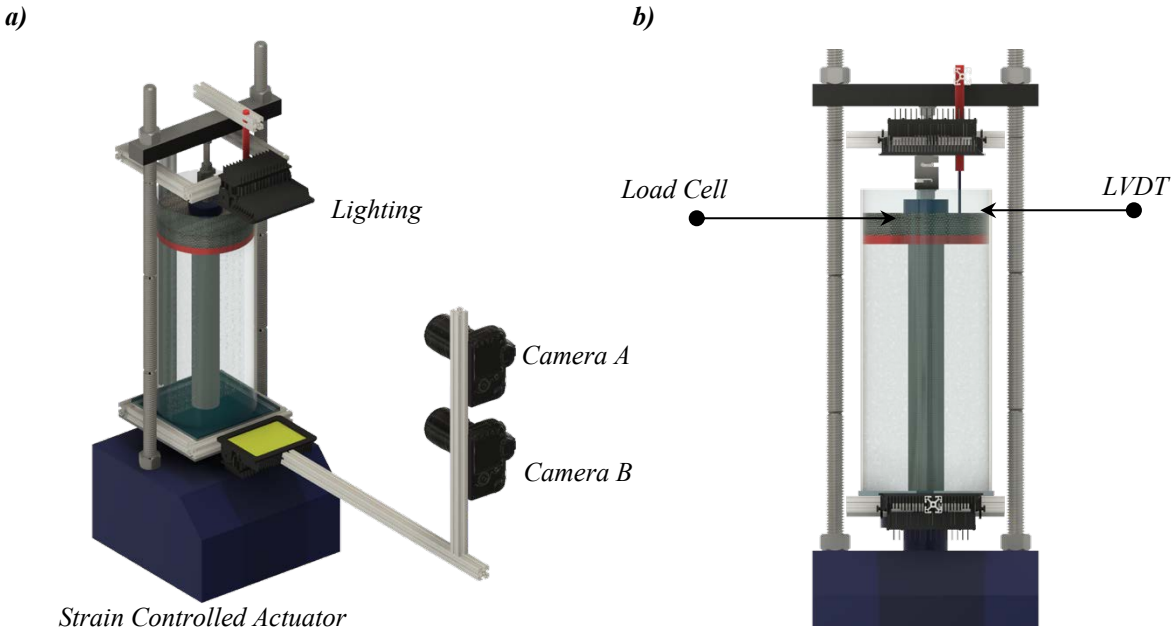

Figure 2.10.- Transparent Unit Cell Chamber testing setup, a) GEC setup with Image acquisition system and b) Transparent Unit Cell Chamber mounted in actuator

2.6.- TYPICAL RESULTS

One of the main objectives of this investigation was to evaluate the suitability of modelling GEC behavior by using laponite, which impose undrained conditions, as a basis for the analysis of the GEC system. Consequently, all variables in the investigation were selected so that they can be considered within the framework of unit cell load and uniaxial load. Accordingly, the selected variables were column geometry, GEC materials, and induced strains. Typical results obtained after testing the base line model of the future testing matrix are presented herein to illustrate the type of data obtained throughout the study. Interpretation of the performance and implication of the results on the analysis of GEC system under study are beyond the scope of this chapter and will be presented in **Chapter 3**.

Testing parameters during test of B-GEC-J34 baseline model were 80 mm diameter, 85 % of relative density, 34 kN/m encasement secant stiffness, and 5 kPa of surrounding soil overburden. From **Figure 2.11**, induced column settlements were increased until 55 mm of column settlement. GEC performance development in the transparent unit cell chamber could be carefully monitored from the imaging and sensing. Recorded images, load, pressures, and displacements collected are presented in this section showing that the methodology provides high quality data were to effectively identify the actual shape of the column at large strains and the potential failure mechanisms.

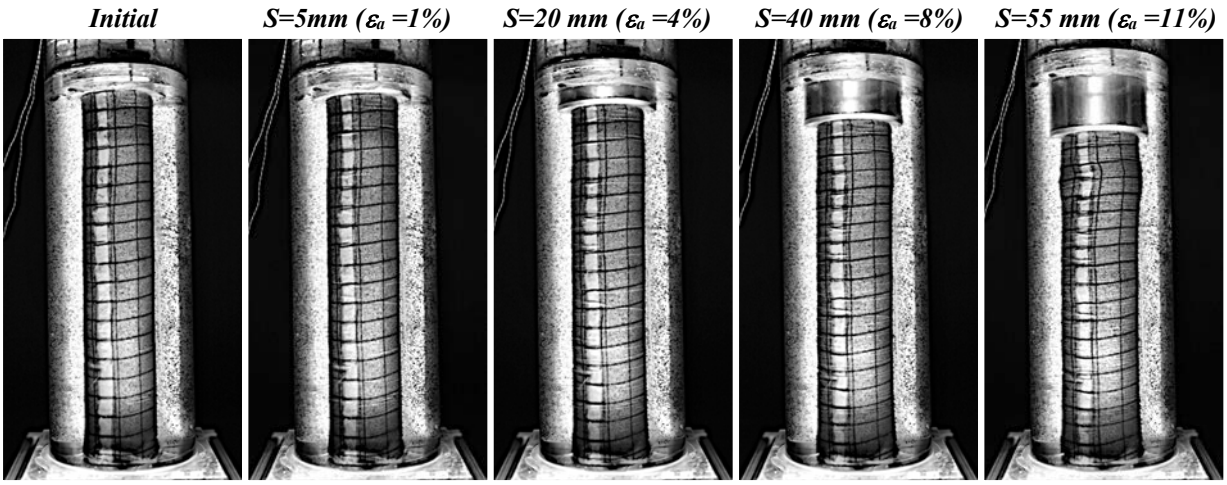

Figure 2.11.- Typical GEC Test at different induced column axial strains, B-GEC-J34 baseline model

2.6.1.- GEOSYNTHETIC ENCASED COLUMN LOAD-SETTLEMENT RESPONSE

The load-settlement response curve of the GEC baseline sample is depicted in **Figure 2.12** in terms of vertical pressure at the top of the column $\sigma_{v,c\,top}$ and average column axial strain $\varepsilon_{a,c}$. The load was applied on a 100 mm diameter loading plate resting on the 80 mm diameter GEC and a circular area of laponite concentric with the column. The $\sigma_{v,c\,top}$ presented in **Figure 2.12** and the following relevant figures is obtained from the total applied load divided by the loading core column plate area. At the same time, the average axial strain was obtained by dividing the settlement of the top column by the initial length of the column (500 mm). The test result shows a typical bearing behavior of a GEC column with no signs of bearing failure, reaching 218 kPa or vertical pressure and $\varepsilon_{a,c}$=11% (55 mm column settlement).

The pressure sensor located at the bottom of the column, as shown in **Figure 2.13**, successfully captures the transfer of load from the top to the bottom column. This sensor also demonstrates potential for quantifying the magnitude of interface shear developed

between the column and the surrounding laponite material by measuring the difference of top and bottom response.

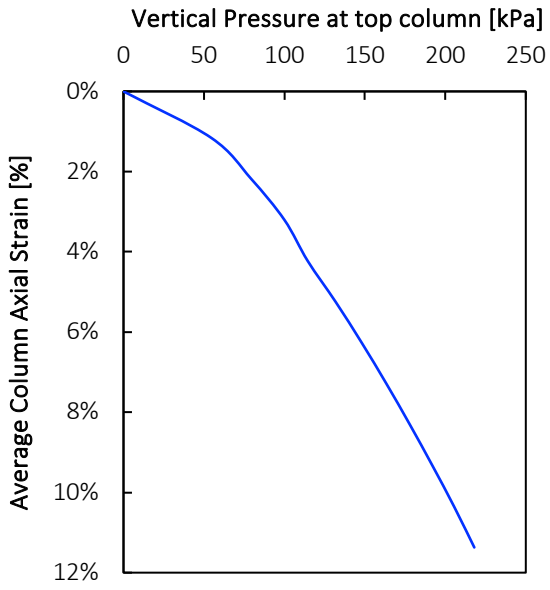

Figure 2.12.- Load-Settlement response, B-GEC-J34 baseline model

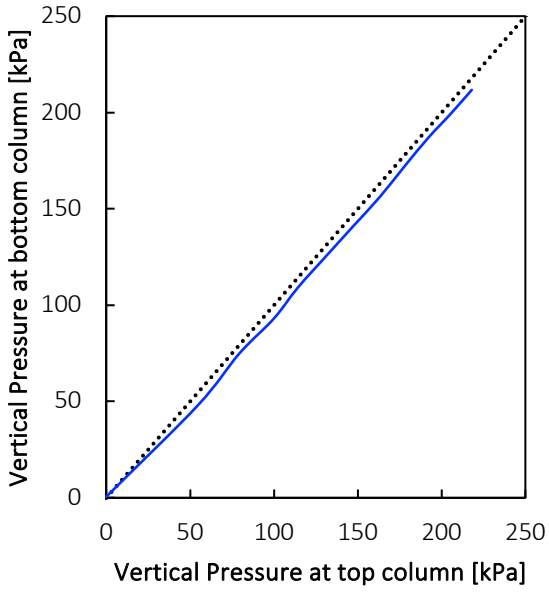

Figure 2.13.- Pressure Top-Bottom column response, B-GEC-J34 baseline model

2.6.2.- GEOSYNTHETIC ENCASED COLUMN STRAIN DATA

Overall, the images captured, and image analysis capabilities enable unique visualization and measurement of the column's vertical and encasement radial displacements, which is a prime advantage of the experimental setup used in this investigation. The test column was monitored using 20 equally spaced references along the encasement length. The resulting plot in **Figure 2.14** shows the depth position of each section from top to bottom obtained through image analysis. As expected, the displacements gradually decrease from the top of the column to the bottom. This detailed spatial displacement data provides great insight into both the overall vertical deformation response of the column as well as the distribution of axial strains along its length during testing. The ability to observe the progression of displacements at different heights allows for a nuanced understanding of the column's behavior under load that could not be achieved from measuring only the total displacement.

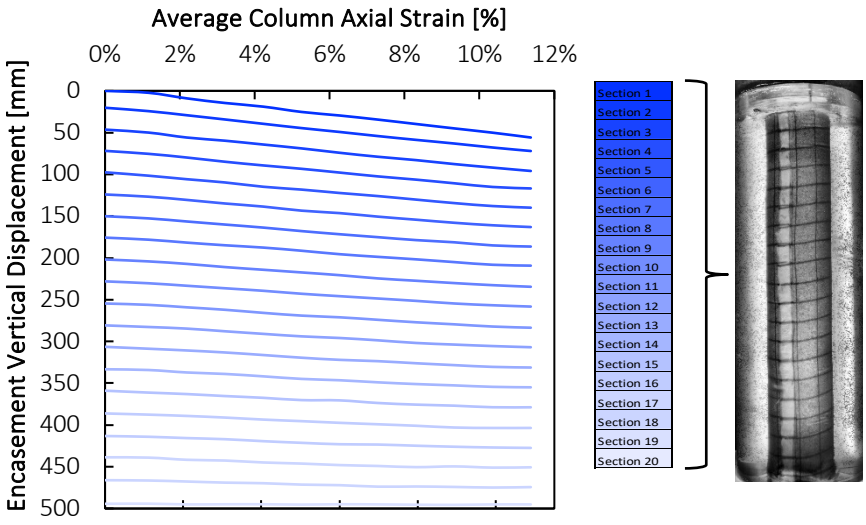

Figure 2.14.- Encasement vertical displacement, B-GEC-J34 baseline model

Another advantage of the imaging analysis methods used in this study is the ability to quantify the geosynthetic encasement radial strain along the entire column length. By tracking changes in the column's outer contour using predefined markers, encasement radial strains can be calculated as the change in diameter divided by the original diameter as shown in **Figure 2.15**. The resulting strain contour plots provide high detail on the progression of radial bulging, which initiates at a depth of about 2 diameters below the surface under early loading. Whereas previous experimental research on GEC was limited to continuously measuring encasement radial strains only at specific depths, the imaging techniques here enable visualization and quantification of the radial bulge progression along the entire column's profile depth. The high-resolution encasement radial strain data gives clear insight into the mechanics of the column's response by capturing the depth progression of encasement radial strains resulting from the pressure applied on top of the column.

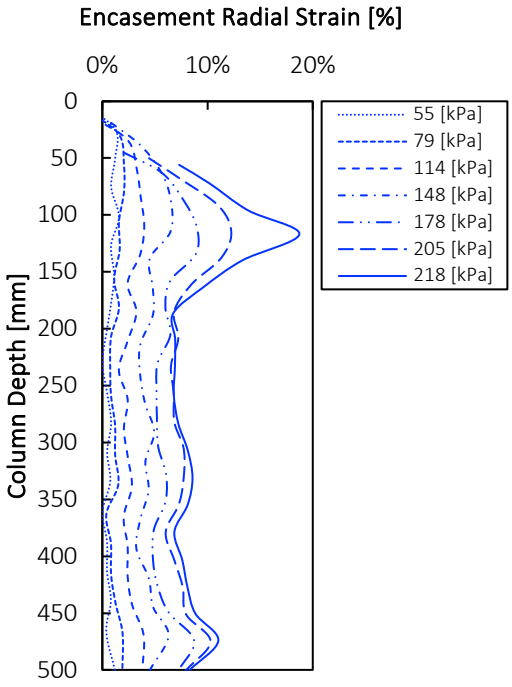

Figure 2.15.- Profile of geosynthetic encasement radial strain at different loading stages, B-GEC-J34 baseline model

In addition to the detailed encasement radial strain contours, **Figure 2.16** quantifies the average radial strain along the column length at each loading stage. This plot illustrates the incremental progression of overall radial strains in the encasement, providing a general but less detailed perspective on the column's deformation. While the averaged plot lacks the high-resolution strain distribution along the column depth, it complements the contour data, enabling the analysis of radial strains from different viewpoints. The progression of averaged strain demonstrates the overall outward deformation of the column across loading stages.

Simultaneously, the detailed contour plots facilitate the study of strain localization and the formation and advancement of the column bulge along its length. Together, these strain quantification approaches offer both general trends and specific mechanics, providing comprehensive insight. The continuous radial strain data captures the complete

picture by showcasing the localized progression and the integrated magnitude of the encasement's deformation response under increasing vertical stress at the top column.

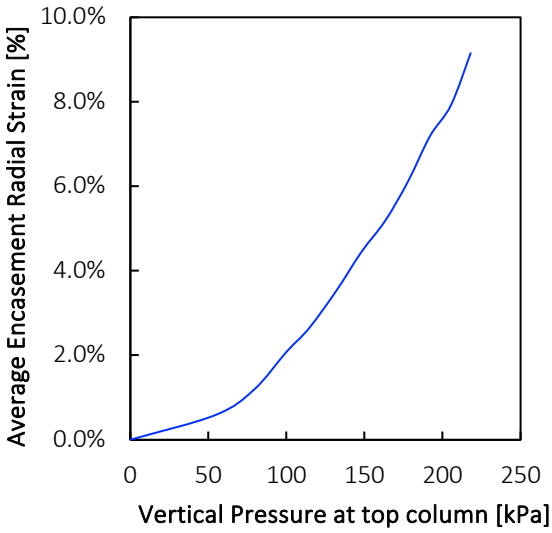

Figure 2.16.- Average geosynthetic encasement radial strain, B-GEC-J34 baseline model

The experimental methods also enabled quantification of volumetric strains in the column throughout loading. By measuring displacement of the overburden plate relative to the column core, total volume change in the test unit cell could be obtained, assuming the surrounding laponite is incompressible. This total volume change was assigned to the column material since it was the only component in the system subjected to possible volume changes. The resulting plot of column axial strain versus volumetric strain percentage shown in **Figure 2.17** clearly captures dilation behavior, which was expected given the high relative density of the sand used as column infill. As average column axial strains and encasement radial strains increased with loading, the column expanded in volume, exhibiting a dilative response.

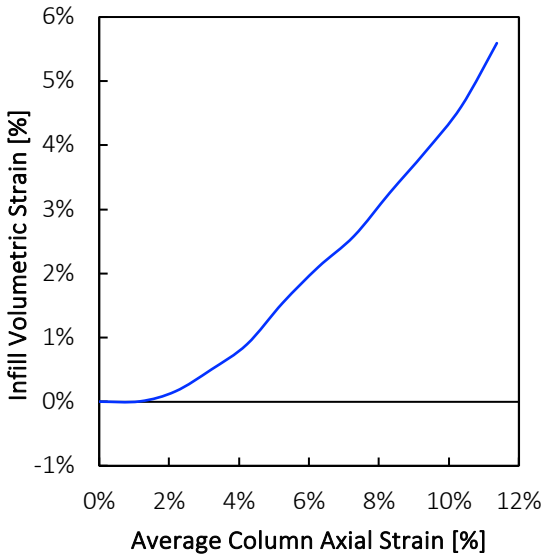

Figure 2.17.- Column infill volumetric strain, B-GEC-J34 baseline model

Previous experimental studies on GECs restricted full characterization of three-dimensional column deformations. The capabilities here to quantify localized encasement radial strains along with axial strains and total volume change provide insight into the progression of strains under loading. This multi-component understanding of the column's deformation enhances interpretation of the physical mechanisms governing the complex soil-column interaction.

2.6.3.- SURROUNDING SOIL BEHAVIOR

Whereas experimental methods in previous investigations focused on column displacements, the DIC analysis here enables detailed visualization and quantification of the surrounding soil movement influenced by the deforming column. Digital image correlation (DIC) was performed on a region of interest encompassing the laponite clay and a portion of the column to visualize soil-column interaction mechanics as shown in **Figure 2.18**. Using the Ncorr 2D DIC MATLAB program, progressive horizontal

displacements were obtained from the DIC images provided in **Figure 2.18**. The DIC results clearly show concentrated horizontal component of displacements in the laponite near the column top and the column interface under increasing load. In the bulging development stage, significant outward soil movement is captured by the DIC analysis. This technique's high sensitivity to small deformations provides unique insight into soil-column interaction. The progression of soil horizontal displacements adjacent to the column improves understanding of the shear transfer mechanics governing the soil-column response. For instance, the DIC analysis reveals that the magnitude and extent of horizontal soil displacements are dependent on the applied load level and the relative stiffness between the column and the surrounding soil. Furthermore, the formation of distinct shear bands in the soil near the column interface can be clearly identified, indicating the development of localized failure mechanisms.

In **Chapter 4**, a detailed study is performed to further investigate the soil-encasement interaction and the influence of various design parameters on the load transfer mechanisms. The insights gained from the DIC analysis in this chapter lay the foundation for a more comprehensive understanding of GEC behavior, which will be explored in greater depth in the subsequent chapters.

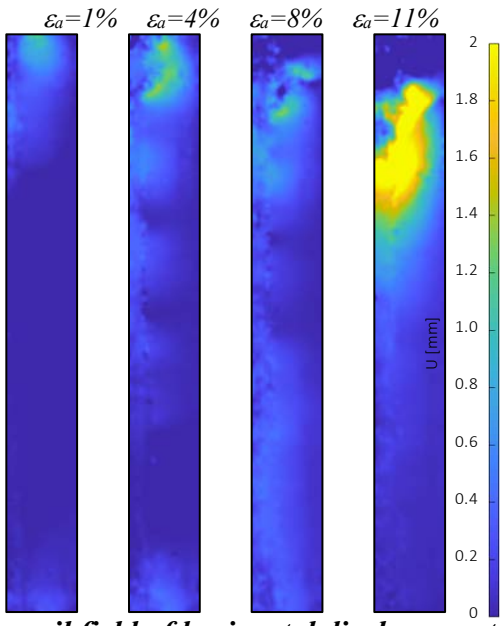

Figure 2.18.- Surrounding soil field of horizontal displacements at 1%,4%, 8% and 11% of average column axial strain, B-GEC-J34 baseline model

The DIC analysis also quantified vertical component of displacements within the region of interest surrounding the column, as shown in **Figure 2.19**. Similar to the horizontal displacements, the results show concentrated vertical displacements in the laponite near the column top and interface as the loading increases. The progression of vertical displacements clearly captures the column settling under the applied pressure load. In the final bulging stage, the DIC analysis measured significant upward soil movements adjacent to the deformed column.

Capturing both horizontal and vertical displacement fields provides a comprehensive depiction of the soil deformation response influenced by the loaded column. The combined analysis of these displacement components offers valuable insights into the complex soil-column interaction mechanisms. For example, the DIC results reveal that the soil near the column top experiences the highest vertical and horizontal displacements. This observation suggests that the load transfer from the column to the

surrounding soil is most pronounced in this region, highlighting the importance of considering the soil-column interaction in GEC analysis.

Moreover, the simultaneous measurement of horizontal and vertical soil displacements enables the calculation of shear strains in the soil mass. These strain fields provide essential information for understanding the development of failure mechanisms and the potential for soil improvement around the GEC. The ability to quantify these strains using DIC analysis represents a significant advancement in the experimental study of GECs, as it allows for a more accurate assessment of the soil response and the effectiveness of the reinforcement system.

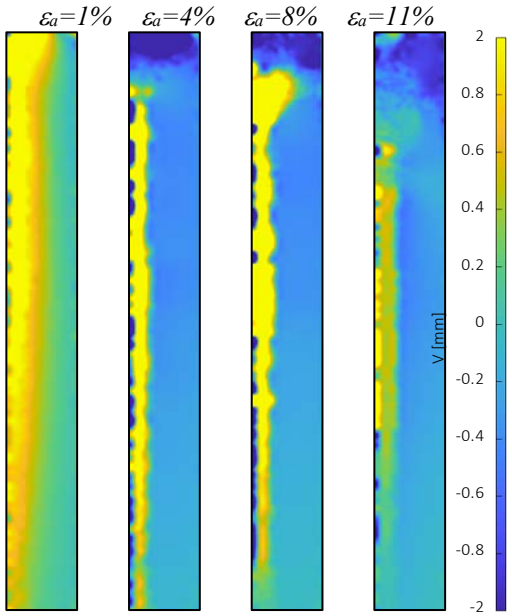

Figure 2.19.- Surrounding soil field of vertical displacements at 1%,4%, 8% and 11% of average column axial strain, B-GEC-J34 baseline model

The DIC analysis also enabled computation of shear strain ε_{xy} development in the soil-column region of interest as displayed in **Figure 2.20**. The results reveal a thin, longitudinal shear band at the soil-column interface that intensifies under increasing load.

In the early loading stage, minimal interface shear can be observed. By the second and third stages, a distinct shear band formed in the laponite next to the column, evidencing non marginal shear transfer. The localized shear band then slightly diminishes in the bulging development stage. The progression of the interfacial shear zone provides unique visualization of the soil-column shear transfer mechanics. Whereas soil and column displacements characterize the kinematic response, quantifying shear strain development specifically captures the dynamic interaction. The emerging and advancing localized shear band proves the mobilization of interface shear stresses as a mode of load transfer from the pressure load applied to the column.

As previously mentioned, the laponite-DIC analysis technique employed in this study provides valuable insights into the progression of shear transfer at the soil-GEC interface. By quantifying soil deformations, column displacements, and shear strains, the experimental data obtained contributes to a more comprehensive understanding of the interactive mechanisms in the composite geosystem. This improved understanding of the soil-column interaction can inform the development of more accurate and efficient design methods for GEC-reinforced foundation soils structures.

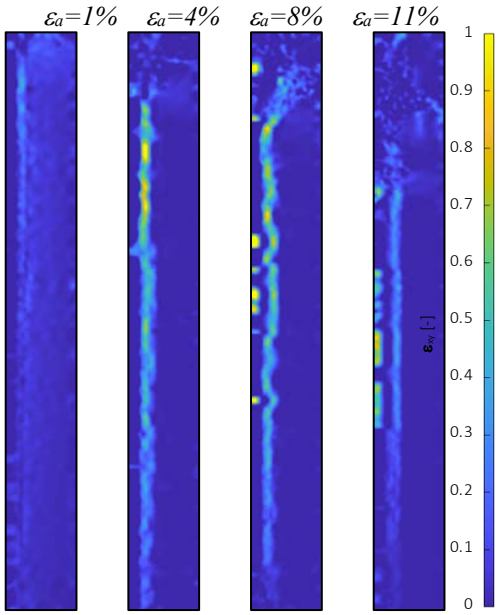

Figure 2.20.- Surrounding soil field shear strain at 1%,4%, 8% and 11% of average column axial strain, B-GEC-J34 baseline model

2.6.4.- REPEATABILITY

The consistent testing protocols adopted in this study proved to yield repeatable results. Such repeatability can be evidenced in **Figure 2.21a** , which presents the load-settlement response curves from two repeat tests conducted using the same GEC baseline configuration (⌀ 80 mm; Dr 85%; $J_{5\%}$ 34 kN/m;σ 5 kPa), which exhibit nearly identical behavior. Furthermore, in **Figure 2.21b** monitoring the column's volumetric strain shows also a very consistent dilation response, within a narrow 1-2% range of variation. The tightly grouped volume change behavior indicates a consistent model construction and testing procedure, as well as reliability in material selection, construction protocols, column relative density, and sensor instrumentation across multiple tests. This repeatability provides confidence in the observed mechanisms and quantified responses, suggesting that they accurately reflect the inherent behaviors of the system under controlled laboratory conditions. The carefully designed methodology and reliable instrumentation of the

transparent unit cell chamber setup ensure the collection of high-quality, consistent data, which is essential for the analysis of GEC performance.

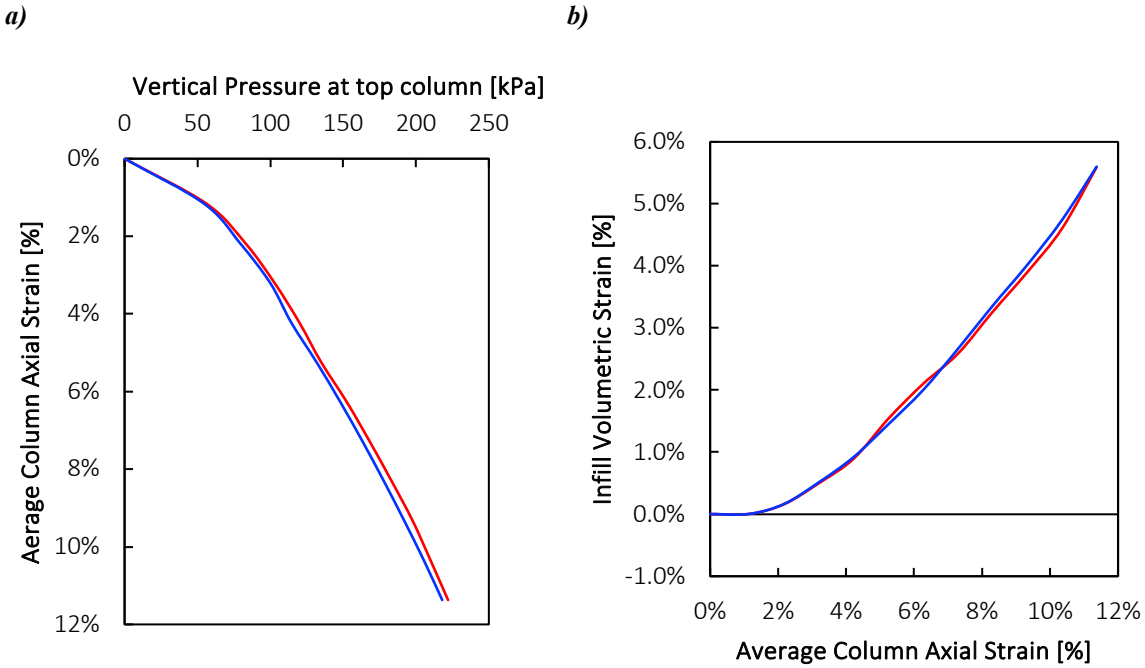

Figure 2.21.- Repeatability of B-GEC-J34 baseline mode, a) Load-Settlement response and b) Column infill volumetric strain testing

2.7.- CONCLUSIONS

In this study, several findings can be drawn regarding the use of laponite as a clay surrogate, the behavior of geosynthetic encased columns (GECs), and the experimental methodology developed in this study:

- The experimental setup and methodology developed, utilizing a transparent unit cell chamber filled with laponite and advanced imaging techniques, proved effective in studying the behavior of GECs under undrained conditions.

- The optimized laponite mix design, consisting of 10% laponite-RD and 0.78% SPP concentration, provided the desired undrained shear strength (>1 kPa) and transparency for optimal visualization and analysis of GEC behavior.

- The load-settlement response curves obtained from the GEC tests from models B-GEC-J34 baseline and B-GEC-J70 exhibited typical bearing behavior without signs of bearing failure, reaching vertical pressures of 218 kPa at 11% average column axial strain.

- The use of transparent clay allowed for the quantification of changes in several relevant variables, such encasement vertical displacements, encasement radial strains along the entire column length, and column infill volumetric strains, providing insight into the progression of GEC strains under loading. This is a significant advancement, as current design methods often assume these variables to be constant with depth. The ability to measure the variation of these parameters along the column length provides valuable data for improving the accuracy of design methods.

- Digital Image Correlation (DIC) analysis of the surrounding laponite allowed for visualization and quantification of soil displacements and soil shear strains, revealing the development of localized shear bands at the soil-column interface and improving understanding of the load transfer mechanisms.

- The consistent testing protocols and reliable instrumentation of the transparent unit cell chamber setup yielded repeatable results, as evidenced by nearly identical load-settlement response curves and volumetric strain behavior across multiple tests with the same GEC configuration.

In summary, the use of laponite as a transparent soil analog opens up new possibilities for in-depth experimental research on GECs. The findings from this study contribute to a better understanding of GEC behavior, the interaction between the GEC and the surrounding soil, and the importance of considering the variation of key parameters along the column depth in the design and analysis of GEC-reinforced soil systems.

2.8.- REFERENCES

Ads, A., Iskander, M., & Bless, S. (2020). Shear Strength of a Synthetic Transparent Soft Clay Using a Miniature Ball Penetrometer Test. *Geotechnical Testing Journal*, *43*(5), 20190020. https://doi.org/10.1520/GTJ20190020

Alexiew, D., & Raithel, M. (2015). Geotextile-Encased Columns, Case Studies over Twenty Years. In *Ground Improvement Case Histories* (pp. 451–477). Elsevier. https://linkinghub.elsevier.com/retrieve/pii/B978008100192900017X

Ali, K., Shahu, J. T., & Sharma, K. G. (2012). Model tests on geosynthetic-reinforced stone columns: A comparative study. *Geosynthetics International*, *19*(4), 292–305. https://doi.org/10.1680/gein.12.00016

Ali, K., Shahu, J. T., & Sharma, K. G. (2014). Model tests on single and groups of stone columns with different geosynthetic reinforcement arrangement. *Geosynthetics International*, *21*(2), 103–118. https://doi.org/10.1680/gein.14.00002

Alkhorshid, N. R. (2017). *Analysis of geosynthetic encased columns in very soft soil* (Publicação G.TD-133/17) [Doctoral]. Universidade de Brasília.

Alkhorshid, N. R., Araujo, G. L. S., Palmeira, E. M., & Zornberg, J. G. (2019). Large-scale load capacity tests on a geosynthetic encased column. *Geotextiles and Geomembranes*, *47*(5), 632–641. https://doi.org/10.1016/j.geotexmem.2019.103458

Alkhorshid, N. R., Araújo, G., & Palmeira, E. (2021). Geosynthetic Encased Column: Comparison between numerical and experimental results. *Soils and Rocks*, *44*(4), 1–12. https://doi.org/10.28927/SR.2021.073121

Almikati, A., Pierozan, R. C., Sadek, S., & Zornberg, J. G. (2023). Geotechnical Characterization of Laponite as Transparent Clay Surrogate. *Geotechnical Testing Journal*, *46*(3), 20220106. https://doi.org/10.1520/GTJ20220106

Ambily, A. P., & Gandhi, S. R. (2007). Behavior of Stone Columns Based on Experimental and FEM Analysis. *Journal of Geotechnical and Geoenvironmental Engineering*, *133*(4), 405–415. https://doi.org/10.1061/(ASCE)1090-0241(2007)133:4(405)

Black, J. A., Sivakumar, V., & Bell, A. (2011). The settlement performance of stone column foundations. *Géotechnique*, *61*(11), 909–922. https://doi.org/10.1680/geot.9.P.014

Black, J. A., & Tatari, A. (2015). Transparent Soil to Model Thermal Processes: An Energy Pile Example. *Geotechnical Testing Journal*, *38*(5), GTJ20140215. https://doi.org/10.1520/GTJ20140215

Bonn, D., Kellay, H., Tanaka, H., Wegdam, G., & Meunier, J. (1999). *Laponite: What Is the Difference between a Gel and a Glass?* 3.

Bonn, D., Tanase, S., Abou, B., Tanaka, H., & Meunier, J. (2002). Laponite: Aging and Shear Rejuvenation of a Colloidal Glass. *Physical Review Letters*, *89*(1), 015701. https://doi.org/10.1103/PhysRevLett.89.015701

Castro, J. (2017). Groups of encased stone columns: Influence of column length and arrangement. *Geotextiles and Geomembranes*, *45*(2), 68–80. https://doi.org/10.1016/j.geotexmem.2016.12.001

Cengiz, C., & Güler, E. (2018a). Seismic behavior of geosynthetic encased columns and ordinary stone columns. *Geotextiles and Geomembranes*, *46*(1), 40–51. https://doi.org/10.1016/j.geotexmem.2017.10.001

Cengiz, C., & Güler, E. (2018b). Shaking table tests on geosynthetic encased columns in soft clay. *Geotextiles and Geomembranes*, *46*(6), 748–758. https://doi.org/10.1016/j.geotexmem.2018.07.009

Chen, J.-F., Li, L.-Y., Xue, J.-F., & Feng, S.-Z. (2015). Failure mechanism of geosynthetic-encased stone columns in soft soils under embankment. *Geotextiles and Geomembranes*, *43*(5), 424–431. https://doi.org/10.1016/j.geotexmem.2015.04.016

Chen, J.-F., Wang, X.-T., Xue, J.-F., Zeng, Y., & Feng, S.-Z. (2018). Uniaxial compression behavior of geotextile encased stone columns. *Geotextiles and Geomembranes*, *46*(3), 277–283. https://doi.org/10.1016/j.geotexmem.2018.01.003

Chini, C. M., Wallace, J. F., Rutherford, C. J., & Peschel, J. M. (2015). Shearing Failure Visualization via Particle Tracking in Soft Clay Using a Transparent Soil. *Geotechnical Testing Journal*, *38*(5), 20140210. https://doi.org/10.1520/GTJ20140210

Cummins, H. Z. (2007). Liquid, glass, gel: The phases of colloidal Laponite. *Journal of Non-Crystalline Solids*, *353*(41–43), 3891–3905. https://doi.org/10.1016/j.jnoncrysol.2007.02.066

Dash, S. K., & Bora, M. C. (2013). Influence of geosynthetic encasement on the performance of stone columns floating in soft clay. *Canadian Geotechnical Journal*, *50*(7), 754–765. https://doi.org/10.1139/cgj-2012-0437

di Prisco. (2006). *Geo-reinforced sand columns: Small scale experimental tests and theoretical modelling*. 4.

di Prisco, C., & Galli, A. (2011). Mechanical behaviour of geo-encased sand columns: Small scale experimental tests and numerical modelling. *Geomechanics and Geoengineering*, *6*(4), 251–263. https://doi.org/10.1080/17486025.2011.578756

Ghazavi, M., Ehsani Yamchi, A., & Nazari Afshar, J. (2018). Bearing capacity of horizontally layered geosynthetic reinforced stone columns. *Geotextiles and*

Geomembranes, *46*(3), 312–318. https://doi.org/10.1016/j.geotexmem.2018.01.002

Ghazavi, M., & Nazari Afshar, J. (2013). Bearing capacity of geosynthetic encased stone columns. *Geotextiles and Geomembranes*, *38*, 26–36. https://doi.org/10.1016/j.geotexmem.2013.04.003

Gniel, J., & Bouazza, A. (2009). Improvement of soft soils using geogrid encased stone columns. *Geotextiles and Geomembranes*, *27*(3), 167–175. https://doi.org/10.1016/j.geotexmem.2008.11.001

Hong, Y.-S., Wu, C.-S., & Yu, Y.-S. (2016). Model tests on geotextile-encased granular columns under 1-g and undrained conditions. *Geotextiles and Geomembranes*, *44*(1), 13–27. https://doi.org/10.1016/j.geotexmem.2015.06.006

Iskander, M. G. (2010). *Modelling with transparent soils: Visualizing soil structure interaction and multi phase flow, non-intrusively*. Springer.

Iskander, M. G., Bathurst, R. J., & Omidvar, M. (2015). Past, Present, and Future of Transparent Soils. *Geotechnical Testing Journal*, *38*(5), 20150079. https://doi.org/10.1520/GTJ20150079

Iskander, M. G., Sadek, S., & Liu, J. (2002). Optical measurement of deformation using transparent silica gel to model sand. *International Journal of Physical Modelling in Geotechnics*, *2*(4), 13–26.

Kempfert, H. G., Raithel, M., & Jaup, A. (1999). *Model tests for analysis of the bearing and deformation behavior of columns foundations*.

Miranda, M. (2014). *Influencia de la densidad y del confinamiento con geotextil en columnas de grava*.

Miranda, M., & Da Costa, A. (2016). Laboratory analysis of encased stone columns. *Geotextiles and Geomembranes*, *44*(3), 269–277. https://doi.org/10.1016/j.geotexmem.2015.12.001

Miranda, M., Da Costa, A., Castro, J., & Sagaseta, C. (2017). Influence of geotextile encasement on the behaviour of stone columns: Laboratory study. *Geotextiles and Geomembranes*, *45*(1), 14–22. https://doi.org/10.1016/j.geotexmem.2016.08.004

Mohapatra, S. R., Rajagopal, K., & Sharma, J. (2016). Direct shear tests on geosynthetic-encased granular columns. *Geotextiles and Geomembranes*, *44*(3), 396–405. https://doi.org/10.1016/j.geotexmem.2016.01.002

Murugesan, S., & Rajagopal, K. (2009a). Investigations on the behaviour of geosynthetic encased stone columns. *Stand Alone*, 2411–2414. https://doi.org/10.3233/978-1-60750-031-5-2411

Murugesan, S., & Rajagopal, K. (2009b). Shear Load Tests on Stone Columns With and Without Geosynthetic Encasement. *Geotechnical Testing Journal*, *32*(1), 101219. https://doi.org/10.1520/GTJ101219

Najjar, S. S. (2013). A State-of-the-Art Review of Stone/Sand-Column Reinforced Clay Systems. *Geotechnical and Geological Engineering*, *31*(2), 355–386. https://doi.org/10.1007/s10706-012-9603-5

Nazari Afshar, J., & Ghazavi, M. (2014). Experimental Studies on Bearing Capacity of Geosynthetic Reinforced Stone Columns. *Arabian Journal for Science and Engineering*, *39*(3), 1559–1571. https://doi.org/10.1007/s13369-013-0709-8

Ni, Q., Hird, C. C., & Guymer, I. (2010). Physical modelling of pile penetration in clay using transparent soil and particle image velocimetry. *Géotechnique*, *60*(2), 121–132. https://doi.org/10.1680/geot.8.P.052

Pierozan, R. C., Almikati, A., Araujo, G. L. S., & Zornberg, J. G. (2022). Optical and Physical Properties of Laponite for Use as Clay Surrogate in Geotechnical Models. *Geotechnical Testing Journal*, *45*(1), 20210100. https://doi.org/10.1520/GTJ20210100

Sadek, S., Iskander, M. G., & Liu, J. (2003). Accuracy of Digital Image Correlation for Measuring Deformations in Transparent Media. *Journal of Computing in Civil Engineering*, *17*(2), 88–96. https://doi.org/10.1061/(ASCE)0887-3801(2003)17:2(88)

Sang, Y., Zhao, J., Duan, F., Sun, W., & Zhao, H. (2019). A novel automatic device to measure deformation inside transparent soil based on digital image correlation technology. *Measurement Science and Technology*, *30*(3), 035202. https://doi.org/10.1088/1361-6501/aafaa0

Stuedlein, A. W., & Holtz, R. D. (2012). Analysis of Footing Load Tests on Aggregate Pier Reinforced Clay. *Journal of Geotechnical and Geoenvironmental Engineering*, *138*(9), 1091–1103. https://doi.org/10.1061/(ASCE)GT.1943-5606.0000677

Wallace, J., Chini, C., Rutherford, C., & Peschel, J. (2015). Visualizing the failure surface of a laboratory vane shear in soft clay using transparent surrogate soil. In V. Meyer (Ed.), *Frontiers in Offshore Geotechnics III* (pp. 1227–1232). CRC Press. http://www.crcnetbase.com/doi/10.1201/b18442-185

Wallace, J. F., & Rutherford, C. J. (2015). Geotechnical Properties of LAPONITE RD®. *Geotechnical Testing Journal*, *38*(5), 20140211. https://doi.org/10.1520/GTJ20140211

White, D. J., Pham, H. T. V., & Hoevelkamp, K. K. (2007). Support Mechanisms of Rammed Aggregate Piers. I: Experimental Results. *Journal of Geotechnical and Geoenvironmental Engineering*, *133*(12), 1503–1511. https://doi.org/10.1061/(ASCE)1090-0241(2007)133:12(1503)

Yuan, B., Xiong, L., Zhai, L., Zhou, Y., Chen, G., Gong, X., & Zhang, W. (2019). Transparent Synthetic Soil and Its Application in Modeling of Soil-Structure

Interaction Using Optical System. *Frontiers in Earth Science*, *7*. https://doi.org/10.3389/feart.2019.00276

Zhang, X., Rajesh, S., Chen, J.-F., & Wang, J.-Q. (2021). Geosynthetic encased column-supported embankment: Behavior with and without basal geogrid. *Geosynthetics International*, 1–56. https://doi.org/10.1680/jgein.21.00038

Zhang, Y., Hu, M., Ye, T., Chen, Y., & Zhou, Y. (2020). An Experimental Study on the Rheological Properties of Laponite RD as a Transparent Soil. Geotechnical Testing Journal, 43(3), 20180348. https://doi.org/10.1520/GTJ20180348

Chapter 3: Evaluation of GEC Behavior from Physical Models involving a Transparent Clay Surrogate

ABSTRACT

Geosynthetic encased columns (GECs) are an innovative ground improvement technique for soft soils. This study investigated the behavior and performance of GECs under undrained loading conditions using laponite as a transparent soft clay surrogate in a physical model. The experimental program involved testing a series of GEC models with varying encasement stiffness, column infill relative density, soil overburden pressure, and column diameter. Encasement tensile rupture was identified as the initial and governing trigger of failure in GECs models with low stiffness and low tensile strength encasement , dictating failure mode and bearing capacity over column infill shear strength. Stiffer encasements enhanced load-settlement response while limiting encasement radial deformations. Denser infill and higher soil overburden pressure increased load capacity and reduced encasement radial strains. Smaller diameter columns achieved higher load capacity due to greater confinement provided by the encasement tensile mobilization. Comparison with analytical methods showed the Elasto-Plastic method agreed better with experimental results, especially for GECs with higher encasement stiffness. Both Rigid-Perfectly Plastic and Elasto-Plastic methods had limitations capturing behavior at lower encasement stiffness and large column axial strains. The findings highlight the importance of optimizing encasement and column properties to maximize GEC performance and provide insights into failure mechanisms and stress-strain response. The experimental results serve as a benchmark for evaluating simplified analytical models at various stages of encasement radial deformation.

3.1.- INTRODUCTION

Geosynthetic encased columns (GECs) are an innovative ground improvement method that has gained increasing popularity in recent years. This technique is commonly implemented as a foundation system for embankments constructed on soft soils, offering a cost-effective and efficient solution to enhance the bearing capacity and reduce the settlement of the underlying weak soil layers. GECs typically consist of a sand or gravel column wrapped with a cylindrical high-tensile strength geotextile encasement. The geosynthetic encasement provides lateral confinement to the granular column infill material, thereby increasing the stiffness and load-bearing capacity of the column while minimizing lateral deformation.

Physical modelling has been used in previous studies as an effective approach to investigate the behavior of GECs and the interactions among their various components. For example, Rajagopal et al. (1999) analyzed triaxial compression tests on river sand columns encased with varying geosynthetics. Malarvizhi and Ilamparuthi (2004) used model clay beds with stone columns to examine load capacity. Ayadat and Hanna (2005) performed loading tests on collapsible soil specimens reinforced with single GEC in a stress-controlled chamber. Murugesan and Rajagopal (2009a, 2009b) conducted laboratory compression tests and shear load tests on GEC in clay. Wu and Hong (2009) carried out triaxial tests on quartz sand specimens encased with geotextiles. Gniel and Bouazza (2009) utilized laboratory compression tests on kaolin clay beds with GEC and ordinary sand columns. Hong et al. (2016) performed 1-g model tests on GEC in soft clay using similarity principles for scaling. Miranda et al. (2017) used instrumented Rowe-Barden oedometer tests on a slice of a unit cell representing an GEC. Alkhorshid et al. (2019) conducted large-scale load tests on GEC installed in very soft clay. Chen et al. (2018)performed uniaxial

compression tests comparing ordinary and encased stone columns. Ghazavi et al. (2013) and Nazari et al. (2014) used large-scale laboratory tests on various stone column configurations in soft clay. Ali et al. (2012, 2014) performed model tests on single columns and groups with different reinforcement schemes. These experimental studies have consistently demonstrated the improvement in bearing capacity and reduction of settlements achieved by using GECs compared to ordinary columns (OCs). However, most of these studies have focused on the overall performance of GECs without providing detailed insights into the internal mechanisms and interactions within the GEC system, such as the development of encasement radial strain and interface shear strains along the column length, and the progression of potential failure modes of the column.

Moreover, none of the aforementioned studies have employed transparent clay as a soil surrogate, which could potentially offer valuable visual insights into the deformation and failure mechanisms of GECs. The use of transparent clay in physical modelling has been limited to relatively small-scale models, typically with volumes less than 5 liters, due to the challenges associated with maintaining transparency and achieving desired geotechnical properties in larger volumes.

To address these research gaps, the present study aims to leverage the advantages of transparent clay in a larger-scale physical model (approximately 17 liters in volume) to investigate the behavior of GECs under undrained loading conditions. By employing advanced image analysis techniques, such as digital image correlation (DIC), this study seeks to provide visual and quantitative insights into the GEC column behavior, the development potential failure mechanisms, and the effect of various design parameters on the performance of GECs. The use of a transparent soil analog in a larger-scale model, combined with state-of-the-art measurement techniques, is expected to bridge the gap

between small-scale laboratory tests and field-scale behavior, contributing to the development of more accurate and reliable design methods for GEC-reinforced foundation soil systems.

The experimental investigation conducted in this study involves testing a series of GEC models prepared using a transparent clay surrogate and tested in a uniaxial displacement-controlled actuator. The variables considered in the parametric evaluation conducted in this study include the Geotextile Encasement Stiffness ($J_{5\%}$), Relative Density (RD) of column infill, Overburden Pressure (σ_{over}) on surrounding soft soil, and Diameter ($\varnothing$) of the column. The focus of this chapter is on the performance behavior of a single GEC and its potential failure mechanisms, as well as on the evaluation of the bearing capacity, stress transfer within the column, and mobilization of confinement stresses in the encasement. To achieve these objectives, a newly designed transparent unit cell chamber is used in the testing program. A description of the experimental setup and the characteristics of the data obtained from the models is presented herein, but the reader is referred to **Chapter 2** for further details.

The outcome of the parametric testing program is to provide detail in the GEC performance by analyzing the load pressure-displacement curves, plots of encasement radial strains of the entire column profile at different loading stages, back calculated encasement tensile stresses, column axial strains, column volumetric strain and soil displacement field vectors to provide a deep picture of the GEC behavior and the failure mechanisms observed.

3.2.- BACKGROUND INFORMATION

Geosynthetic Encased Columns (GECs) are increasingly used to improve soft soils. The encasement provides additional confinement, enhancing load capacity over ordinary stone columns. Extensive research evaluated GEC behavior through analytical, in-situ, numerical, and experimental studies such as in this investigation.

3.2.1.- EXPERIMENTAL STUDIES DEMONSTRATING IMPROVED LOAD CAPACITY OF ENCASED COLUMNS

Experimental research demonstrated that encasing stone columns in geosynthetics provides substantial improvements in load carrying capacity compared to ordinary unreinforced columns in soft soils.

Rajagopal et al. (1999) performed triaxial compression testing evaluating the effects of different woven, non-woven, and geogrid encasements on the strength parameters of sand columns. Results showed negligible increase in friction angle but considerable enhancement of apparent cohesion, increasing with more encasement stiffness. Malarvizhi and Ilamparuthi (2004) found GEC doubled load capacity over OC in clay beds. Ayadat and Hanna (2005) showed higher geotextile encasement stiffness and longer encased sand columns increased composite load capacity in collapsible soils. Murugesan and Rajagopal (2009a) found GEC sustained 3-5 times higher stresses than OC at similar settlements.

Large-scale laboratory studies by Ghazavi et al. (2013) and Nazari et al. (2014) revealed increased ultimate bearing capacity from OC to partial or total encased GEC. Capacity further improved with stronger encasement materials and greater vertical length. Similar trends were observed in column groups. Alkhorshid et al. (2019) showed full-scale

field testing of GEC using various geotextiles and gravel achieved up to 7121% higher load capacity over OC. Overall, these experimental investigations clearly demonstrate the significant benefits of encasement in boosting the load carrying capacity of stone columns in soft soils, owing to the enhanced lateral confinement provided by the geosynthetic reinforcement.

3.2.2.- ENHANCED COLUMN STRUCTURAL INTEGRITY AND REDUCED DEFORMATIONS

In addition to increased load capacity, testing also showed encasement enhances overall column structural integrity by restricting deformations. Gniel and Bouazza (2009) found encased columns exhibited 30-80% lower axial strains and more uniform encasement radial expansion compared to excessive bulging in OC. Murugesan and Rajagopal (2009a) showed GEC withstood 3-5 times higher pressures at similar settlements as OC. Encasement reduced localized bulging failures. Miranda et al. (2015, 2016) demonstrated GEC had 11-25 times higher stress concentration factors than OC, indicating greater load carried by the column and lower stresses in surrounding soil. Settlement reduction factors improved from 0.8 to 0.6 with encasement. Hong et al. (2016) observed stiffer geotextile encasements produced more uniform column deformations rather than localized bulging. Wu and Hong (2009) found looser sands showed the largest encasement radial strain reductions from encasement. These findings highlight the role of encasement in restricting column deformations while transferring greater loads, enhancing overall stability and resilience.

3.2.3.- EFFECTS OF COLUMN FILL DENSITY

Research showed column fill density is another key factor influencing GEC performance, with higher density gravel improving behavior. Wu and Hong (2009) found encasement provided greater enhancement for looser sand specimens, especially at lower confining pressures. However, Miranda et al. (2017) showed columns with 80-100% relative density supported 1.7 times higher stresses and exhibited up to 50% lower encasement radial strains than 30-50% relative density columns. Settlement reduction also improved from 0.8 to 0.6 with higher density fill. These results demonstrate the increased lateral confinement from denser gravel fill enables greater load carrying capacity while restricting bulging deformations in GEC.

3.2.4.-EFFECTS OF ENCASEMENT STIFFNESS AND LENGTH

Studies evaluated the effects of varying geosynthetic stiffness and encasement length on column response. Rajagopal et al. (1999) found higher apparent cohesion with stiffer and more encasement cells within a cluster. Malarvizhi and Ilamparuthi (2004) showed stiffer encasements provided greater capacity increases. Gniel and Bouazza (2009) observed larger reductions in axial strain for full-length versus partial encasement GEC. Ghazavi et al. (2013) and Nazari et al. (2014) found stronger geosynthetics and greater encasement length enhanced load capacity of encased columns. Alkhorshid et al. (2019) showed the strongest geotextile tested provided the maximum 7121% capacity increase over ordinary columns. These findings demonstrate stiffer and longer encasements provide higher confinement and load transfer, improving overall encased column performance.

3.2.5.- TYPES OF SOILS USE AS CLAY SURROGATE

To date researchers used extremely soft natural clays, bentonite clays or synthetic kaolin to examine the performance of GEC and OC. Using very soft clays with undrained shear strengths of 2.5-15 kPa allows assessment of geotextile effectiveness in improving behavior under low confining stresses.

Murugesan and Rajagopal (2009a) used a natural lacustrine clay with liquid limit 49%, plastic limit 17%, undrained shear strength S_u of 2.5 kPa, and moisture content 47±1%. Ghazavi et al. (2013) and Nazari et al. (2014) used a clay with liquid limit 33%, plastic limit 20%, S_u 15 kPa at 28% moisture content. Miranda et al. (2017) utilized kaolin clay with S_u 12 kPa when consolidated under 50 kPa. Hong et al. (2016) tested columns in clay with liquid limit 38%, plastic limit 21%, 40% moisture content, and S_u 1.25-1.36 kPa. Alkhorshid et al. (2019) prepared a bentonite-mixed soil with liquid limit 60%, plasticity index 21%, S_u below 5 kPa, and hydraulic conductivity $4.2 \cdot 10^{-5}$ cm/s to simulate a soft deposit.

Laponite, a synthetic clay, has recently emerged as a material that mimics undrained clay behavior while allowing visual observation of deformations. Its transparency is optimal for optical measurements, and its geotechnical properties are those of soft clays (Pierozan et al., 2022b; Almikati et al., 2023b). Although laponite's low coefficient of consolidation ($c_v = 0.007$ m^2/yr at 48 kPa for an 11% laponite and 0.41% SPP mixture) may limit its use in drained studies, it can be considered an incompressible material for short-term loading. A 10% laponite and 0.78% SPP mix provides a balance between undrained shear strength (1-1.4 kPa for depths of 50-500 mm), optical transmittance (for a 300 mm layer).

Overall, clays with undrained shear strengths of 1-15 kPa facilitate detailed experimental examination of geotextile effectiveness in improving column performance. Natural soft clays provide realistic field conditions but limit visual observations. Laponite clay overcomes this but requires attention in the dosage design. This effort is made to understanding GEC behavior mechanisms by adding a direct observation feature in the investigation.

In summary, extensive research showed that geosynthetic encasement provides significant improvements in load capacity, reduced deformation, higher stiffness, and enhanced overall performance of OC in soft soils through the additional confinement provided by the encasement. While prior studies have evaluated encased columns under various conditions, they have been limited in their ability to provide detailed observations and quantitative measurements of the deformations along the column and in the surrounding soil during loading. Most of these studies relied on conventional soil materials, such as natural clay, which do not allow for direct visual observation of the internal mechanisms and interactions within the GEC system. In contrast, the use of laponite, a transparent synthetic clay that emulates the behavior of soft clays, enables continuous and non-intrusive measurement of displacements along the entire column and in the surrounding soil under undrained loading conditions. This unique capability of laponite allows for a more comprehensive understanding of the complex soil-structure interactions, column deformation, and failure mechanisms associated with GECs.

3.3.- SETUP AND MATERIALS

The experimental setup used in this study focuses on capturing key stages of the GEC behavior under specific loading conditions, rather than attempting to fully replicate the entire consolidation process that occurs in natural soft clay. The approach involves evaluating targeted stages of load or strain to reveal GEC performance under well-defined conditions. The study concentrates on specific aspects and parameters that are relevant to understanding the fundamental behavior of GECs, rather than conducting a comprehensive review of all factors involved. The setup employed in this study distinguishes itself from previous experimental research by simultaneously satisfying three conditions:

1. The physical boundary condition is defined by a cylindrical chamber that represents the tributary volume around the column, known as the unit cell.

2. The surrounding transparent soft soil, which is modeled using laponite, is subjected to a constant overburden load that simulates the in-situ stress conditions.

3. The GEC is loaded independently using a displacement-controlled plate, allowing for the evaluation of the column response under various loading scenarios.

By combining these three conditions, the experimental setup enables the investigation of GEC behavior under well-controlled boundary conditions and loading mechanisms. This approach allows for a more focused study of the key factors influencing GEC performance, such as the geosynthetic encasement stiffness, column diameter, and overburden pressure, while maintaining a simplified and manageable experimental testing program.

3.4.- MATERIALS

The laponite mixture utilized contains 10% laponite and 0.78% SPP by gravimetric concentration, the undrained shear strength reads 1.5 kPa at a depth of 50 mm at 14 days of aging at 21°C, while maintaining excellent transparent properties suitable for testing.

The column infill is Monterey sand No. 30, it is a clean uniformly graded sand. Three relative densities RD of 65%, 85% and 95% were employed with a e_{max} of 0.78, e_{min} of 0.56, the dry unit weight γ_d measured as 15.91 kN/m^3, and a specific gravity G_s of 2.6 g/cm^3.

Four different polyester geosynthetic encasements were carefully chosen for this study:

1. GTX08: A non-woven geotextile with a secant stiffness at 5% strain (J5%) of 08 kN/m. This material represents a low stiffness and low strength encasement.

2. GTX11: A non-woven geotextile with a J5% value of 11 kN/m, representing a low stiffness and low strength encasement.

3. GTX34: A woven geotextile with a J5% value of 34 kN/m, representing a medium stiffness and medium strength encasement.

4. GTX70: A woven geotextile with a J5% value of 70 kN/m, representing a high stiffness and high strength encasement.

The geosynthetic encasement is assembled with a 10 mm longitudinal overlap, which is glued using a flexible adhesive specifically designed for polyester fabric. Tensile strength tests were conducted on both seamed and unseamed samples of all four

geosynthetic materials to evaluate the performance of the joints. The results indicated that the seamed and unseamed geotextiles exhibit similar tensile strength and stiffness properties, confirming the suitability of the joint construction procedure for the test.

Table 3.1 provides a summary of the geosynthetic encasement properties, including the material type, secant stiffness ($J_{5\%}$), and ultimate tensile strength.

Table 3.1.- Mechanical properties of geosynthetics encasements

Parameter	GTX08	GTX11	GTX34	GTX70
Ultimate Tensile strength [kN/m]	0.81	1.01	3.25	8.12
Secant Tensile stiffness 5% [kN/m]	08	11	34	70
Rupture strain [%]	15.8	8.4	13.2	15.1

3.4.1.- EXPERIMENTAL SETUP AND SAMPLE PREPARATION

The transparent unit cell chamber in **Figure 3.1** physically it consists of three elements: first is the main body cylinder acrylic 8 inches (203.2 mm) diameter and 2 ft (609.6 mm) height that holds the core volume of laponite and the installed GEC model, second is the ring overburden plate made of acrylic consisting of a rigid ring shaped plate covering the foot-print of the laponite, the ring plate apply a constant overburden pressure to the tributary area of the column with a dead weight on top and it is free to move vertically; third is the core column plate, a closed-cylinder shaped plate fitting perfectly inside the inner circle of the ring plate and coupled to the actuator. The core plate moves in downward direction when the constant displacement-controlled load is applied.

a) ***b)***

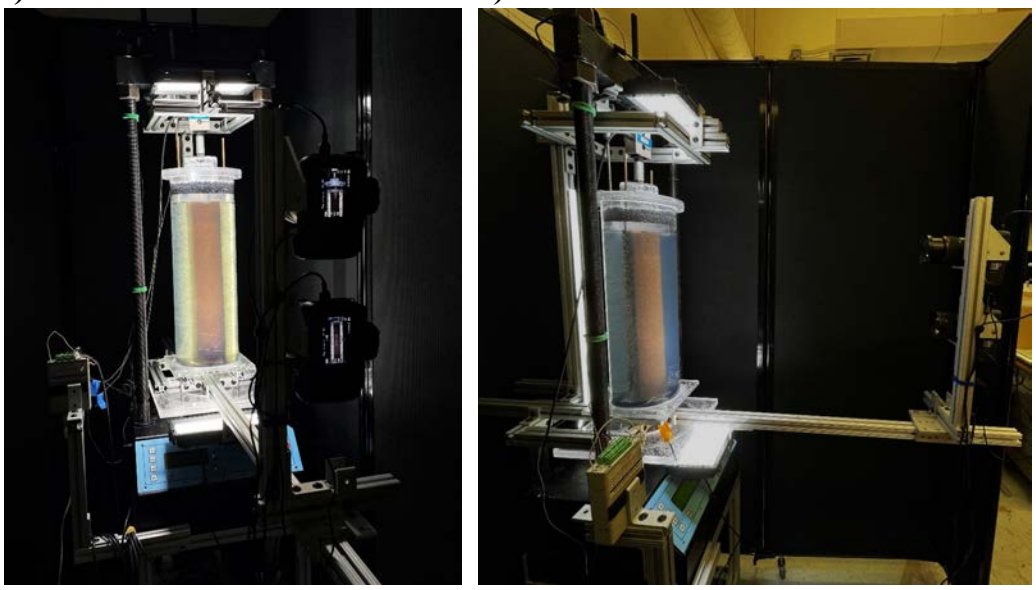

Figure 3.1.- Testing Setup and instrumentation, a) OC model mounted in GEC setup, b) Side view of OC model

The testing setup features a modified HM-3000 Humboldt actuator holding a transparent unit cell chamber and an image acquisition system with two high-resolution cameras. The actuator was calibrated for a constant 1 mm/min displacement rate, the load applied to the top column is recorded trough a load cell and a pressure sensor at the column's base measures the pressure at the bottom of the column.

3.5.- SCOPE OF THE TESTING PROGRAM

To achieve the main objective of this study, which is to evaluate the performance and behavior of GECs under different stages of loading, a set of key variables were carefully selected. These variables were chosen to enable a comprehensive analysis of the factors influencing GEC performance and to provide insights into the underlying mechanisms governing their behavior. The selected variables are as follows:

1. The encasement secant stiffness material: Three different materials were adopted; GTX08 (J5% = 08 kN/m), GTX11 (J5% = 11 kN/m), GTX34 (J5% = 34 kN/m) and GTX70(J5% = 70 kN/m).

2. The relative density of column infill: Monterey Sand No.30 at three different relative densities was used (RD: 65%, 85% and 95%).

3. The overburden pressure on the surrounding soft soil: Three constant pressures were applied (σ: 2.5 kPa, 5 kPa and 15 kPa).

4. The diameter of the GEC: Three different diameters were selected (60 mm, 80 mm and 100 mm).

In support of the 1-g model testing, a complementary testing program was undertaken to evaluate the strength mobilization of the encasement resulting in the confinement provided to the column, and of the column soil that could influence the performance of the GEC model. The tests performed in this study were grouped into 5 test series (A, B, C, D, and E), each aimed at investigating the effect of one variable as shown in **Table 3.2**. Series A, consisting of OC at different overburden pressures performed to set a reference against the rest of GEC models, Series B performed to investigate the effect of

the encasement secant stiffness, series C performed to investigate the effect of the relative density of the soil column, series D performed to investigate influence the diameter of the column and series E performed to investigate the effect of the overburden pressure in the surrounding soft soil.

Table 3.2.- Experimental GEC Evaluation Testing matrix

#	Test	Encasement J kN/m	Diameter mm	Overburden kPa	RD %	L/D -	Ae %
1	**∅0.08-J34-RD85-σ5 Baseline****	**34**	**80**	**5**	**85**	**12.5**	**17.64**
2	A-OC-**σ2.5**	NA	80	***2.5***	85	12.5	17.64
3	A-OC-**σ5**	NA	80	***5***	85	12.5	17.64
4	A-OC-**σ10**	NA	80	***10***	85	12.5	17.64
5	B-GEC-**J08**	***08***	80	5	85	12.5	17.64
6	B-GEC-**J11**	***11***	80	5	85	12.5	17.64
7	B-GEC-**J34** **	***34***	80	5	85	12.5	17.64
8	B-GEC-**J70**	***70***	80	5	85	12.5	17.64
9	C-GEC-**RD65**	34	80	5	***65***	12.5	17.64
10	C-GEC-**RD85****	34	80	5	***85***	12.5	17.64
11	C-GEC-**RD95**	34	80	5	***95***	12.5	17.64
12	D-GEC-**∅60**	34	***60***	5	85	16.7	9.92
13	D-GEC-**∅80****	34	***80***	5	85	16.7	17.64
14	D-GEC-**∅100**	34	***100***	5	85	10	27.56
15	E-GEC- **σ2.5**	34	80	***2.5***	85	12.5	17.64
16	E-GEC- **σ5****	34	80	***5***	85	12.5	17.64
17	E-GEC- **σ10**	34	80	***10***	85	12.5	17.64

All models were built following the same procedure, as described in **SECTION 2.5**, each column model in this study was named using a letter that identifies the test series (A to E), followed by the type of column (OC or GEC) and the symbol of the varied parameter from the baseline model with its respective value used in the model (e.g. for $J_{5\%}$ 34 kN/m is J34).

Model B-GEC-J34 was designed as the baseline test for this parametric study to represent the most common values seen in published case histories of ground improvement using GEC. According to Alexiew and Raithel (2015), a typical GEC has a diameter of 0.80 m, a length between 5-15 m, a replacement ratio of 15%, is installed in a soft soil with an S_u < 20 kPa, the column soil has typically a friction angle about 35°, is designed for a service vertical load around 150 kPa, and has an encasement secant stiffness between 2500-3500 kN/m. With this baseline established, the scaling laws governing 1-g conditions, presented in **Table 3.3**, were derived and applied to the baseline model with a scale of λ=10. While the other parametric models in this study do not strictly adhere to specific prototype values, their primary objective is to investigate the effects of varying individual parameters relative to the defined baseline case. By systematically altering key variables such as the geosynthetic encasement stiffness, column infill relative density, overburden pressure, and column diameter, the parametric study aims to provide insights into the sensitivity of GEC performance to these factors.

Table 3.3.- 1g GEC Scaling factors, with λ=10

Parameter	Unit	Scaling factor	Typical Prototype Value	Model Value
$J_{5\%}$	$\left[\frac{kN}{m}\right]$	λ^2	2000 – 5000	20 – 50
S_u	$[kPa]$	λ	<25	0.5 – 2
∅	$[m]$	λ	0.6 – 1.2	0.06 – 0.12
σ_{over}	$[kPa]$	λ	80 – 150	8 – 15

3.6.- EVALUATION OF THE GEC PERFORMANCE

3.6.1.- GEC MODEL FAILURE MODE OBSERVED

The failure mechanism of geosynthetic encased columns (GECs) under axial compression loading depends on several factors, including properties of the column infill, encasement stiffness and tensile strength, surrounding soil conditions, and loading conditions. This section discusses the GEC tensile breakage as primary failure mode observed during the testing program, with a focus on the separate mobilization of the composite materials: column infill, and geotextile encasement until reaching failure.

Three models are presented in detail to illustrate different column behaviors reaching failure: i) the unreinforced model OC serving as reference, ii) the low stiffness and low strength B-GEC-J08 model presenting an encasement ductile failure, and iii) the relative high stiffness and low strength encasement B-GEC-J11 model showing a sudden tensile breakage failure of the encasement.

a) *b)*

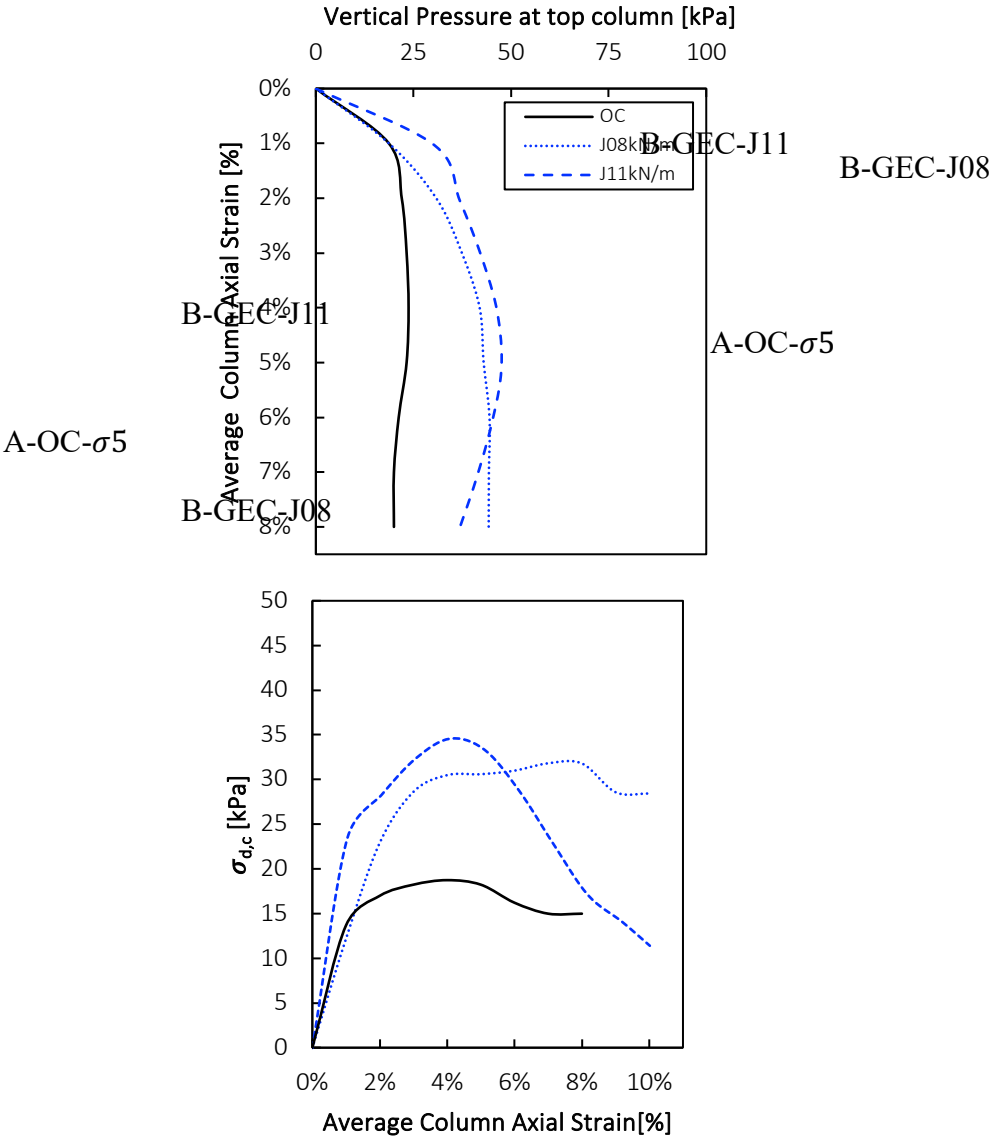

Figure 3.2.- Bearing behavior of failed models: A-OC-σ5, B-GEC-J08 and B-GEC-J11, a) Load-Settlement response, b) Column infill deviatoric Stress-Average column axial strain

a) *b)* *c)*

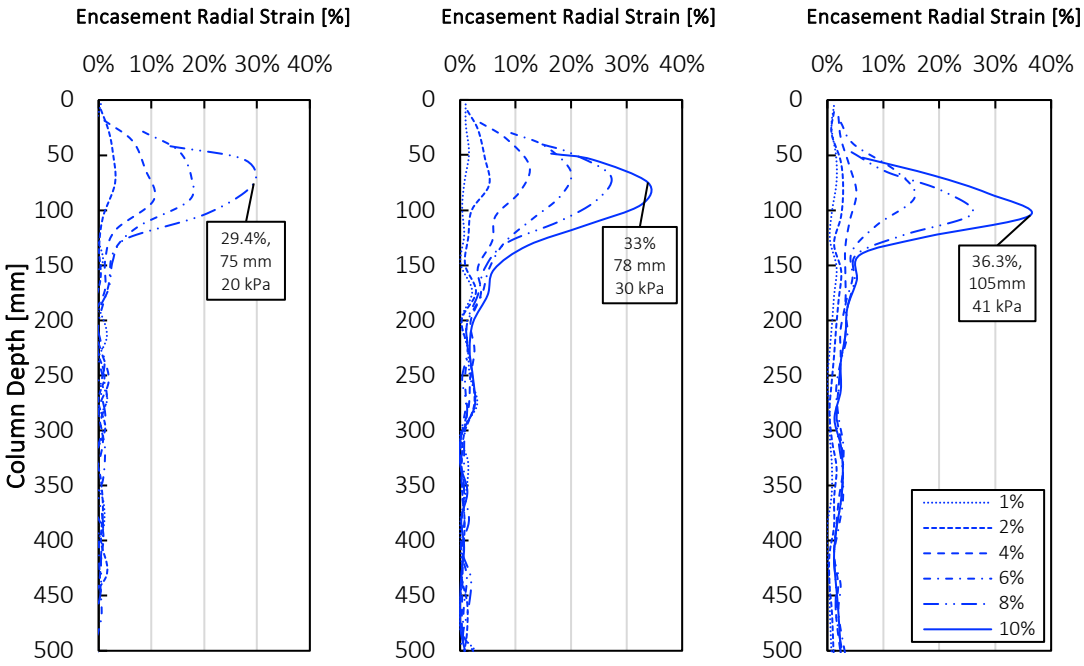

Figure 3.3.- Profiles of geosynthetic encasement radial strain of failed models, a) A-OC-σ5, b) B-GEC-J08, and c) B-GEC-J11

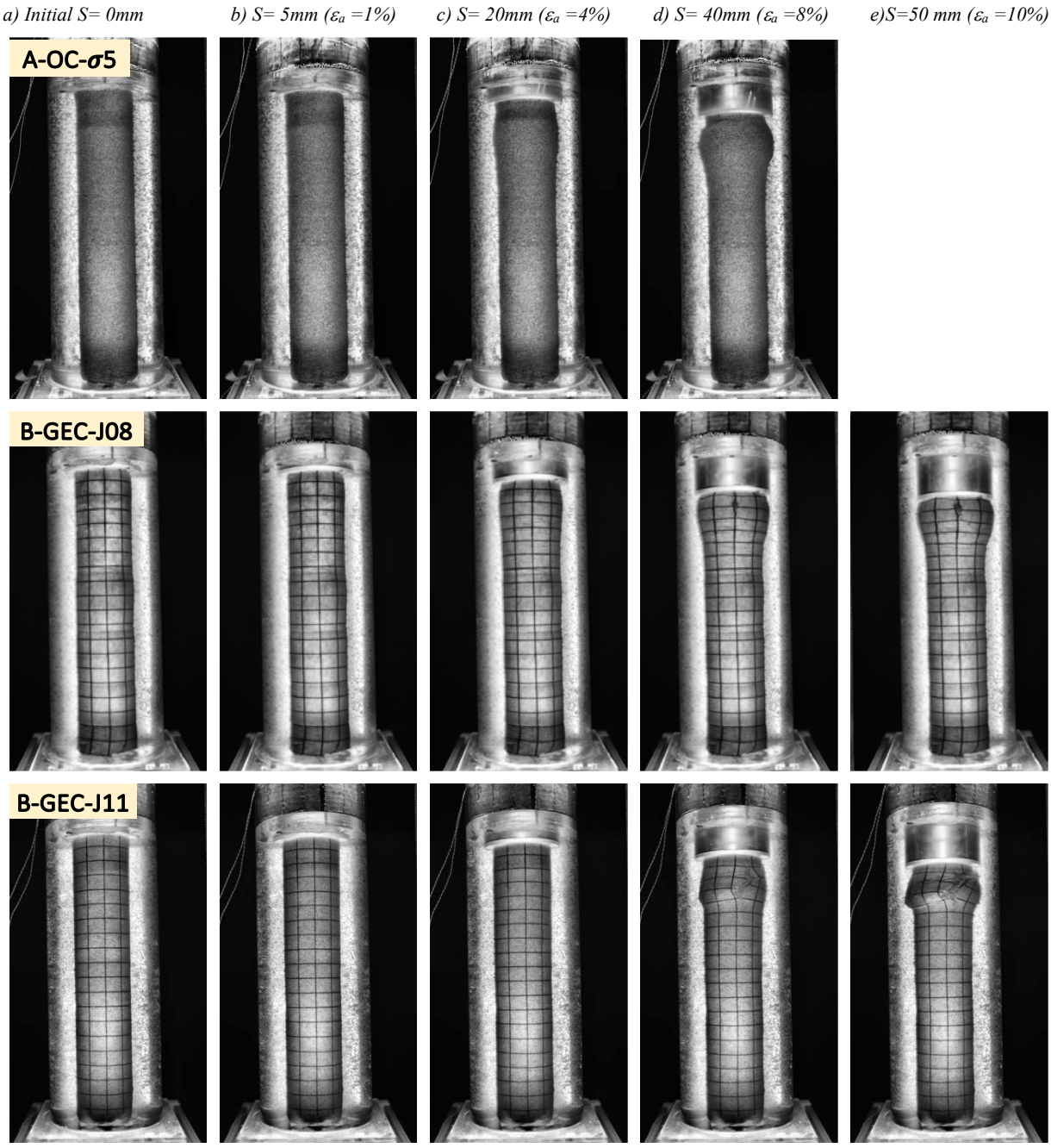

Figure 3.4.- Image sequence of models failed: A-OC-σ05, B-GEC-J08, and B-GEC-J11 test at 0%, 1%, 4%, 8% and 10% average column axial strains

Unreinforced Column, model A-OC-σ5

The unreinforced column (A-OC-σ5) model exhibited early bulging shear failure since lacking encasement, as evidenced by the image sequence in Error! Reference source not found. and column infill radial strain profiles in **Figure 3.3a** obtained from image analysis and using the following equation **Eq. 3-1** that applies also to GEC models:

$$\varepsilon_r = \frac{\Delta d}{d_0} = \frac{\Delta r}{r_0} \qquad \textit{Eq. 3-1}$$

Where, ε_r is the radial strain of the column infill or encasement, Δ_d is the change of diameter of the column infill or encasement from the initial diameter d_0, and Δ_r is the change of column infill or encasement radius from the initial radius r_0.

Under 5 kPa of overburden pressure, the OC column did not show signs of failure until 2% axial strain when shear bulging failure initiated at 1 diameter from the top of the column, the peak of bearing capacity recorded was 21 kPa shown in **Figure 3.2a**. The column bulging reached a maximal deformation of 30% radial strain located at 1 diameter depth when the column was axially compressed 8%. Therefore, the low overburden did not provide enough confinement, resulting in shear bulging failure.

This A-OC-σ5 model is an important reference for comparison to the GEC models. Additionally, the A-OC-σ5 model early failure reinforces the relevance of the geosynthetic encasement role in stabilizing the column and preventing failure at large settlements, even with low surrounding soil confinements.

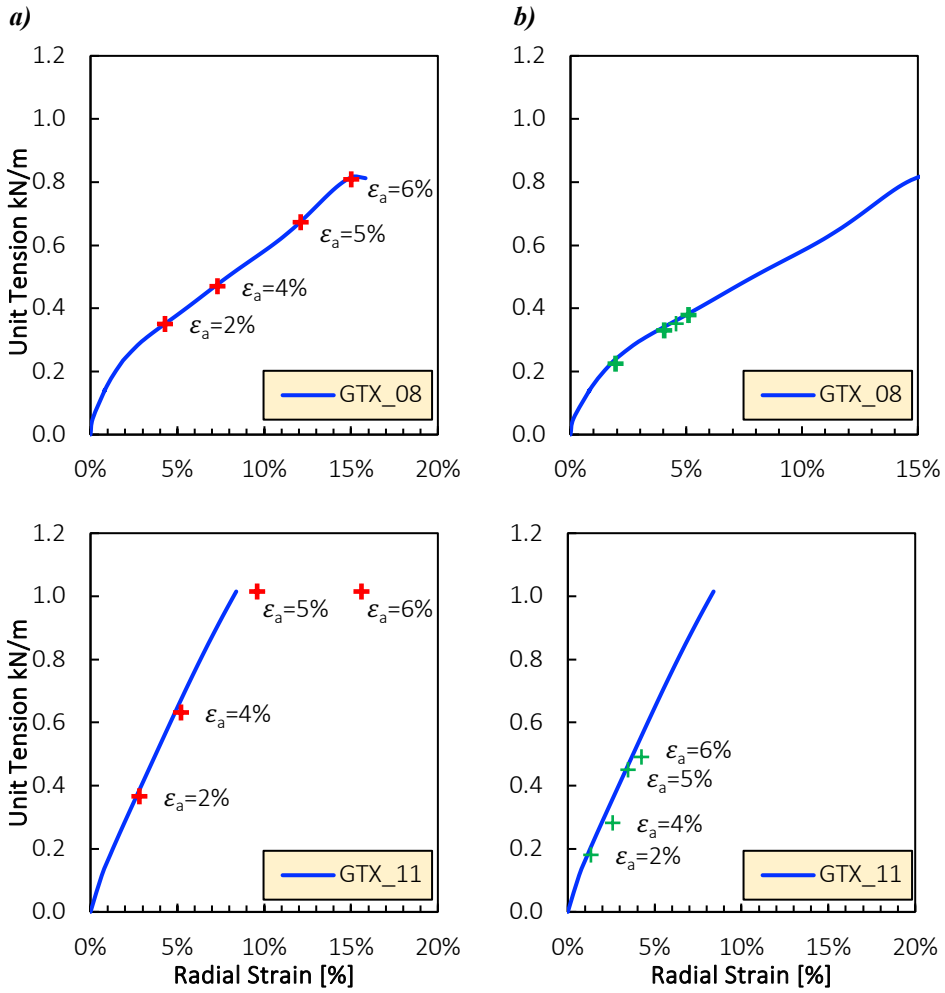

Figure 3.5.- Encasement tensile mobilization of models failed: B-GEC-J08 & B-GEC-J11, a) Maximal encasement radial strain, and b) Average encasement radial strain

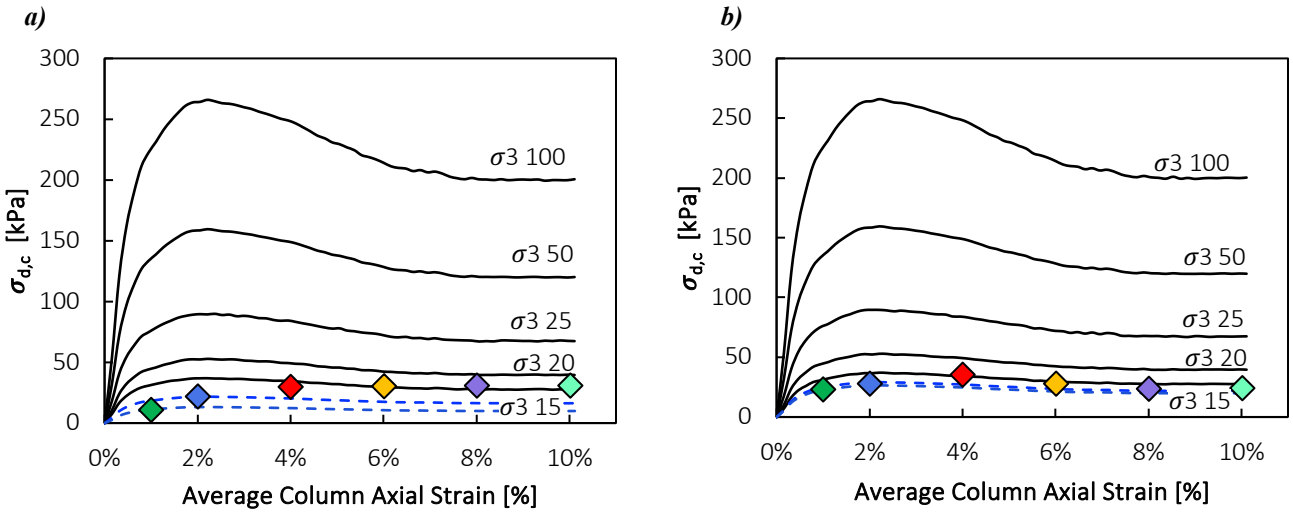

Figure 3.6.- Column infill mobilization of failed models: a) B-GEC-J08 & b) B-GEC-J11

GEC Ductile Failure, model B-GEC-J08

The model B-GEC-J08 failed gradually in a ductile manner, allowing large deformations of the encasement before its tensile breakage. This behavior is evident in the load -settlement response shown **Figure 3.2** and the encasement radial strain profile at different average column axial strains in **Figure 3.3b.** Under 5 kPa overburden pressure, this low stiffness and strength encasement started deforming radially early at 2% average column axial strain. Encasement radial deformation increased up to 6% average column axial strain when encasement tensile breakage became noticeable at 1 column diameter. The peak bearing capacity of 44 kPa was reached at 6% axial strain observed in **Figure 3.2** with minimal drop in vertical pressure afterwards. Loading continued, and at 8% average column axial strain, encasement tensile rupture fully developed, with visible localized bulging. At the maximum 10% average column axial strain, the residual vertical pressure remained almost constant at 43 kPa.

The image sequence in **Figure 3.4**, particularly from model B-GEC-J08, showed a small vertical tearing in the encasement that limited further increase in bearing capacity. From B-GEC-J08 model, a noticeable bulging shape was observed at 1 diameter depth even before encasement rupture. However, the bulging did not define GEC failure. The final failure contour was similar to the A-OC-σ5 model, with bulging at the top and an intact column below. **Figure 3.3** shows the column profile of the encasement radial strains at 1%, 2%, 4%, 6%, 8% and 10% average axial column strains, allowing to obtain the maximal encasement radial strain value and the average profile encasement radial strain for each average axial column strain stage.

To understand the encasement and column infill behavior at failure, further analysis was conducted. Encasement radial strains from model B-GEC-J08 were mapped to a wide tensile plot (ASTM-D4595), and the encasement tensile strain for tests in the cross-machine direction was assumed equivalent to the encasement radial deformation behavior in the model. **Figure 3.5** illustrates how the maximal encasement tensile strains rapidly increase along the tensile-strain curve with increasing average column axial strain. The failure at 6% average column axial strain is explained by the encasement reaching a maximal tensile strain of 15.5%, surpassing the allowed deformation and its tensile capacity, leading to ductile failure.

To analyze column infill strength, triaxial tests were performed on 85% relative density (RD) Monterey sand under 15 kPa, 20 kPa, 25 kPa, 50 kPa and 100 kPa confinements. The GEC model stress state, considering the column infill vertical stress $\sigma_{v,c}$ and column infill confinement $\sigma_{h,c}$, was compared to the triaxial test envelopes. The vertical stress in the column infill ($\sigma_{v,c}$) was computed directly from the average load measured at the top and bottom of the column using Error! Reference source not found.:

$$\sigma_{v,c} = \frac{\sigma_{v,c\ top} + \sigma_{v,c\ bottom}}{2} \qquad \textit{Eq. 3-2}$$

where $\sigma_{v,c\ top}$ and $\sigma_{v,c\ bottom}$ are the stress measured at the top and bottom of the column, respectively.

The column infill confinement ($\sigma_{h,c}$) comprised the soil confinement ($\sigma_{h,s}$), known and constant in the model setup, and the encasement confinement ($\sigma_{h,g}$), as shown in Error! Reference source not found.:

$$\sigma_{h,c} = \sigma_{h,g} + \sigma_{h,s} \qquad \textit{Eq. 3-3}$$

The encasement confinement ($\sigma_{h,g}$) was obtained using Error! Reference source not found., which incorporates the average encasement radial strain ($\varepsilon_{r,g\ avg}$) and its secant stiffness at 5% strain ($J_{5\%}$):

$$\sigma_{h,g} = J_{5\%} \cdot \frac{\varepsilon_{r,g\ avg}}{r_g} \qquad \textit{Eq. 3-4}$$

where r_g is the geosynthetic encasement radius.

Figure 3.6 interpolates from B-GEC-J08 and B-GEC-J11 models, the column infill deviatoric stress ($\sigma_{d,c}$) from 1-10% average axial column strain between different triaxial envelopes of the tested triaxial confinement stresses. The column infill deviatoric stress ($\sigma_{d,c}$) was calculated using Error! Reference source not found.:

$$\sigma_{d,c} = \sigma_{v,c} - \sigma_{h,c} \qquad \textit{Eq. 3-5}$$

The analysis showed a maximum column infill confinement ($\sigma_{h,c}$) of 16 kPa at 6% average column axial strain (failure point). Thus, at 3% average column axial strain, the column infill failed, but overall B-GEC-J08 model failure occurred at encasement rupture.

Despite rupture, the column infill confinement ($\sigma_{h,c}$) remained constant up to 10% average column axial strain.

GEC Brittle Failure, model B-GEC-J11

The B-GEC-J11 model exhibited sudden encasement tensile rupture with substantial loss of bearing pressure after reaching peak strength, followed by a pronounced diagonal column infill shear plane failure, as evident in the vertical pressure-axial strain plot (**Figure 3.2**) and encasement radial strain profile (**Figure 3.3c**). Under 5 kPa overburden pressure, this relatively high stiffness, low strength encasement exhibited uniform encasement radial strain until 5% average column axial strain. At this point, abrupt encasement tensile breakage occurred, localized at a depth of 1.5 diameters. A peak encasement radial strain of 10% was measured at the rupture location. It is inferred that the higher encasement stiffness developed confinement stresses deeper in the column, resulting in the localized tensile failure at that depth once the limit was reached. The encasement from B-GEC-J11 presented encasement tensile rupture at a deeper length compared to B-GEC-J08 model. Loading continued and at 8% strain, encasement rupture fully formed across a visible 45° column infill shear plane. In terms of load bearing, the maximal vertical pressure of 47 kPa occurred at 5% average column axial strain (**Figure 3.2**) but then decreased significantly to 35 kPa at 10% average column axial strain. Images from B-GEC-J11 model in **Figure 3.7**, reveal diagonal tearing of the encasement and shear plane formation near the top, while the deeper portion of the column stayed intact.

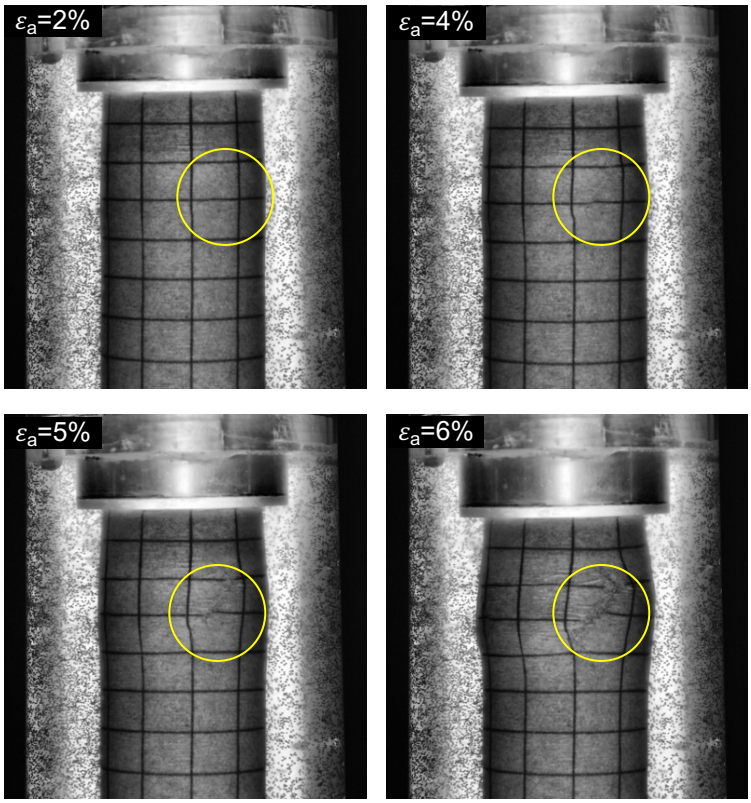

Figure 3.7.- Observed progress at 2%, 4%, 5% and 6% average column axial strain of encasement tensile breakage in model B-GEC-11

Analysis of encasement and column infill strength mobilization was also performed as explained for the GEC ductile failure model. **Figure 3.5** shows that due to the short encasement elastic range and limited plastic deformation capacity of this encasement previously characterized with the wide tensile test, encasement tensile strains reached the failure limit of 10% rapidly by 5% of average column axial strain. However, from **Figure 3.6**, the column infill already failed around 2-3% average column axial strain, while peak strength for the overall B-GEC-J11 model reached at 5% average column axial strain. Additionally, the mobilized encasement confinement in **Figure 3.6** confirms a substantial loss beyond encasement rupture. Thus, in this model the confinement provided by the encasement governed the integrity of the GEC until its encasement tensile rupture.

In essence, the abrupt encasement tensile breakage failure caused column infill shear plane failure as a second mode of failure, despite slightly exceeding the performance of the more ductile B-GEC-J08 model initially. The relatively high stiffness and low tensile strength encasement led to instability for the reinforced column, which is not suitable for achieving the desired performance in prototype conditions.

Findings from this experimental testing program revealed encasement tensile rupture as the initial and governing trigger of failure in GECs, even though shear bulging is often considered the most observed failure mode in field applications (Najjar, 2013). The GEC models enabled detailed visualization and quantification, showing that encasement tensile breakage precipitates shear failure of the column infill material. Until tensile encasement rupture occurs, typically at a depth of 1-2 column diameters, the system performance continues improving. However, insufficient confinement provided by the low stiffness and strength encasement leads to tensile failure, subsequently causing localized column infill shear failure and bulging at the weaker portion of the column. Measurements of encasement tensile strains are relevant to quantify the mobilized encasement confinement and directly evaluate this progression. Although not optimal, the GEC models tested still doubled the bearing capacity compared to the unreinforced column, despite ultimate instability.

The prototype's transparency enabled robust visualization and analysis of the sequence of failure mechanisms and the relative contributions of the encasement and column infill at each stage of the dominant GEC failure mode observed. Initial encasement tensile rupture, precipitated by insufficient encasement tensile strength and ductility, was found to trigger subsequent shear failure in the soil column. This failure characterization highlights the need for encasements with greater tensile capacity and deformation

compatibility to prevent premature rupture and delay the triggering of shear failure in the column infill material. Enhancement of tensile properties is thus important to further reinforce the composite system and improve its overall performance.

3.6.2.- GEC MODEL PERFORMANCE OBSERVED

The performance of GEC models was analyzed to identify optimal design conditions that maximize the stabilization provided by the encasement confinement while minimizing the risks associated with insufficient or excessive reinforcement. The primary objective was to quantify the level of confinement that could be effectively provided before detrimental effects on the system performance occur. Two representative GEC models from the testing program were selected to illustrate different performance outcomes: the B-GEC-J34 baseline model, featuring a medium stiffness encasement, and the B-GEC-J70 model case, characterized by a high stiffness encasement. Comparing these two models helps elucidate the key factors that contribute to substantial performance improvements and those that may lead to instability in the GEC system.

Analyzing the behavior of GECs at different reinforcement levels enables the characterization of the compromises between leveraging the encasement for enhanced tensile strength and stiffness and potentially compromising the column's performance through excessive rigidity or loading. The detailed examination of these two models highlights the importance of tailoring the confinement provided by the encasement to facilitate performance gains while avoiding over-design.

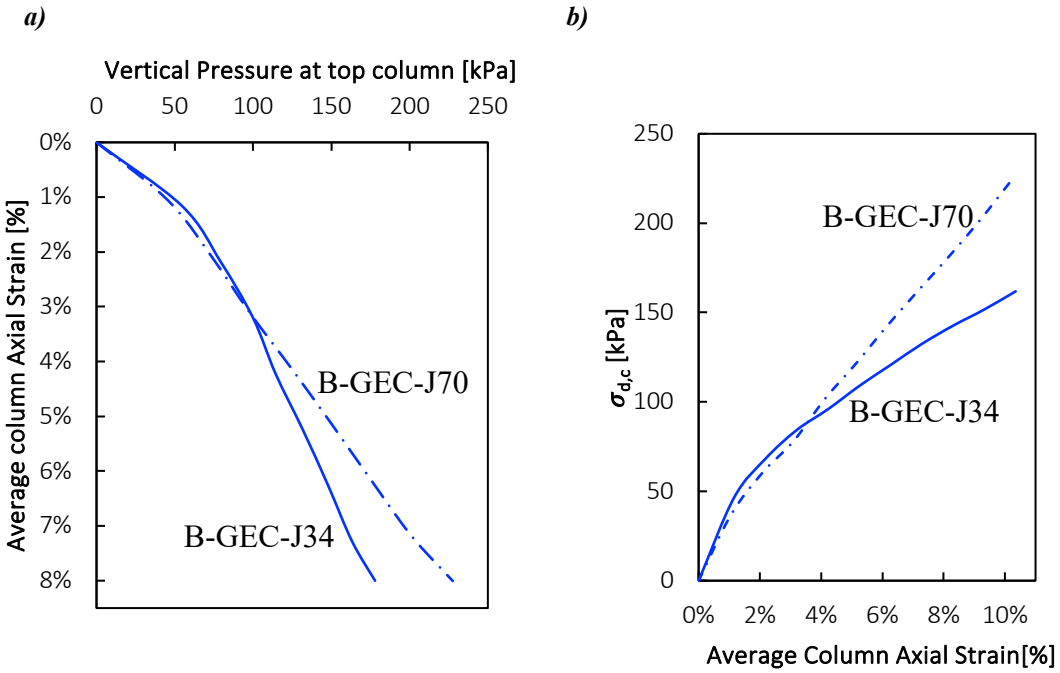

Figure 3.8.- Bearing behavior of models: B-GEC-J34 and B-GEC-J70, a) Load-Settlement response, b) Column infill deviatoric Stress-Average column axial strain

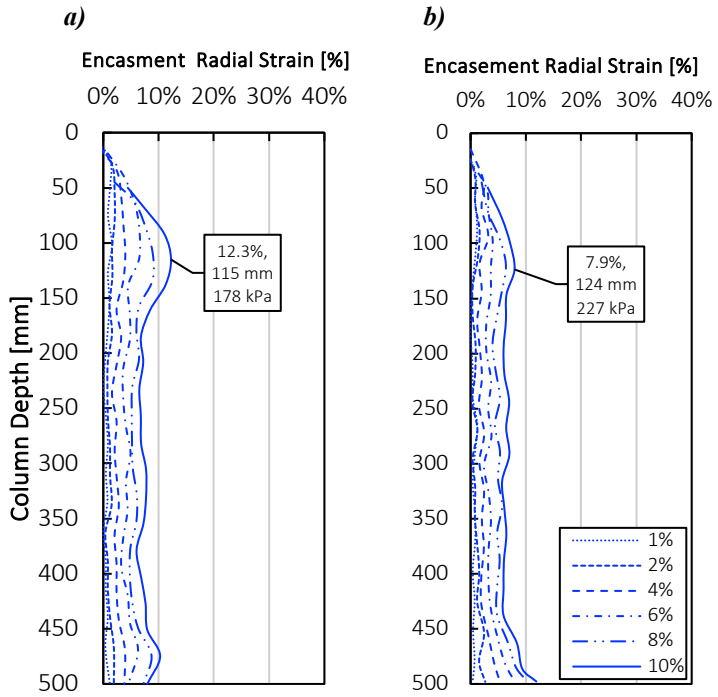

Figure 3.9.- Profiles of geosynthetic encasement radial strain of models: a) B-GEC-J34, and c)B-GEC-J70

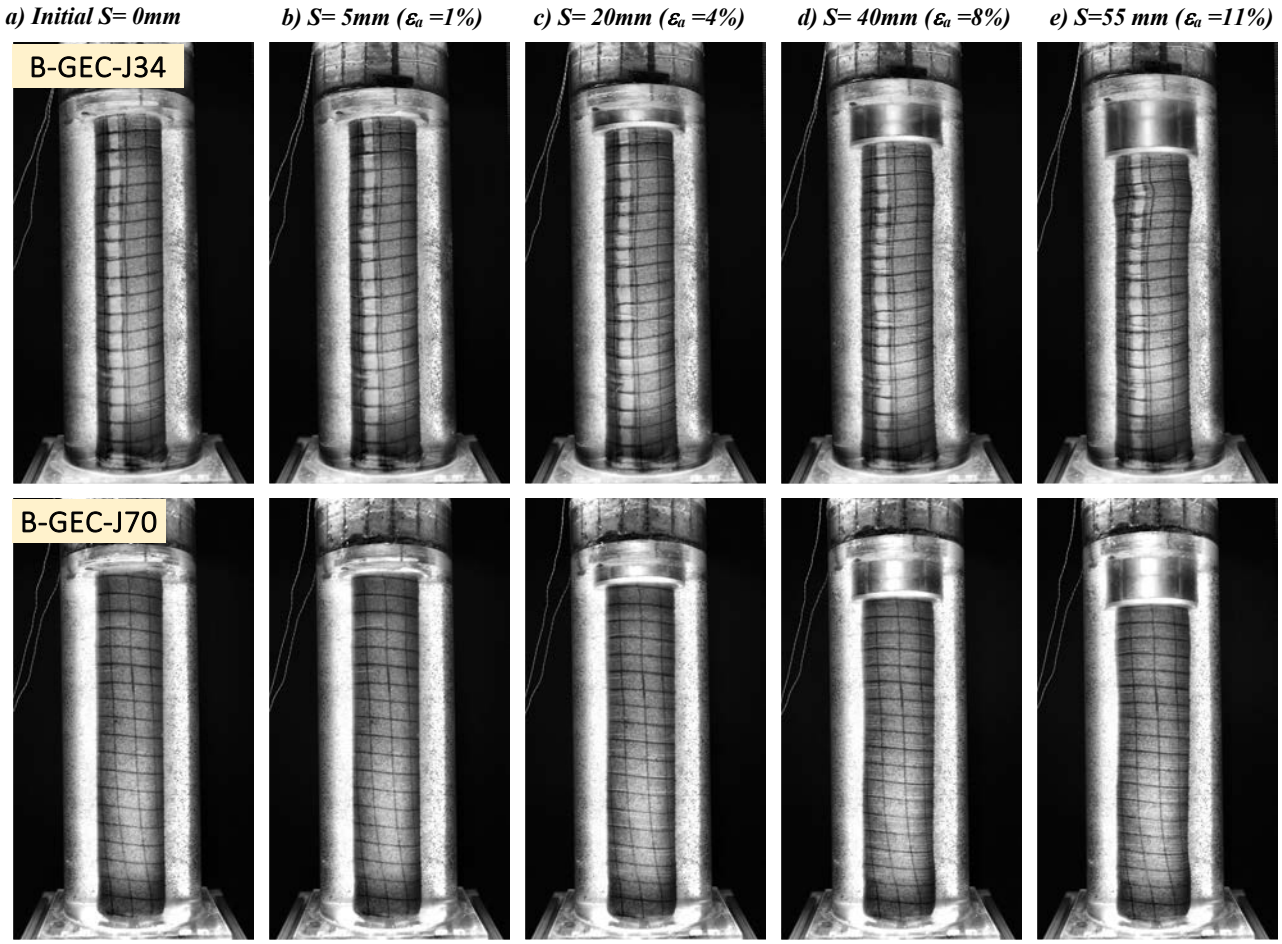

Figure 3.10.- Image sequence of models: B-GEC-J34, and B-GEC-J70 test at 0%, 1%, 4%, 8% and 11% average column axial strains

GEC Baseline, model B-GEC-J34

The B-GEC-J34 baseline model exhibited no signs of failure up to 10% average column axial strain under high vertical loads (**Figure 3.10**). The encasement radial strain profile (**Figure 3.9**) showed nearly uniform deformation through 8% average column axial strain, with slight bulging and no damage to the encasement. At 10% average column axial strain, visible bulging developed at 1.5 column diameters depth without encasement

damage. The load-settlement response (Error! Reference source not found.) confirmed no failure occurred, as the encasement continuously provided sufficient confinement to the column infill.

The B-GEC-J34 model demonstrated remarkable stability, with no notable failures even at 50 mm of column total settlement. The encasement's tensile strength significantly reduced bulging in the column compared to the unreinforced (A-OC-σ5) and lower encasement stiffness models (B-GEC-J08 and B-GEC-J11). The 10% average column axial strain did not trigger failure due to the encasement's confinement along the entire length including at depths of initial subtle bulging regions. **Figure 3.11** shows the maximum encasement radial strains increasing along the allowable tensile strength path of the encasement without exceeding its maximal tensile capacity, allowing large encasement radial deformations at the bulging depth without encasement breakage failure. Bulging did not indicate overall failure of the GEC system, and the mobilization of encasement confinement enabled constant incremental enhancements in bearing capacity, provided that tensile strains remained within permissible bounds.

From the column infill perspective, internal shearing residual strength was assumed present, but increasing mobilized encasement confining stresses prevented outright failure at the cost of permissible encasement radial deformation. **Figure 3.12** illustrates how the increasing mobilized confining pressure ($\sigma_{h,c}$) allowed the stress state of the column infill to progress along the triaxial envelopes at various average column axial strain stages. The encasement enabled the mobilized confining pressure to reach 140 kPa at 10% average column axial strain, despite the column infill having reached its peak strength between 2-3% average column axial strain, after which the residual strength governed its stress state.

In summary, this prototype-representative model encasement delivered stabilization without damage under significant column axial deformations, mobilizing about 90% of the available encasement strength. This demonstrates that the encasement secant stiffness and ultimate tensile capacity are relevant governing parameters in determining GEC performance.

GEC with High Stiffness Encasement, model B-GEC-J70

The B-GEC-J70 model exhibited excellent performance among all the 80 mm diameter GECs, with no signs of tensile breakage failure or encasement damage up to 10% average column axial strain, as seen in Error! Reference source not found. and **Figure 3.10**. The GEC presented visually uniform encasement radial deformations along its full length. The encasement radial deformation profile from **Figure 3.9** identified a slight peak of encasement radial strain at 1.5 column diameters depth and at the bottom of the column. Throughout the test, the encasement showed no tearing, and the column infill did not show any shear plane or significant bulging formation.

The B-GEC-J70 model maintained a similar load-displacement response to the B-GEC-J34 baseline model up to 3.5% average column axial strain. After that point, it developed a higher rate of bearing capacity due to faster encasement confinement mobilization, as shown in **Figure 3.11**. The maximum encasement radial strain measured did not exceed 50% of the allowable deformation throughout testing, indicating the encasement remained in the elastic range. This enabled uniform encasement radial deformations and rapid confinement mobilization at lower strains due to the encasement's steep tensile strength-strain slope. **Figure 3.12** shows the column infill experienced high confinement levels up to 160 kPa, following a stress path similar to the B-GEC-J34

baseline model. This demonstrates the encasement's ability to provide adequate confinement even if the column infill has already reached shear failure due to large average column axial deformations by mobilizing only 50% of its encasement tensile strength capacity.

The column infill deviatoric stress ($\sigma_{d,c}$) versus axial strain relationship was found to be the most suitable representation of the true stress state of the GEC model. By considering both vertical column stress and mobilized encasement confinement, it captures the performance and onset of column failure in detail. In contrast, plots of load-settlement response may portray the overall system behavior but can miss when yielding and loss of encasement confinement begins to increase at lower rate or be reduced . The analysis showed encasement confinement mobilization governs the GEC model performance, so confining stress-strain relations accounting for this provides more insight.

Finally, the results demonstrated that the tensile breakage capacity of the encasement controls GEC failure in very soft soils, indicating bearing capacity depends primarily on encasement stiffness and tensile strength rather than column infill shear strength. Encasement stiffness impacts GEC deformation patterns, with lower stiffness encasements leading to uneven encasement radial deformation and encasement radial strain concentration in the top 2 column diameters, which can prompt column infill shear plane or column bulging failures. Stiffer encasements distribute deformation more uniformly along the column. When bulging occurs, the allowable mobilized encasement's horizontal stresses restrain further deformation. Bulging may arise without determining the failure condition, which only occurs once the encasement yields or breaks. In summary, encasement stiffness and tensile strength properties dictate failure mode and bearing

capacity over column infill shear strength, with higher stiffnesses reducing encasement radial strains while increasing column load capacity.

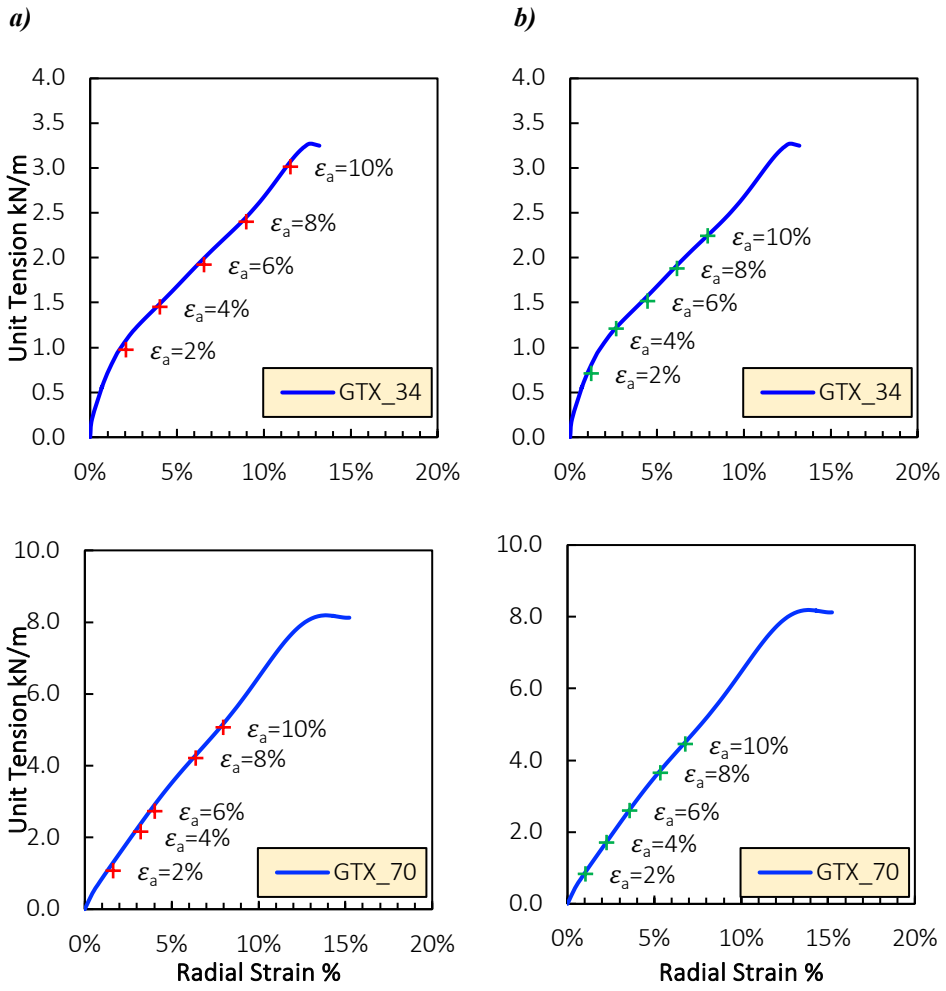

Figure 3.11.- Encasement tensile mobilization of models: B-GEC-J34 baseline & B-GEC-J70 , a) Maximal encasement radial strain, and b) Average encasement radial strain

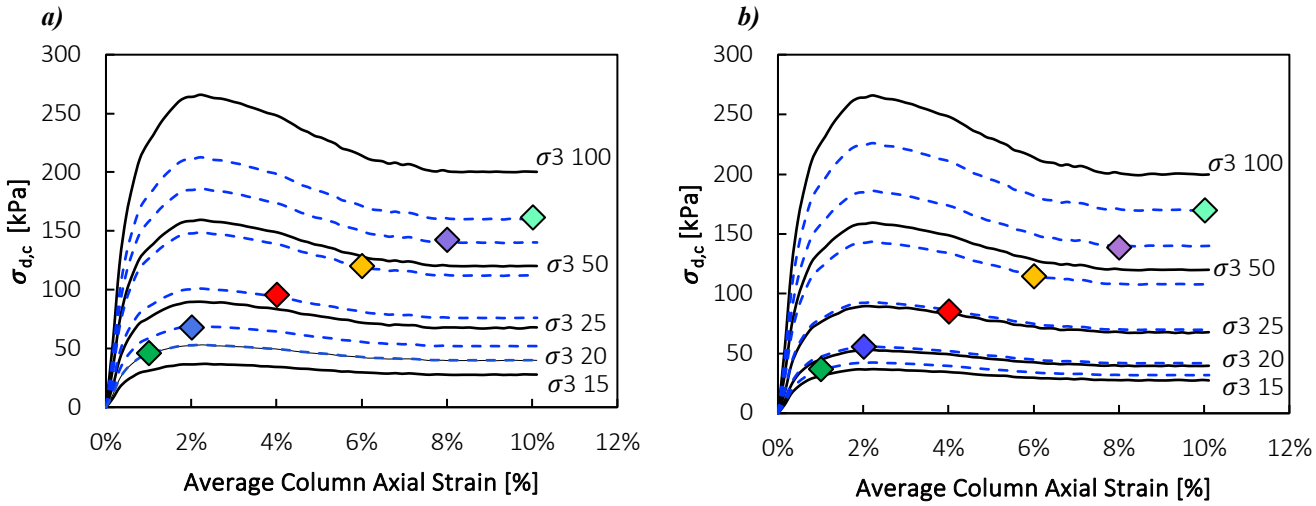

Figure 3.12.- Column infill mobilization from models: a) B-GEC-J34 baseline & b) B-GEC-J70.

3.7.- PARAMETRIC EVALUATION

A parametric evaluation was conducted to assess the impact of various parameters on GEC performance. The evaluation draws on the load-displacement response (**Figure 3.13**), column infill volume change (**Figure 3.14**), and average encasement radial strain (**Figure 3.15**) at a maximum average column axial strain of 8%. Each figure is described in detail below.

3.7.1.- EFFECT OF ENCASEMENT STIFFNESS

The encasement stiffness was varied using four values: $J_{5\%}$ = 8, 11, 34 (baseline), and 70 kN/m. Increasing the encasement stiffness provided greater lateral confinement to the column infill, enhancing the load-settlement response. From **Figure 3.13a**, at 8% average column axial strain, the vertical pressure reached 178 kPa for the B-GEC-J34 model, while the B-GEC-J70 model achieved 227 kPa, a 28% increase. In contrast, the B-GEC-J08 and B-GEC-J11 models reduced capacity by 79% to just 36 and 47 kPa, respectively

The improved confinement from higher stiffness encasements also restricted column infill volumetric and encasement radial strains. From **Figure 3.14a**, at 8% average column axial strain, the B-GEC-J70 model limited column infill volume dilation to 1.82%, a 40.5% decrease from the 3.05% column infill volumetric strain in the B-GEC-J34 model. Meanwhile, the B-GEC-J08 and B-GEC-J11 models underwent significant column infill dilation, reaching 2% volumetric strain because both columns failed at earlier axial strains, allowing the column infill to dilate freely. For the average encasement radial strain in **Figure 3.15a**, a virtual case of constant volume has been added to show the hypothetical variation of the radius with increasing axial strain. The B-GEC-J70 model restricted the

average encasement radial deformation to 5.32%, being the closest to the constant column infill volume case, with a 13.1% reduction compared to the 6.12% average encasement radial strain in the B-GEC-J34 model. The B-GEC-J08 and B-GEC-J11 models also accumulated low average encasement radial strain at 5.4%; however, the peaks of maximal encasement radial strain are not captured in the average encasement radial strain due to non-uniform radial deformation.

Overall, the encasement stiffness test results quantitatively demonstrate that selecting stiffer geosynthetic encasements enhances the vertical load capacity while limiting column infill volumetric and encasement radial strains. The $J_{5\%}$ = 70 kN/m encasement outperformed the intermediate $J_{5\%}$ = 34 kN/m case, while the $J_{5\%}$ = 8 and 11 kN/m encasements led to reduced capacity and greater strains across all metrics because the encasement failed during the testing. Optimizing encasement stiffness is relevant for improving the performance of GEC foundations.

Load-Settlement Response

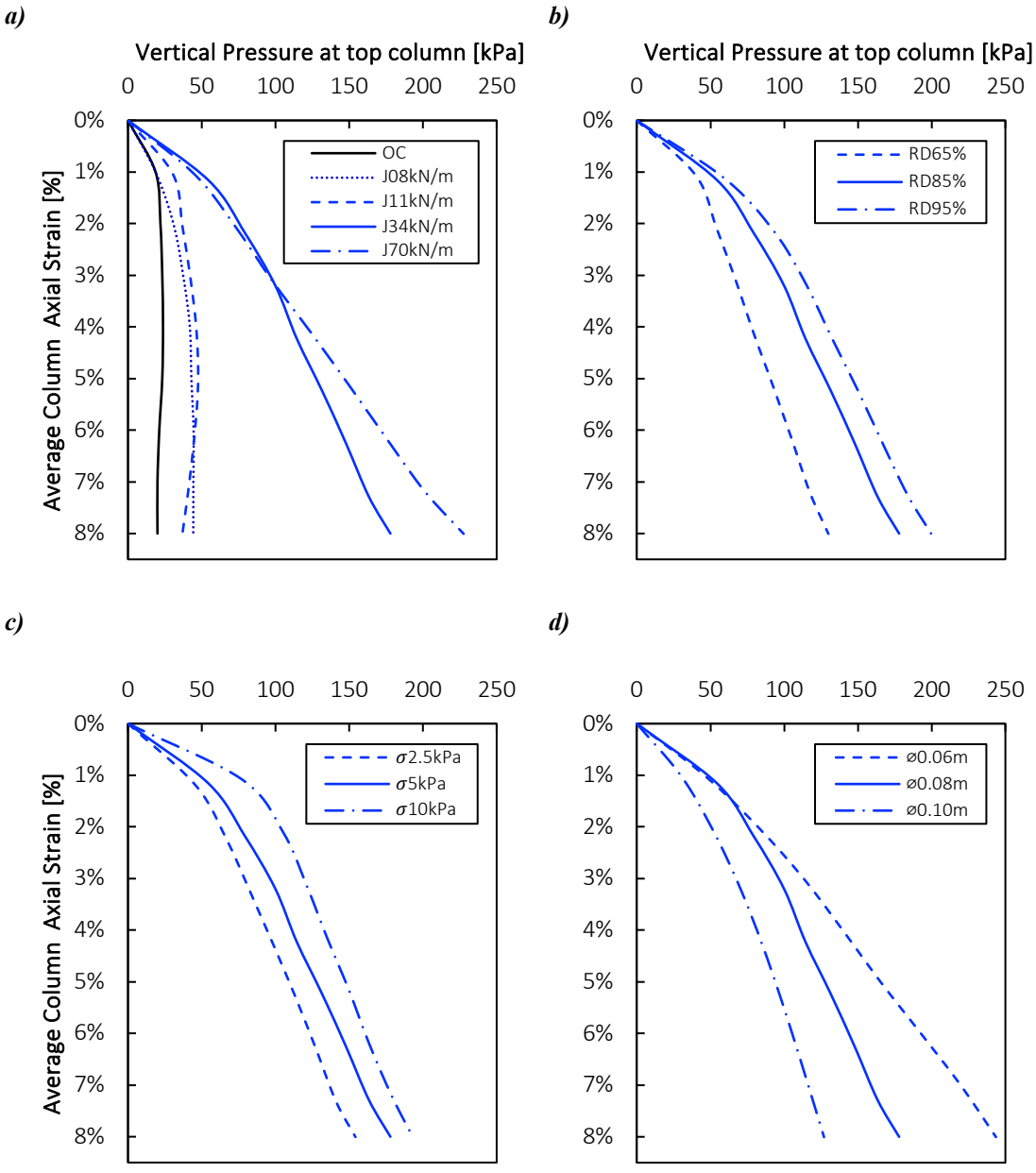

Figure 3.13.- Load-Settlement response, a) Encasement secant stiffness effect, b) Column infill relative density effect, c) Overburden pressure effect, and d) Column diameter effect

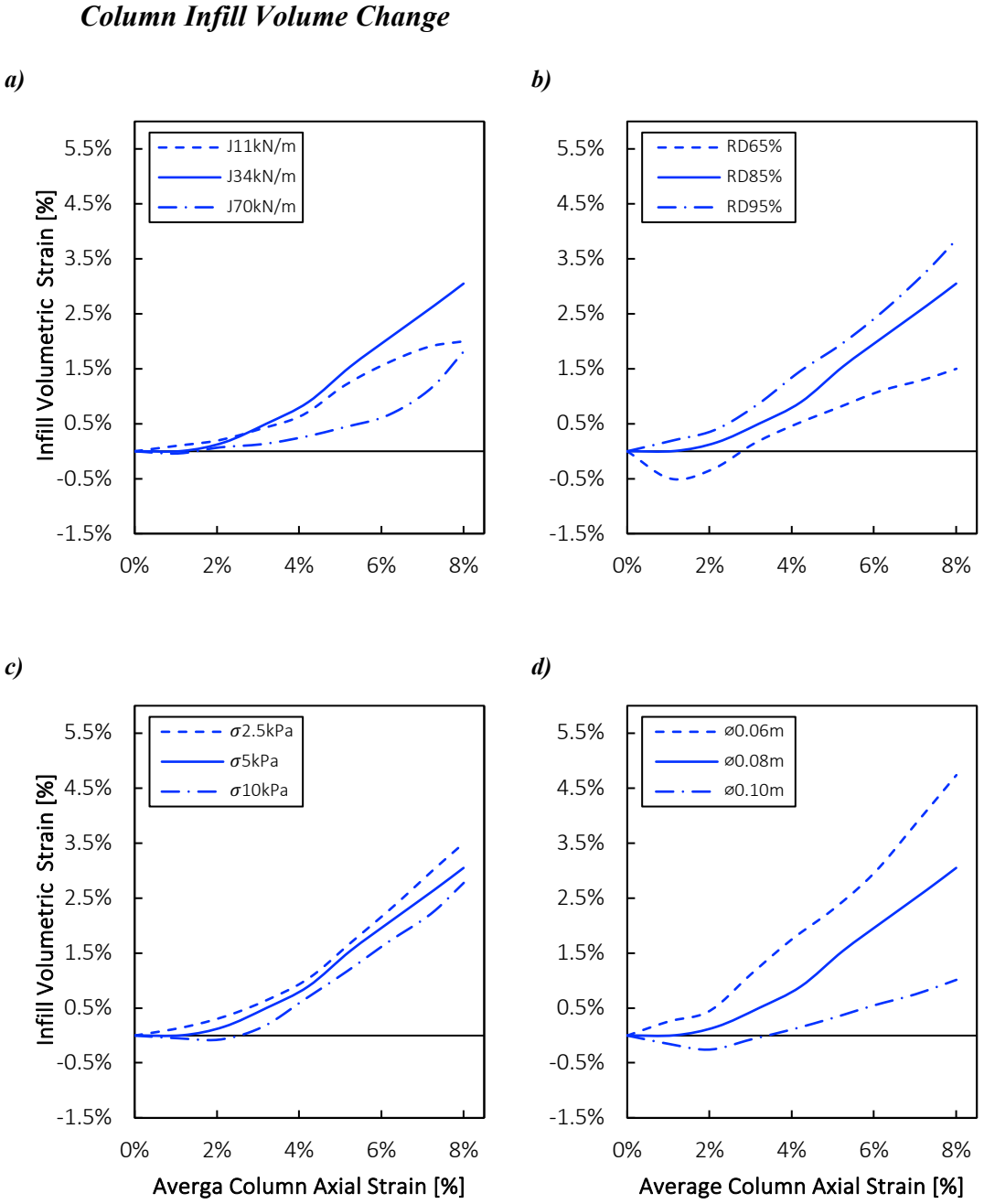

Figure 3.14.- Volumetric change response, a) Encasement secant stiffness effect, b) Column infill relative density effect, c) Overburden pressure effect, and d) Column diameter effect

Average Encasement Radial Strain

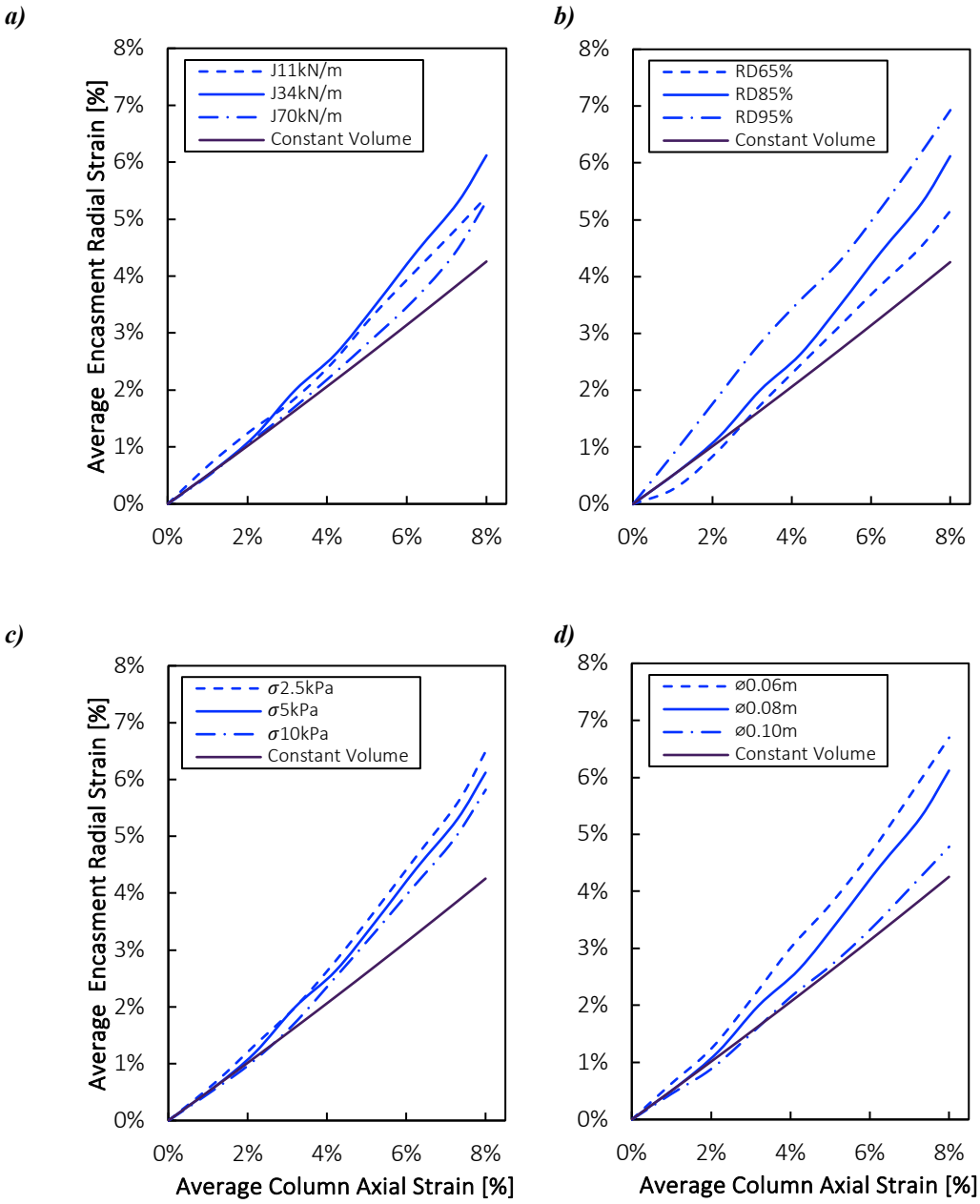

Figure 3.15.- Average encasement radial strain response, a) Encasement secant stiffness effect, b) Column infill relative density effect, c) Overburden pressure effect, and d) Column diameter effect

3.7.2.- EFFECT OF RELATIVE DENSITY

The relative density (RD) of the soil column was varied using three values: RD 65%, RD 85% (baseline), and RD 95%. Increasing the relative density enhances interparticle contact forces, providing greater resistance to compression and improving load capacity. From **Figure 3.13b**, at 8% average column axial strain, the vertical pressure reached 178 kPa for the RD 85% baseline case. The densest RD 95% column achieved a higher pressure of 200 kPa, a 12% increase in capacity. In contrast, the loosest RD 65% column had a 27% lower capacity of 130 kPa.

From **Figure 3.14b** the denser model also displayed higher column infill dilation. At 8% average column axial strain, the RD 95% column underwent 3.85% of column infill volumetric dilation, a 26.2% increase over the 3.05% in the RD 85% baseline model. Meanwhile, the loose RD 65% model accumulated significantly less column infill volume change at 1.5% , a 50% decrease compared to the baseline. For average encasement radial strain shown in **Figure 3.15b**, the dense RD 95% column restricted deformation to 6.93%, a 13.2% increase compared to the 6.12% average encasement radial strain in the baseline RD 85% model. The looser RD65% model accumulated lower encasement radial strain at 5.16%, a 15.7% reduction from the baseline.

Overall, the relative density test results quantitatively demonstrate that denser GEC columns provide higher vertical load capacity while undergoing greater column infill volumetric dilation and even encasement radial strains. The dense RD 95% model outperformed the baseline RD 85% case, while the loose RD 65% column displayed poorer response across key metrics. Selecting an appropriately high relative density for the column fill is important to maximize the functioning of GEC foundations, since the mobilization

of the encasement depends highly in its the uniform encasement radial deformation which is highly affected when the overall volume increases.

3.7.3.- EFFECT OF OVERBURDEN PRESSURE

The constant overburden pressure applied on the surrounding soft soil was varied using three values: σ_{low} = 2.5kPa, σ_{medium} = 5kPa (baseline), and σ_{high} = 10kPa. Test results demonstrated that raising the overburden stress furnished greater initial confinement, moderately enhancing load carrying capacity. This outcome is attributed to the baseline encasement already providing substantial restraint. Hence, the supplemental stability and reduced stress ratio between the column and adjacent soil from additional overburden provided incremental improvements.

From **Figure 3.13c** Quantitatively, at 8% average column axial strain, the vertical pressure sustained by the column reached 178 kPa with the medium σ 5 kPa overburden in the baseline model. However, the model with high σ 10kPa overburden achieved a higher pressure of 193 kPa, constituting an 8% enhancement versus the baseline capacity. In contrast, the model with low σ 2.5 kPa overburden exhibited a 13% inferior capacity of 154 kPa.

Figure 3.14c shows that the higher σ 10 kPa overburden pressure also provided improved restriction of column infill volumetric and encasement radial strains. At 8% average column axial strain, the σ 10 kPa model underwent 2.78% column infill volumetric strain, a 9% decrease from the 3.05% in the σ 5 kPa baseline model. Meanwhile, the lower σ 2.5 kPa overburden model accumulated significantly more volumetric change at 3.5%, a 15% increase from the baseline model. For average encasement radial strain in **Figure 3.15c**, the σ 10 kPa model limited deformation to 5.82%, a 5% reduction compared to the

6.12% in the baseline σ 5 kPa case. The lower σ 2.5 kPa model underwent the most encasement radial strain at 6.5%, a 6% increase.

Overall, the overburden pressure test results quantitatively demonstrate that greater initial confining stresses enhance the vertical load carrying capacity while restricting strains. The σ 10 kPa model moderately outperformed the σ 5 kPa baseline case, while the lower σ 2.5 kPa model displayed poorer response across key metrics. Appropriately estimating the overburden pressures is important for optimized functioning of GEC foundations.

3.7.4.- EFFECT OF COLUMN DIAMETER

The column diameter was varied using three sizes: Ø 60 mm, Ø 80 mm (baseline), and Ø 100 mm. Decreasing the diameter provides greater relative confinement from the encasement, substantially enhancing bearing capacity. From **Figure 3.13d** at 8% average column axial strain, the vertical pressure reached 178 kPa for the Ø 80 mm baseline column. The smaller Ø 60 mm column achieved the highest pressure of 244 kPa given the lower column sectional area, a 37% increase in capacity. In contrast, the largest Ø 100 mm column had a 29% lower bearing capacity of just 127 kPa. As a remark, in terms of load (kN) the order will be inverted, however the evaluation remained in terms of vertical pressure applied for analysis consistency.

As observed in **Figure 3.14d** the greater relative restraint on the narrow Ø 60 mm column also experimented higher volumetric and encasement radial strains. At 8% axial strain, the Ø 60 mm column underwent 4.74% volumetric strain, a 55% increase over the 3.05% in the Ø 80 mm baseline model. Meanwhile, the Ø 100 mm column accumulated significantly less volume change at 1.01%, a 67% decrease. For average encasement radial

strain in **Figure 3.15d**, the Ø 60 mm column reached 6.7%, a 9.4% increment compared to the 6.12% average encasement radial strain in the baseline Ø 80 mm model. The Ø 100 mm column underwent the lower encasement radial strain at 4.8%, a 21.8% decrease compared to the baseline model.

Overall, the column diameter test results quantitatively demonstrate that smaller diameter GEC columns achieve substantially higher vertical load capacity while limiting volumetric strains. This enhanced performance is attributed to the greater tensile mobilization of the encasement for a given axial strain when the diameter is reduced. Specifically, the narrow Ø 60 mm column stimulates larger encasement radial strains, which more effectively activates the hoop stiffness and tensile capacity of the encasement to furnish superior confinement. This Ø 60 mm column considerably outperformed the Ø 80 mm baseline case, achieving a 37% increase in capacity at 8% axial strain. In contrast, the larger Ø 100 mm column displayed a 29% reduction in load capacity along with heightened column infill volumetric and encasement radial strains across key metrics. Selecting an appropriate column diameter is therefore imperative to optimize encasement tensile mobilization and maximize the performance of GEC foundations.

3.8.- COMPARISON BETWEEN EXPERIMENTAL AND ANALYTICAL RESULTS

The encasement radial strains measured in the GEC baseline model were compared to those from four analytical models that predict the encasement radial change in a GEC column:

1. A basic constant column infill volume model.

2. The Raithel and Kempfert (2000) method, which is a popular design approach adopted by the German Standard EBGEO (2011). This method uses a rigid-perfectly plastic column infill model with constant volume assumptions.

3. The Pulko (2011) method that considers an elasto-plastic column infill behavior and incorporates dilatancy effects within the column infill.

While the specifics of these analytical models can be found in the source references, the key details and assumptions are summarized in the following sections. The goal of this comparison is to benchmark the encasement radial strain results from the GEC baseline model against established analytical approaches.

3.8.1.- ANALYTICAL MODELS

Rigid-Perfectly Plastic analytical model (Raithel & Kempfert, 2000)

The analytical method by Raithel and Kempfert (2000) is based on the unit cell concept with the following assumptions: equal settlement of column infill and surrounding soil, active earth pressure condition mobilized in the column infill, linear-elastic constitutive model for the geosynthetic encasement, and drained surrounding soil characterized by effective stress parameters. The required input parameters include area

replacement ratio (a_E), tensile secant stiffness modulus of the geosynthetic encasement ($J_{5\%}$), constrained soil modulus varying with depth/stress level (E_s), soil Poisson's ratio (ν_s), friction angle of column infill material (φ_c), and the coefficient of lateral earth pressure at rest (K_0) of the surrounding soil. Based on force equilibrium and strain compatibility, the method allows calculation through iterations of: encasement tensile force (F_R), settlement of column/surrounding soil (S), average encasement radial strain ($\varepsilon_{r,g}$), and vertical stresses of the column infill and the surrounding soil ($\sigma_{v,c}$ and $\sigma_{v,s}$). The method considers the influence of deformations on stresses in the system and vice versa (second-order theory). Advantages include the consideration of time-dependent consolidation of surrounding soil. Disadvantages are the inability to capture some detailed aspects revealed by more complex models and experimental results such as the detailed encasement radial strains along the column length or the differential settlement between the column and the surrounding soil. The closed-form analytical expressions used for the predictions in this study are provided in Raithel and Kempfert (2000).

Elasto-Plastic analytical model (Pulko, 2011)

The analytical method proposed by Pulko et al. (2011) is based on a unit cell model with the following assumptions: regularly spaced end-bearing stone columns, surrounding soil modeled as elastic, elasto-plastic Mohr-Coulomb column infill material with constant dilation angle (ψ) per Rowe's theory, and elastic geosynthetic encasement; equal settlement on top of column and soil, with no interface shear; soil remains elastic under loading; and first-order strain theory is used. The main inputs required are geometrical parameters (column spacing, size, and replacement ratio), column infill material properties (modulus, Poisson's ratio, friction angle, dilation angle, and unit weights of soil and column), load magnitude, and encasement stiffness. Key advantages include a closed-form analytical

solution that is easy to implement and can predict settlements, column and soil vertical stresses, and encasement tensile forces. It has been validated through finite element analyses and accounts for dilatancy and compressibility of the column. Disadvantages are the assumption of constant dilation angle that may overestimate stiffness at large strains. The closed-form analytical expressions used for the predictions in this study are provided in Pulko et al. (2011).

3.8.2.- COMPARISON BETWEEN EXPERIMENTAL RESULTS AND ANALYTICAL PREDICTIONS

Figure 3.16 presents a comparison between the measured encasement radial strain profiles for two GEC models with varying encasement secant stiffness (B-GEC-J34 baseline model and B-GEC-J70 model) and the predicted encasement radial strain profiles from two analytical methods: Rigid-Perfectly Plastic method by Raithel & Kempfert, (2000) and Elasto-Plastic method by Pulko et al., (2011). The comparison is made at three different average column axial strain levels: low ($\varepsilon_a = 2\%$), medium ($\varepsilon_a = 4\%$), and high ($\varepsilon_a = 8\%$).

For both models in **Figure 3.16**, the measured encasement radial strain profiles (dashed blue lines) exhibit a non-linear decrease with depth, with higher encasement radial strains concentrated at the top of the column. The continuous blue line represents the average encasement radial strain measurements and fades the variation and peaks measured but give a better understand of the trend. B-GEC-J34 baseline model, having a lower encasement secant stiffness, shows higher overall encasement radial strains and a more pronounced non-linear decrease with depth compared to B-GEC-J70 model, which has a higher secant stiffness and displays lower and more uniform encasement radial strains along the column depth.

The Rigid-Perfectly Plastic (red line) shown also in **Figure 3.16** generally overpredicts the encasement radial strains compared to the average encasement radial strains measured profiles, especially at higher average column axial strain levels. This can be attributed to several assumptions made in the method:

- Active earth pressure condition: The model assumes that the column material is always in an active state of stress, which may not be the case at all axial strain levels. This assumption could lead to overprediction of encasement radial strains.

- Linear-elastic behavior of geosynthetic encasement: The model considers the geosynthetic encasement to behave linear-elastically. However, at large encasement radial deformations, the geosynthetic material may exhibit non-linear behavior, which could result in a stiffer response than predicted by the linear-elastic assumption. This may contribute to the overprediction of encasement radial strains at higher axial strain levels.

In contrast, the Elasto-Plastic Method (green line) provides a better match to the average measured encasement radial strain profiles, particularly for B-GEC-J70 at low to medium average column axial strain levels. However, it tends to underpredict the encasement radial strains at very large average column axial strain levels. This can be explained by the following assumptions made in the method:

- Constant column infill dilation angle: The model uses a constant dilation angle based on Rowe's theory to describe the column infill volumetric behavior. However, the dilation angle may vary with stress level and column axial strain, and assuming a constant value may overestimate the column stiffness at large strains, contributing to the underprediction of encasement radial strains.

- First-order strain theory: The model employs first-order strain theory, which assumes small deformations. At very large column axial strains, second-order effects such as geometric nonlinearity and stress redistribution may become significant. Neglecting these effects could lead to discrepancies between the predicted and measured encasement radial strain profiles.

The measured encasement radial strain profiles exhibit distinct peaks and fluctuations that are not fully captured by the average encasement radial strain and the predicted encasement radial strain of the analytical methods evaluated. These peaks are more prominent in the B-GEC-J34 baseline model and at higher column axial strain levels, indicating localized deformations, stress concentrations, or potential failure zones within the GEC system.

The comparison highlights the importance of considering the secant stiffness of the geosynthetic encasement and the limitations of analytical models when analyzing and designing GECs. The Elasto-Plastic Method demonstrates better agreement with the measured encasement radial strain profiles, especially for GECs with higher secant stiffness encasement, while both methods show limitations in capturing the behavior of GECs with lower encasement secant stiffness and at very large column axial strains.

In summary, the assumptions made in each analytical method can explain some of the observed differences between the predicted and measured encasement radial strain profiles. Future research should focus on developing advanced analytical and numerical models that can better account for the complex stress-strain relationships in GECs, particularly for systems with lower encasement secant stiffness and under large column axial deformations.

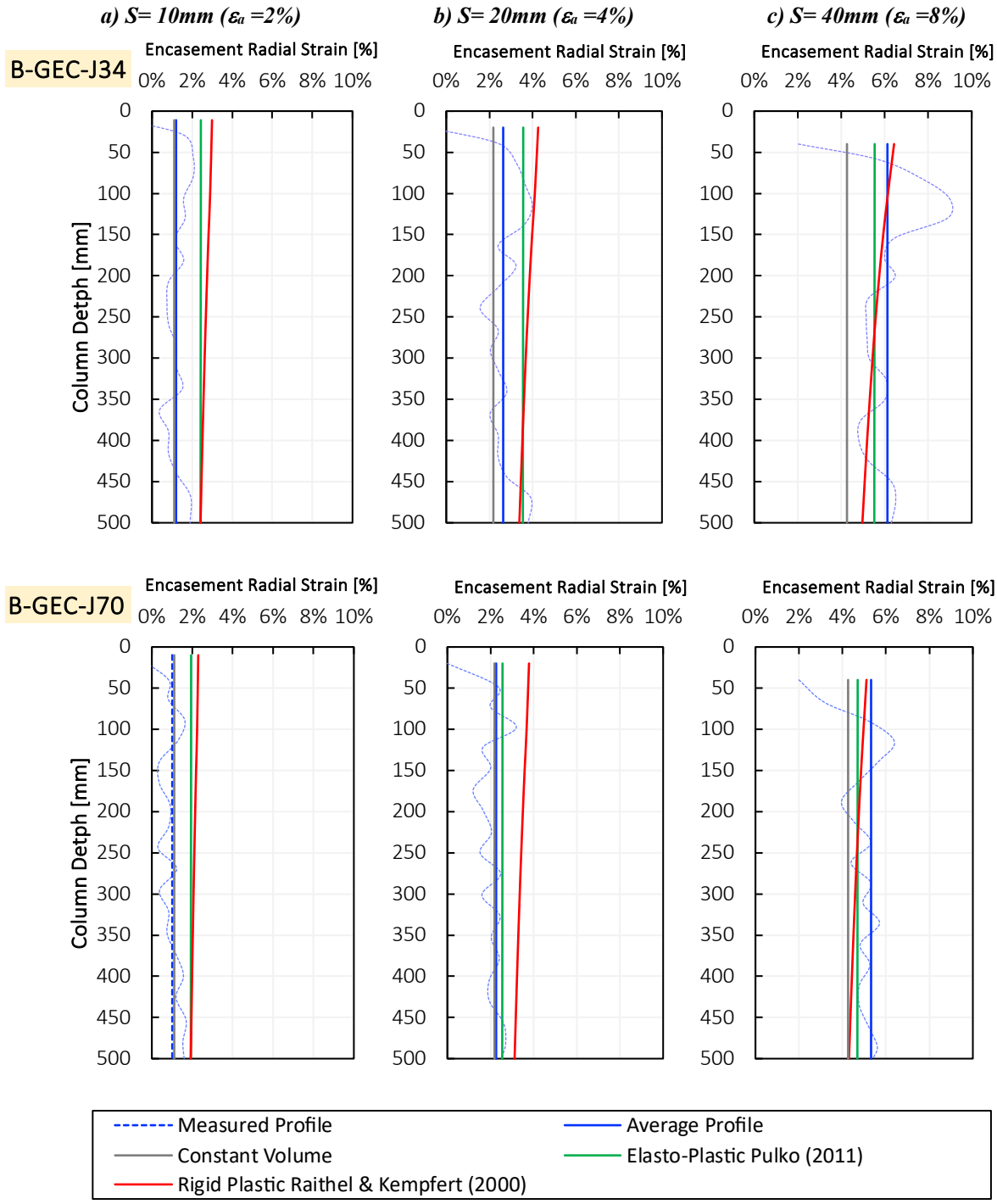

Figure 3.16.- Experimental vs analytical results from B-GEC-J34 baseline model and B-GEC-J70 model

3.9.- CONCLUSIONS

In conclusion, this experimental study provided valuable insights into the behavior and performance of geosynthetic encased columns (GEC) in soft soils through detailed analysis of failure mechanisms, stress-strain response, parametric evaluations, and comparison between experimental results and analytical predictions. The key conclusions drawn from this research are as follows:

- Encasement tensile rupture was identified as the initial and governing trigger of failure in GECs models with low tensile strength and low secant stiffness encasements, even though shear bulging is often considered the most observed failure mode in field applications.

- Encasement stiffness and tensile strength properties were found to dictate failure mode and bearing capacity over column infill shear strength, with higher encasement stiffnesses reducing encasement radial strains while increasing column load capacity.

- Selecting stiffer geosynthetic encasements was shown to enhance the load-settlement response while limiting column infill volumetric and encasement radial strains.

- Denser infill GEC columns were quantitatively demonstrated to provide higher vertical load capacity while undergoing greater column infill volumetric dilation and encasement radial strains.

- Greater initial confining stresses from overburden pressure were found to enhance the vertical load carrying capacity while restricting encasement radial strains in GECs.

- Smaller diameter GEC columns were quantitatively demonstrated to achieve substantially higher vertical load capacity while limiting column infill volumetric strains due to the greater tensile mobilization of the encasement for a given column axial strain.

- The results from the predicted Elasto-Plastic analytical method demonstrated better agreement with the measured encasement radial strain profiles, especially for GECs with higher secant stiffness encasement, while both the Rigid-Perfectly Plastic and Elasto-Plastic methods showed limitations in capturing the behavior of GECs with lower encasement secant stiffness and at very large column axial strains.

In summary, this study provided valuable insights into the failure mechanisms, stress-strain response, and key parameters governing the performance of geosynthetic encased columns in soft soils. The findings highlight the importance of optimizing the encasement and column properties to maximize the benefits of GEC reinforcement systems. The experimental results also serve as a benchmark for evaluating the accuracy of simplified analytical models at various stages of column deformation.

3.10.- REFERENCES

Alexiew, D., Kuster, V., & Assinder, P. (2011). *An Introduction to Ground Improvement using Geotextile Encased Columns (GEC)*. 22.

Alexiew, D., & Raithel, M. (2015). Geotextile-Encased Columns, Case Studies over Twenty Years. In *Ground Improvement Case Histories* (pp. 451–477). Elsevier. https://linkinghub.elsevier.com/retrieve/pii/B978008100192900017X

Ali, K., Shahu, J. T., & Sharma, K. G. (2012). Model tests on geosynthetic-reinforced stone columns: A comparative study. *Geosynthetics International*, *19*(4), 292–305. https://doi.org/10.1680/gein.12.00016

Ali, K., Shahu, J. T., & Sharma, K. G. (2014). Model tests on single and groups of stone columns with different geosynthetic reinforcement arrangement. *Geosynthetics International*, *21*(2), 103–118. https://doi.org/10.1680/gein.14.00002

Alkhorshid, N. R., Araujo, G. L. S., Palmeira, E. M., & Zornberg, J. G. (2019). Large-scale load capacity tests on a geosynthetic encased column. *Geotextiles and Geomembranes*, *47*(5), 632–641. https://doi.org/10.1016/j.geotexmem.2019.103458

Almikati, A., Pierozan, R. C., Sadek, S., & Zornberg, J. G. (2023). Geotechnical Characterization of Laponite as Transparent Clay Surrogate. *Geotechnical Testing Journal*, *46*(3), 20220106. https://doi.org/10.1520/GTJ20220106

Ayadat, T., & Hanna, A. M. (2005). Encapsulated stone columns as a soil improvement technique for collapsible soil. *Proceedings of the Institution of Civil Engineers - Ground Improvement*, *9*(4), 137–147. https://doi.org/10.1680/grim.2005.9.4.137

Chen, J.-F., Wang, X.-T., Xue, J.-F., Zeng, Y., & Feng, S.-Z. (2018). Uniaxial compression behavior of geotextile encased stone columns. *Geotextiles and Geomembranes*, *46*(3), 277–283. https://doi.org/10.1016/j.geotexmem.2018.01.003

Ghazavi, M., & Nazari Afshar, J. (2013). Bearing capacity of geosynthetic encased stone columns. *Geotextiles and Geomembranes*, *38*, 26–36. https://doi.org/10.1016/j.geotexmem.2013.04.003

Gniel, J., & Bouazza, A. (2009). Improvement of soft soils using geogrid encased stone columns. *Geotextiles and Geomembranes*, *27*(3), 167–175. https://doi.org/10.1016/j.geotexmem.2008.11.001

Hong, Y.-S., Wu, C.-S., & Yu, Y.-S. (2016). Model tests on geotextile-encased granular columns under 1-g and undrained conditions. *Geotextiles and Geomembranes*, *44*(1), 13–27. https://doi.org/10.1016/j.geotexmem.2015.06.006

Malarvizhi, S. N., & Ilamparuthi, K. (2004). *Load versus Settlement of Claybed stabilized with Stone & Reinforced Stone Columns*. GeoAsia.

Miranda, M., & Da Costa, A. (2016). Laboratory analysis of encased stone columns. *Geotextiles and Geomembranes*, *44*(3), 269–277. https://doi.org/10.1016/j.geotexmem.2015.12.001

Miranda, M., Da Costa, A., Castro, J., & Sagaseta, C. (2015). Influence of gravel density in the behaviour of soft soils improved with stone columns. *Canadian Geotechnical Journal*, *52*(12), 1968–1980. https://doi.org/10.1139/cgj-2014-0487

Miranda, M., Da Costa, A., Castro, J., & Sagaseta, C. (2017). Influence of geotextile encasement on the behaviour of stone columns: Laboratory study. *Geotextiles and Geomembranes*, *45*(1), 14–22. https://doi.org/10.1016/j.geotexmem.2016.08.004

Murugesan, S., & Rajagopal, K. (2009a). Investigations on the behaviour of geosynthetic encased stone columns. *Stand Alone*, 2411–2414. https://doi.org/10.3233/978-1-60750-031-5-2411

Murugesan, S., & Rajagopal, K. (2009b). Shear Load Tests on Stone Columns With and Without Geosynthetic Encasement. *Geotechnical Testing Journal*, *32*(1), 101219. https://doi.org/10.1520/GTJ101219

Nazari Afshar, J., & Ghazavi, M. (2014). Experimental Studies on Bearing Capacity of Geosynthetic Reinforced Stone Columns. *Arabian Journal for Science and Engineering*, *39*(3), 1559–1571. https://doi.org/10.1007/s13369-013-0709-8

Pierozan, R. C., Almikati, A., Araujo, G. L. S., & Zornberg, J. G. (2022). Optical and Physical Properties of Laponite for Use as Clay Surrogate in Geotechnical Models. *Geotechnical Testing Journal*, *45*(1), 20210100. https://doi.org/10.1520/GTJ20210100

Rajagopal, K., Krishnaswamy, N. R., & Madhavi Latha, G. (1999). Behaviour of sand confined with single and multiple geocells. *Geotextiles and Geomembranes*, *17*(3), 171–184. https://doi.org/10.1016/S0266-1144(98)00034-X

Wu, C.-S., & Hong, Y.-S. (2009). Laboratory tests on geosynthetic-encapsulated sand columns. *Geotextiles and Geomembranes*, *27*(2), 107–120. https://doi.org/10.1016/j.geotexmem.2008.09.003

Chapter 4: Evaluation of GEC-Soil interaction from Physical Models Involving a Transparent Clay Surrogate

ABSTRACT

An experimental study was conducted that included visualizing the interface shear behavior between an end-bearing geosynthetic encased column (GEC) and surrounding transparent clay. Laponite, a synthetic transparent clay, enabled continuous visualization and Digital Image correlation (DIC) analysis of the development of shear bands in the clay adjacent to the GEC. The evaluation also allowed quantification of the interface shear contribution to the GEC bearing capacity. Additionally, tracking displacements within an embedded marker plane evaluated evolving soil deformations throughout loading. The results revealed that interface shear activation differed along the GEC depth since vertical displacements were nonuniform during uniaxial loading. Early loading stages displayed shear bands extending up to 0.5 diameters from the GEC, but this zone diminished drastically a post peak shear strength of laponite at higher displacements. Visualization of the interface shearing enabled quantification of the soil volume activated in load transfer. The early transient shear bands did not significantly impact end-bearing GEC behavior, as the encasement stiffness increased and interface interaction faded, shifting load transfer to the tip. The strain influence zone remained within 0.5 column diameter, suggesting negligible disturbance in the surrounding soil. This research achieved high resolution of the interface shear behavior during GEC-soil interaction under simulated field conditions.

4.1.- INTRODUCTION

Geosynthetic Encased Columns (GECs) effectively improve soft soil foundations by transferring loads to deeper firm layer. However, the degree of load transfer and the contribution of interface shear resistance between the geosynthetic encasement and surrounding soil are not well understood. Quantifying this interface shear behavior is essential for the design and performance evaluation of GECs.

Directly visualizing the interface shear mechanisms can be achieved by developing a specialized experimental methodology using transparent soils. Recent studies have implemented transparent clays like laponite, enabling imaging techniques to observe soft soil deformation. Mixed laponite forms a soft, thixotropic, and transparent colloid while exhibiting comparable properties to natural high plasticity clays. This study embeds markers within a laponite cross-section surrounding a model GEC to track interface shear displacements and soil field strains. This enables continuous, non-intrusive measurement and visualization of progressive interface shear development and its contribution to vertical load transfer.

The objectives are to first evaluate GEC load transfer performance and laponite shear strength behavior under applied loading. Subsequently, the interface shear between the soil and the geosynthetic encasement will be analyzed under controlled conditions to characterize shear influence zones around columns and the specific role of interface shear in GEC performance. Outcomes will elucidate interface shear mechanisms and their impact on improving very soft clay foundations. Visualization and quantification of deformations and shear aim to clarify GEC load transfer behavior and the significance of interface shear in the performance of GECs.

4.2.- BACKGROUND INFORMATION

Laponite as a Transparent Clay Surrogate for Shear Visualization

Laponite is a synthetic transparent clay surrogate capable of allowing visualization of shear failure mechanisms in physical models (Iskander, 2010). The transparency of laponite enables the use of optical measurement techniques to non-intrusively observe deformations within the soil mass. Of particular interest is the ability of laponite to exhibit shear strength comparable to very soft clays (Ads et al., 2020; Almikati et al., 2023b). The laponite mixture shear strength can be engineered to reach a target value that will stabilize over time due to the thixotropic nature of the material. The progression of shear failure surfaces and deformation characteristics around various shear strength testing devices can be visualized using transparent laponite and particle tracking methods. Techniques such as digital image correlation (DIC) have been implemented to measure displacements and soil shear strains during shear (Chini et al., 2015). The shearing behavior and transparency make laponite a suitable soil surrogate to study soil-structure interaction mechanisms along interfaces using non-intrusive optical measurements. Additionally, markers embedded in transparent soils allow for measuring displacements and soil shear strains under loading with higher precision. Integrating these approaches enables observing geosynthetic encased column interface behavior during loading, revealing the contribution of interface shear to the overall performance.

GEC Load Transfer and Interface Shear: Insights from Analytical and Numerical Studies

Several studies have investigated the role of interface shear between the encasement geosynthetic and the surrounding soil in the load transfer and deformation behavior of GECs using analytical and numerical approaches. While GEC axial capacity relies

primarily on the composite stiffness of the column material and the column infill radial confinement provided by the geosynthetic encasement (Tan & Zhao, 2018), characterizing interface shear may provide relevant insights into the mechanical response and failure mechanisms of these systems.

Some analytical models for GECs directly incorporate interface shear by calculating shear stress from earth pressure and interface friction/cohesion parameters (L. Zhang & Zhao, 2015). Results showed that including interface shear improved the prediction of axial load transfer and deformation trends compared to models that neglected this aspect. However, these analytical models often make simplifying assumptions, such as ignoring the shear interaction between the soil column and the geosynthetic encasement.

Numerical simulations have also been employed to study the role of interface shear in GECs. Advanced numerical models have adopted interface shear constitutive relationships between discrete GEC components, such as the soil column, geosynthetic encasement, and surrounding soil (Tan, Feng, Hu, & Abbas, 2021). By fitting an assumed interface shear resistance, these simulations matched experimental results and demonstrated that interface shear can have a substantial effect on the overall capacity of GECs (Tan, Feng, Hu, & Zhao, 2021). Additional simulations revealed the initiation of shear failure zones originating from GEC boundaries (Tan & Zhao, 2018), providing qualitative validation of the underlying interface shear mechanisms. Even unit cell approaches that exclude explicit interface elements have shown shear localization along observed bulging zones and column yielding (Ng & Tan, 2015), highlighting the importance of interface shear in the overall behavior of GECs.

These studies exemplify how interface shear can trigger behaviors such as the development of soil plasticity zones, bulging, and differential settlements in GECs. Although the direct contribution of interface shear to the overall capacity may be relatively low, experimental investigation remains relevant for a comprehensive characterization of GEC behavior and failure mechanisms. Quantitative visualizations of interface shear through advanced laboratory techniques can provide fundamental insights into the role of interface shear in the performance of GECs.

4.3.- LAPONITE SHEAR AND PHYSICAL CHARACTERISTICS

Before analyzing the interface shear behavior between the GEC model and the surrounding laponite clay surrogate, two preliminary investigations were carried out. First, the undrained shear strength of the laponite was evaluated as a function of vane depth and the magnitude of vane circumferential displacement. This allowed characterization of how laponite shear strength varies with depth and with the level of shear displacement, providing a baseline for interpreting the shear behavior observed later in the GEC testing. The second investigation focused specifically on the laponite-geosynthetic interface using a tailored pullout test. With no other stresses or materials involved, the pullout test provided insight into the fundamental shearing behavior between the geosynthetic encasment and the laponite. Together, these two tests furthered understanding of the shear strength properties of laponite and the laponite-geosynthetic interface interactions prior to integrated GEC model testing.

4.3.1.- UNDRAINED VANE SHEAR TEST

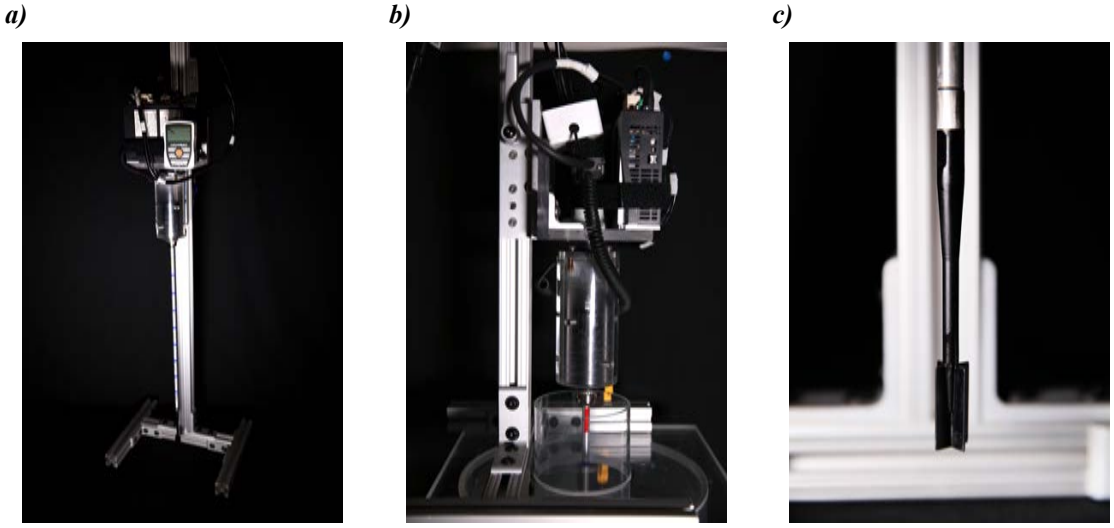

Figure 4.1.- a) Vane shear setup, b) Motor and Torque Gauge, and c) Vane Blade

A tailored laboratory vane shear device was purposely configured to directly probe the undrained shear strength (S_u) profile of the large cell of laponite containing 35 liters in volume, as illustrated by the experimental setup in **Figure 4.1**. The vane shear setup incorporates a high-precision digital torque gauge (Mark-10 MTT03-10Z, maximum 7 Ncm) coupled to a closed loop stepper motor (Oriental Motor, ARM46AC-T10) rotating at 1°/min meeting ASTM D4648M standards for measuring undrained shear strength. The apparatus is outfitted with a vane blade (2:1 height-to-diameter blade ratio) attached to a 600 mm length aluminum shaft, the vane setup is mounted on a rail support which enables precise stepwise insertion of the vane to specify depths for precise strength profiling. Continuous measurement of the torque during vane rotation captures the evolution of shear resistance detecting the development to the peak and post-peak strain softening behavior manifested in the test material, as shown in **Figure 4.2**.

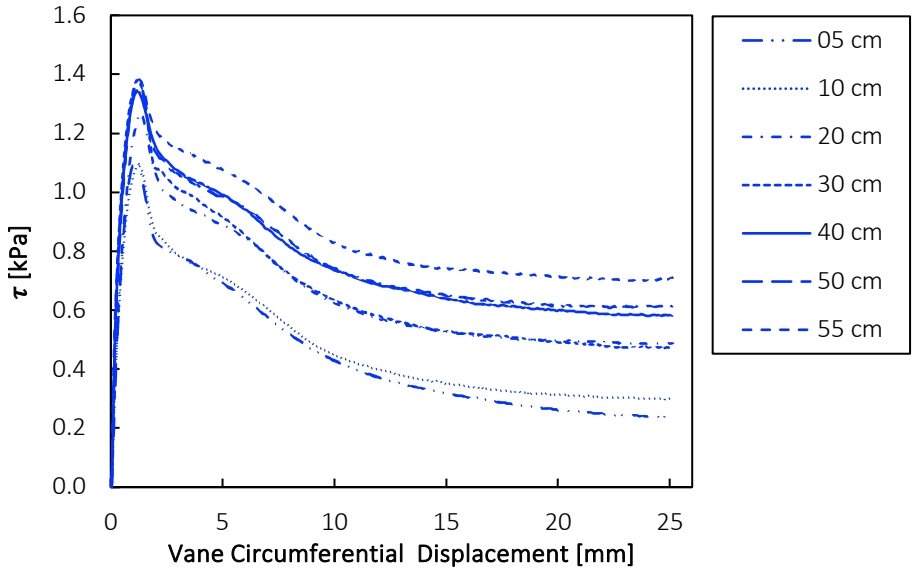

Figure 4.2.- Vane Shear Test results from mix L10-S0.78 after 14 days aging, measurements from 5 to 55 cm depth

From **Figure 4.2** it is shown the results from one of the samples tested (B-GEC-J34 the baseline model), in this plot the shear strength is presented against the circumferential displacement which is the distance in mm of the perimetral travel of the vane blade (⌀: 15.24 mm), the plot is limited to 25 mm of circumferential displacement equivalent to a 180° rotation, with the purpose of understanding the undrained shear strength with displacement and in order to be compared latterly with the interface shear occurring between the encasement and the surrounding soil in the models tested.

Vane shear tests were performed prior to installing the GEC models in the transparent cell on each of the 17 samples of the testing program outlined in **Table 3.2** using a L10-S0.78 mix aged 14 days and following the method in **SECTION 2.4.1**. Laponite undrained shear strength (Su) peak values measured in these samples ranged from 1.1 to 1.4 kPa. Greater peak S_u values were recorded at deeper locations (50-550 mm depth). The peak strength was mobilized at a very low shear circumferential displacement of 1 mm to 1.25 mm (9° blade rotation). This was followed by softening behavior that dropped to residual strength levels. Residual strength values were reached after approximately 20 mm (140° blade rotation) of shear displacement and ranged from 0.6 kPa to 1.0 kPa, as depicted in **Figure 4.2**. The residual plateau maintained a relatively consistent difference from the peak values recorded at various depths.

In **Figure 4.3** the peak undrained shear strength (S_u) at each tested depth was normalized by the corresponding effective vertical stress ($\sigma_{v'}$). The resulting $S_u/\sigma_{v'}$ ratio ranged from 2.25 near the surface to approximately 0.25 at the bottom of the cell, consistent with typical values for normally consolidated soils. The $S_u/\sigma_{v'}$ profile can be divided into two distinct regions: i) the upper third (0-200 mm depth): $S_u/\sigma_{v'}$ ranged from 2.25 to 0.5, and ii) the bottom two-thirds (200-600 mm depth): $S_u/\sigma_{v'}$ ranged from 0.5 to 0.25. This

normalized strength index provides insights into the undrained shear behavior of laponite at various depths. The observed decreasing trend of the normalized undrained shear strength (Su/σv') with depth highlights the growing influence of the effective vertical stress on the shear strength behavior of laponite. This finding emphasizes the importance of imposing a constant overburden stress in the final GEC model setup. By maintaining a consistent overburden stress, the influence of the effective vertical stress on the shear strength can be minimized, allowing for focused investigation of other factors affecting the shear behavior of laponite in the model. This approach will enable a clearer understanding of the inherent properties and mechanisms governing the shear strength of laponite.

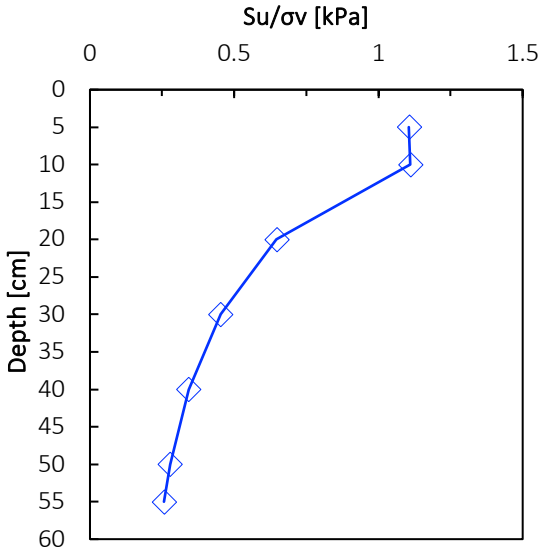

Figure 4.3.- Su/σv Profile from a 60 cm depth cell using laponite mix L10-S0.78 after 14 days aging

4.3.2.- PULLOUT TEST

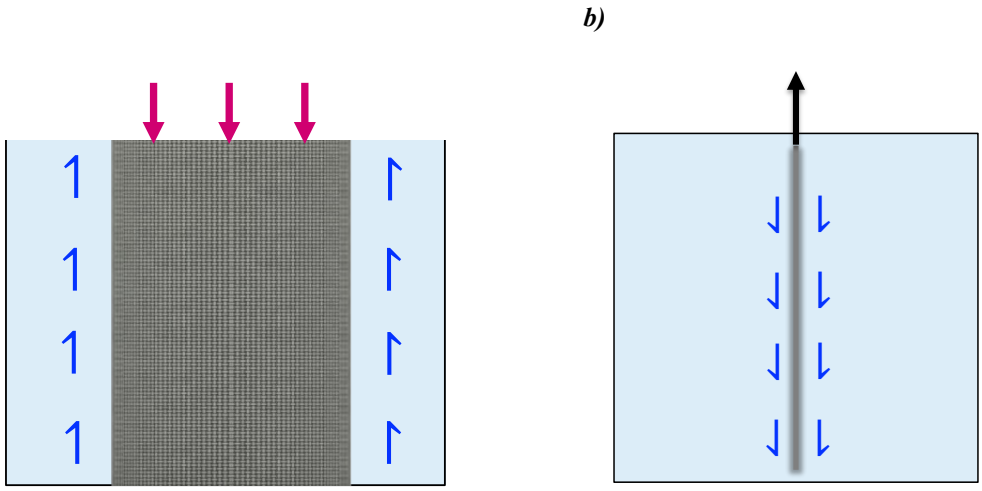

Figure 4.4.- Conceptual behavior of interface shear in GEC model, a) Interface shear in GEC model, and b)Interface shear in designed Pullout test

To gain understanding of the interaction between laponite and geosynthetic materials, a simplified pullout test setup was designed and implemented. The motivation behind this test stemmed from the need to isolate and examine the shearing behavior at the laponite-geosynthetic interface, without the influence of external stresses or other materials that may complicate the analysis. **Figure 4.4** illustrates the rationale behind the induced relative displacement between the geosynthetic and the soft soil in both the GEC model conditions and the proposed pullout test. In the GEC model, the geosynthetic is subjected to a downward displacement relative to the surrounding soil, while in the pullout test, the geosynthetic is pulled upward. Despite the inverse direction of the shearing displacement, the relative displacement between the geosynthetic and the soil remains the same in both cases. This similarity allows for a comparison of the interface behavior observed in the GEC model and the pullout test, enabling a better understanding of the shear strength and displacement mechanisms at the laponite-geosynthetic interface.

To achieve this goal, a simple yet effective test setup was designed using a 100 mm cubic box shown in **Figure 4.5** filled with laponite L10-S0.78. The laponite was allowed to age for 14 days, reaching an undrained shear strength (Su) of 1.1 kPa at a depth of 50 mm. Prior to filling the box with laponite, a 50 mm wide and 100 mm long geosynthetic sample was suspended at the center of the box. This installation method ensured that the fabric remained straight when subjected to the pullout test after the 14-day aging period.

a) ***b)***

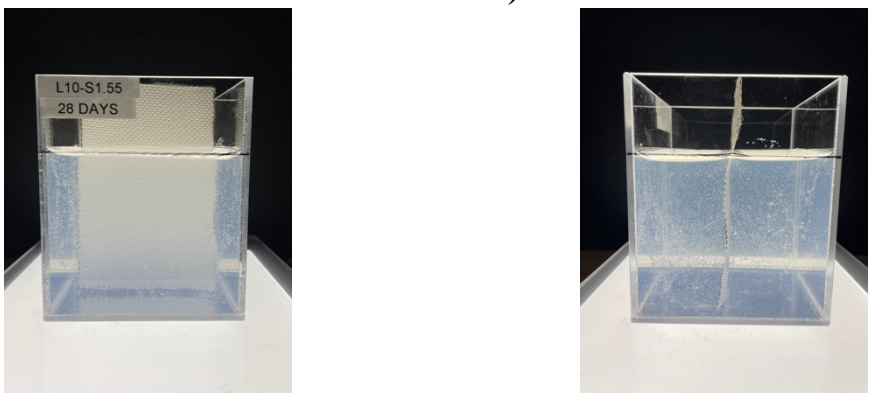

Figure 4.5.- Pullout test result for geotextile GTX34, a) Front view from pullout test box, and b) Side view of the pullout test box

As shown in **Figure 4.6**, the pullout test itself involved attaching a custom clamp that covered the entire width of the geosynthetic sample. This clamp was connected to a 4.5 kgf load cell (Interface SM S-10), which in turn was coupled to a displacement-controlled actuator (GeoJac). The geotextile was then pulled out vertically 38 mm at a controlled rate of 1 mm/min, while the displacement was accurately monitored using a 50 mm LVDT (Omega).

a) *b)*

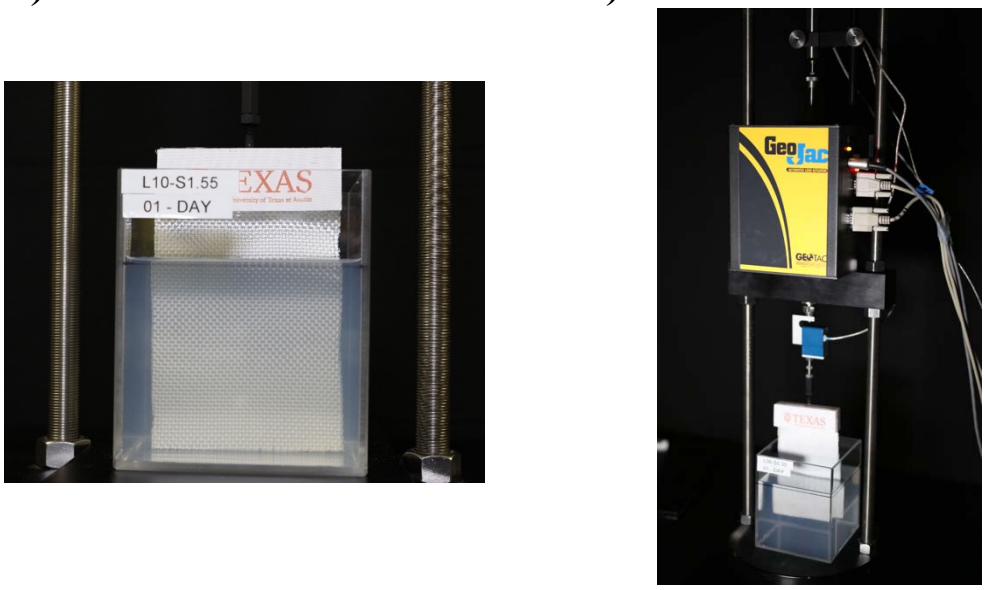

Figure 4.6.- Transparent Vertical Pullout test, a) Front view of sample and b) Pullout Setup

The plot in **Figure 4.7** from the pullout test shows the relationship between the shear resistance (kPa) and frontal displacement $\delta_{frontal}$ (mm) of the geosynthetic embedded in laponite. The shear resistance was calculated by dividing the pullout force by the area of the geosynthetic in contact with the laponite, considering the actual surface contact during the pullout process. The frontal displacement $\delta_{frontal}$ represents the horizontal distance travelled by the geosynthetic as it is being pulled out of the laponite during the test. By using the shear resistance instead of the pullout force, the plot accounts for the changing contact area between the geosynthetic and laponite during the pullout process, providing a more accurate representation of the interface behavior.

The curve exhibits a softening behavior, starting with an initial linear increase in shear resistance up to a peak value of approximately 0.71 kPa at around 2.5 mm of $\delta_{frontal}$. This linear portion indicates shear resistance is directly proportional to the displacement. Upon reaching the peak, the curve undergoes a gradual softening phase, with the shear

resistance decreasing to about 0.58 kPa at 5 mm displacement and further declining to roughly 0.49 kPa at 10 mm. This post-peak softening behavior suggests a progressive weakening of the geosynthetic-laponite interface resistance as the displacement continues. After 10 mm, the shear resistance stabilizes and attains a residual value of approximately 0.47 kPa, which remains relatively constant with further displacement until the end of the test at 25 mm. This residual strength characterizes the steady-state resistance of the geosynthetic-laponite interface under sustained slow displacement rate.

Figure 4.7 effectively captures the key stages of the pullout behavior, including the initial elastic response, peak shear resistance, post-peak softening, and residual strength. The plot provides valuable insights into the maximum shear strength that can be mobilized and the post peak behavior at the interface given the relative displacement occurring between the geosynthetic and the laponite.

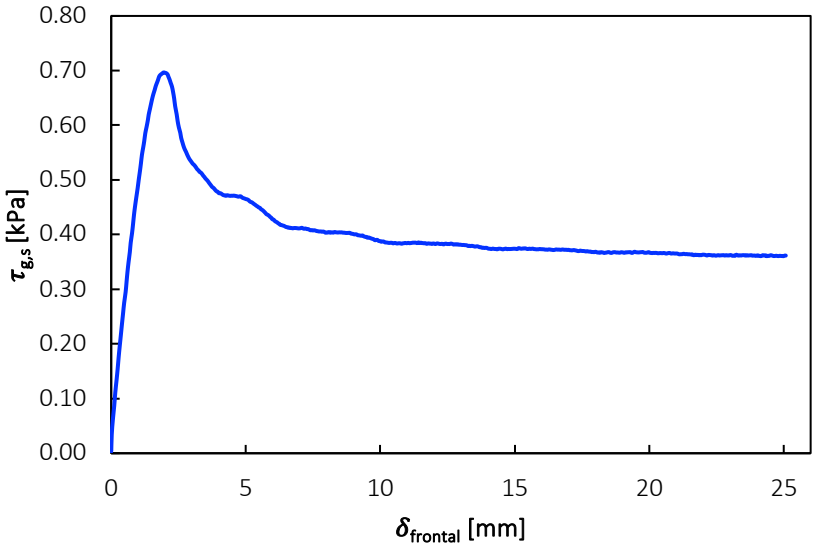

Figure 4.7.- Pullout test result for GTX34 using laponite mix L10-S0.78 after 14 days aging

4.4.- EXPERIMENTAL METHODOLOGY

After gaining understanding of the shear strength of laponite and the interface shear strength between laponite and the selected geosynthetics, the methodology was designed to capture the interface resistance between the GEC models: B-GEC-J08, B-GEC-J34 (baseline) and B-GEC-J70, and the surrounding laponite (mix L10-S0.78 after 14 days aging), which serves as a soft clay surrogate. To achieve this goal, the research employed a twofold methodology:

1. Capturing the shearing contribution by measuring the load applied on top of the GEC model and the load measured at its base using high-resolution load and pressure sensors.

2. Focusing on digital image correlation (DIC) to track the displacement of markers installed within a predefined diametral sectional plane.

By coupling these two methodological approaches, the research aims to obtain a clear picture of the interface shear behavior occurring in the system. The load and pressure measurements provide valuable information about the overall interface shear resistance and load transfer mechanisms, while the DIC analysis offers insights into the localized encasement vertical displacements and soil deformations at the interface. The combination of these techniques enables a comprehensive understanding of the interface shear behavior.

4.4.1.- SETUP AND MODEL CONSTRUCTION

The setup employed corresponds to the one described in **SECTION 2.5**, the transparent unit cell chamber. The instrumentation to assess the load applied at the top of the column and the load transferred at the bottom of the column relied on the

instrumentation described in **SECTION 2.3.6** also for this study the markers as displayed in **Figure 2.8** played an important role for the quality of images obtained for each test performed.

4.4.2.- LOAD TRANSFER MEASUREMENT

The load transfer within the GEC model was quantified using the instrumentation detailed in section **SECTION 2.3.6**. The load applied at the top column was measured using a load cell with a capacity of 2270 kgf (Interface SSM-AJ-5000). The load at the base was computed by dividing the readings from a pressure sensor with a capacity of 500 kPa (Tokyo Measurements PDB) by the area of the column base, assuming a uniform pressure distribution at the bottom. To ensure the accuracy of the measurements, particularly from the bottom sensor, a precise calibration process was carried out. The reliability of this instrumentation approach for measuring load transfer was validated through multiple tests and materials, confirming that the obtained measurements were highly accurate and not influenced by external factors.

By employing this methodology, the load transfer mechanism within the GEC model can be effectively quantified. The use of high-resolution load and pressure sensors, along with meticulous calibration and installation procedures, ensures that the obtained measurements are reliable and representative of the actual load transfer within the system.

4.4.3.- IMAGE ACQUISITION AND PROCESSING

To effectively utilize our Digital Image Correlation (DIC) tool for analyzing the displacement field of installed markers, obtaining high-quality images that clearly capture the speckle pattern is crucial. The images should exhibit good contrast, resolution, and

focus to enable accurate tracking of the markers. Proper lighting and high-resolution cameras were employed to ensure the quality of images suitable for the DIC analysis.

The images used in this study were captured using a Canon EOS 5DSR DSLR camera body, which boasts a 50-megapixel resolution. The camera was equipped with a Sigma 50mm F1.4 ART DG HSM prime lens and fixed to the loading frame through a rigid arm at a distance of 1.05 m, which is the optimal focal distance considering the dimensions of the model. The manual camera settings were as follows: ISO 100, aperture f/2, and exposure time of 1/100 seconds. Images were acquired every minute, corresponding to 1 mm of vertical settlement of the GEC.

As shown in Figure 4.8, to enhance the captured images a Contrast Limited Adaptive Histogram Equalization (CLAHE) filter was applied. CLAHE is an image processing technique that improves the contrast in images by performing local contrast enhancement. This method enhances the visibility of details in both dark and bright areas of the image. By limiting the contrast amplification to a predefined value, known as the clip limit, CLAHE achieves a more balanced contrast enhancement while reducing noise amplification. This step is relevant for providing high contrast of the markers in the laponite and generating a suitable speckle pattern for tracking.

The combination of high-resolution camera equipment, optimal camera settings, and the application of the CLAHE filter ensures that the acquired images are of sufficient quality for accurate DIC analysis. The resulting images, with enhanced contrast and clearly visible markers, form the foundation for precise displacement field measurements and subsequent analysis of the shearing behavior within the GEC model.

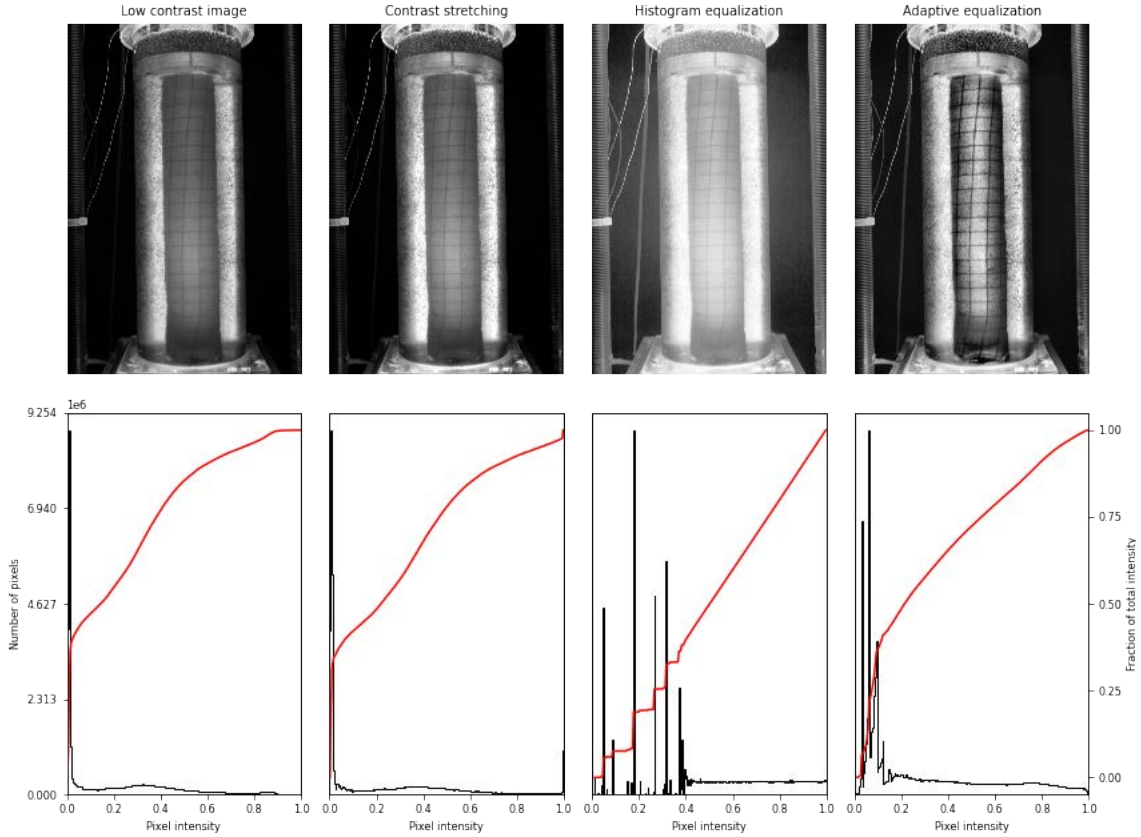

Figure 4.8.- Image processing steps: Low contrast, Contrast stretching, Histogram equalization and Adaptative equalization

4.4.4.- DIGITAL IMAGE CORRELATION

To perform digital image correlation (DIC) on each sequence of processed images, Ncorr, an open-source 2D DIC software package implemented in MATLAB, was utilized due to its robust capabilities and approach. Ncorr is capable of computing full field displacements and strains from series of images, making it suitable for analyzing the different sets of processed image sequences.

The core workflow in Ncorr involves several steps. First, a region of interest (ROI) is defined in the reference (undeformed) image. Next, a subset size is specified, which represents the window used to track the speckle pattern. Subset-based image matching is

then performed between the reference and deformed images to determine the displacement vectors at each subset center. Following this, the full field u (horizontal) and v (vertical) displacement values are computed. Finally, for strain computation, Ncorr employs a least squares plane fit to a circular group of displacement data points. The size of this group can be adjusted by specifying the strain radius. This approach helps to minimize the effect of noise in the displacement data, resulting in more accurate strain calculations.

Ncorr employs the reliability-guided (RG) method to enhance the accuracy and efficiency of the DIC analysis. The RG method identifies and removes unreliable displacement values that may result from image noise, poor contrast, or large deformations. It operates by iteratively performing the correlation, using reliable neighboring points as the initial guess for each subset, rather than conducting independent correlations. This approach improves the robustness of the DIC analysis, particularly for challenging datasets, further information can be consulted a the source reference (Blaber et al., 2015).

When applied to the tested GEC model images, Ncorr would take an initial image as the reference and then calculate the u and v displacements of the markers within the sectional plane as they evolve over subsequent images. This enables quantification of the displacement field over the entire test. The primary outputs from the Ncorr analysis would be the u and v displacement fields within the plane, representing the movement of the laponite markers relative to their initial positions.

The shear displacements were computed using the Ncorr approach. However, prior to the computation, the vertical displacements were corrected to account for the upward movement of the laponite within the transparent unit cell chamber. This correction was necessary due to the incompressible nature of laponite and the fact that the only outlet for

displacement is in the upward direction. By applying this correction, the computed displacements solely represent the actual shearing occurring within the laponite, eliminating the influence of the upward component caused by the material's incompressibility. This approach ensures that the analyzed displacements accurately reflect the shear behavior at the interface, providing a more precise understanding of the shear mechanisms in the GEC system.

Finally, with high quality images that enable accurate tracking of the speckle pattern, Ncorr serves as a powerful tool to noninvasively quantify the evolution of displacements and shear strains in a sectional plane of a laponite cell. This analysis can provide valuable insights into displacement behavior or other phenomena of interest, depending on the experimental conditions. The open-source nature of Ncorr allows for customization and automation, facilitating streamlined analysis workflows tailored to specific research needs.

4.5.- INTERFACE SHEAR TEST RESULTS

The results of the interface shear evaluation of the GEC models are presented in three parts: firstly, the overall magnitude of the interface shear, indirectly measured through load transfer evaluation, provides insights into its contribution to load-carrying capacity at different test stages; secondly, the shear strength in the laponite clay surrogate is detailed along the entire GEC column profile and throughout the test, focusing on understanding how shear strength behaves within the surrounding soft soil; and finally, Digital Image Correlation (DIC) analysis examines the spatial component of interface shear strength through computed shear strain displacements, evaluating the development and propagation of shear bands within the surrounding soft soil and providing a comprehensive understanding of the shearing mechanisms at the GEC column-laponite clay surrogate interface.

4.5.1.- LOAD TRANSFER RESULTS

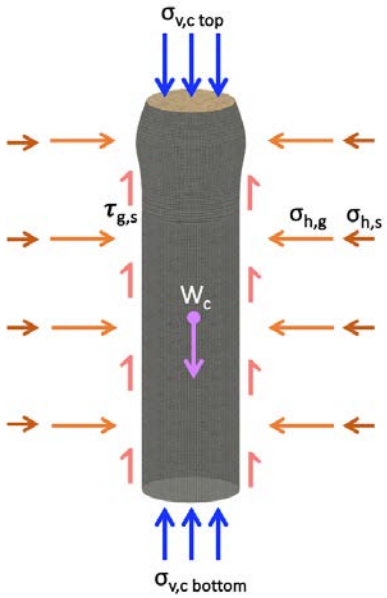

Figure 4.9.- Free body diagram of column infill under axial loading

From **Figure 4.9** it is shown a free body diagram of the column infill axially loaded; the vertical equilibrium is given by:

$$\sigma_{v,c\ top} \cdot A_{top} + W_c = \sigma_{v,c\ bottom} \cdot A_{bottom} + \tau_{g,s} \cdot A_c \qquad \textbf{\textit{Eq. 4-1}}$$

where: $\sigma_{v,c\ top}$ is the applied vertical stress at the top of the column, W_c is the weight of the column infill, $\sigma_{v,c\ bottom}$ is vertical stress at the bottom of the column, $\tau_{g,s}$ is the total interface shear stress between the geosynthetic encasement and surrounding soil, A_{top} and A_{bottom} are the top and bottom area of the column and A_c is the shaft area of the column.

From the equation **Eq. 4-1**, the only unknown variable is the total interface shear stress $\tau_{g,s}$. By assessing the load transfer of the GEC model, the change in interface shear can be obtained at every millimeter of GEC model settlement. **Figure 4.1** presents the load at the bottom against the load at the top of the column plot for the B-GEC-J34 baseline model. A 1:1 line is also plotted as a reference meaning 100% load transfer from top to bottom. The results obtained for this model demonstrate a small but non-negligible deviation from the 1:1 line, indicating that the load transfer is not 100% efficient. Given the conditions of the testing setup, this gap can be fully attributed to the contribution of interface shear to the load-carrying capacity of the system.

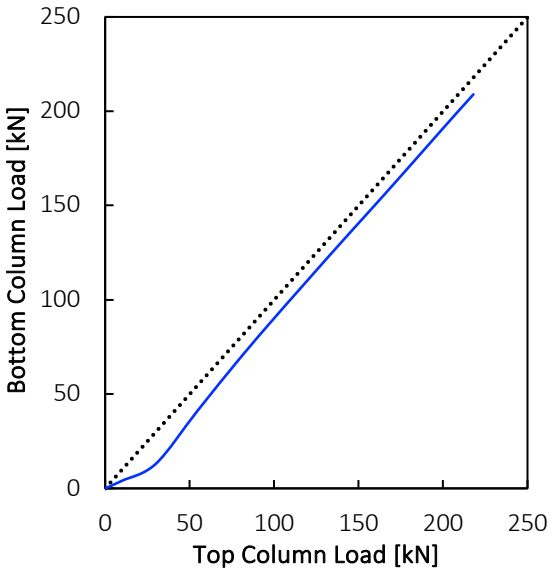

Figure 4.10.- Top-Bottom column load response from baseline model B-GEC-J34

Figure 4.11 provides valuable insights into the relationship between the axial strain of the column and the load transfer efficiency. The load transfer efficiency (η) in **Eq. 4-2** is expressed as the percentage ratio of the bottom load to the top load in the column:

$$\eta = \left(\frac{q_{v,c\ bottom}}{q_{v,c\ top}}\right) \cdot 100\% \qquad \textit{Eq. 4-2}$$

A load transfer efficiency of 100% would indicate that the entire applied load is transferred to the base of the column, with no contribution from interface shear. However, it is important to note that a certain level of interface shear contribution is desirable, as it helps to distribute the load along the length of the column and reduces the stress concentration at the base.

The plot in **Figure 4.11** reveals that when the column axial strain increases from 0% to 2%, the load transfer efficiency increases substantially, reaching a plateau value of around 95%. This suggests that the peak interface shear strength is mobilized rapidly with

displacement, and the residual interface shear strength is reached. The most significant finding is the large contribution of interface shear at very low axial strains of the column, where it is carrying a large amount of the load applied to the GEC model. This observation highlights that the first mechanism activated in the load transfer process is the mobilization of interface shear strength. As the axial strain increases beyond 2%, a gradual transition from the interface shear-dominated regime to other load transfer mechanisms takes place. Although the residual interface shear strength is not negligible, accounting for 5% of the carried load, the primary focus should be on the role of interface shear at very low column axial strains.

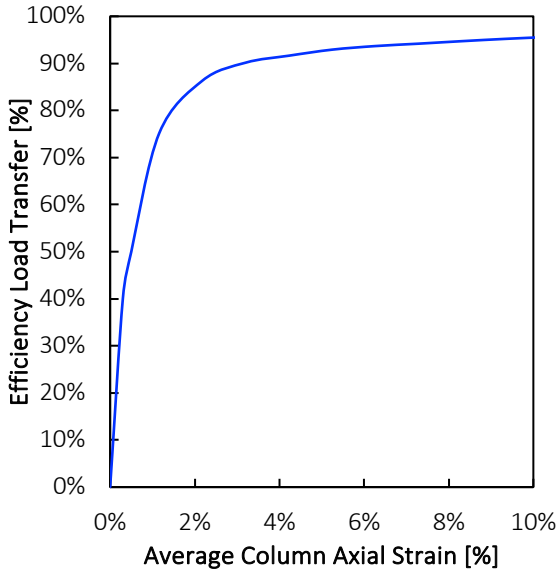

Figure 4.11.- Efficiency load transfer from baseline model B-GEC-J34

4.5.2.- INTERFACE SHEAR BEHAVIOR

The relevance of the interface shear strength between the GEC and the surrounding soft soil has been evidenced from the load transfer results. **Figure 4.12** shows the total interface

shear obtained according to **Eq. 4-3** by taking the remaining load to reach 100% load transfer from **Figure 4.10** divided by the column shaft area of the GEC model.

$$\tau_{g,s} = \frac{q_{v,c\ top} - q_{v,c\ bottom}}{A_c} \qquad \textit{Eq. 4-3}$$

The plot reveals that the total interface shear developed around the column is rapidly mobilized, reaching a peak of 0.82 kPa, followed by a post peak softening behavior that decreases to a value of 0.7 kPa. This softening is not as drastic as the one observed in the pullout test from the same geosynthetic and laponite mix from **Figure 4.7**.

It is important to note that the total interface shear strength corresponds to the overall interface shear developed along the column. However, not all sections of the column profile contribute the same interface shear strength, as the vertical displacements of the column are not uniform as shown in **SECTION 2.6.2** and **Figure 2.14**. To address this issue, a detailed discretization of the total interface shear measured in the GEC model has been also completed.

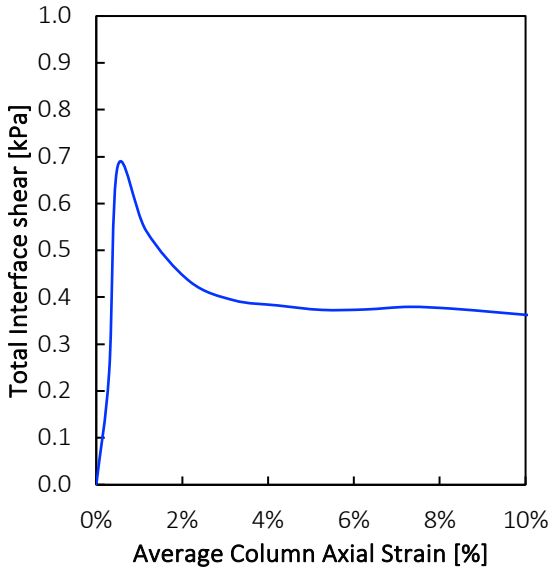

Figure 4.12.- Computed Interface shear from baseline model B- GEC-J34

The load carried by the interface shear has been plotted in **Figure 4.13** as a percentage of the total load carried by the column at different settlements, given in mm, which is assumed to be the maximal displacement value at the interface. The plot reveals that at very low settlements, the interface shear contribution increases rapidly, reaching up to 60% at 2 mm of column settlement, but then suddenly drops. This high level of load-carrying contribution is not sustained, indicating that it is not reliable to depend on it. At larger column settlements, the interface shear contribution remains between 5-10%, which is not negligible.

Interestingly, the drop in the contribution from 60% to 7% (an 88% fall) is more drastic compared to the evaluation from the total shear interface computed from the instrumentation, which showed a decrease from 0.7 kPa to 0.4 kPa (a 42% drop). This discrepancy highlights the importance of understanding that both pieces of information complement each other. The interface shear strength, even if it exhibits a softening behavior, maintains a more sustainable and reliable post-peak and residual value compared to its load-carrying contribution percentage. The drastic drop in the load-carrying contribution of the interface shear is primarily due to the activation of the GEC system, which allows most of the load to be transferred to the bottom, with only the residual interface shear strength contributing to the load transfer.

The shearing behavior at the interface is of utmost importance during the rapid transition that occurs when the encasement tensile strength of the GEC becomes highly mobilized, a process which is thoroughly explained in **Chapter 3**. This observation is consistent with the concept of a swift shift from a regime dominated by interface shear to one where vertical load transfer mechanisms prevail. This change can be attributed to the complete activation of the encasement stress confinement around the GEC column, which

allows for more efficient load transfer through the column itself, reducing the relative contribution of the interface shear.

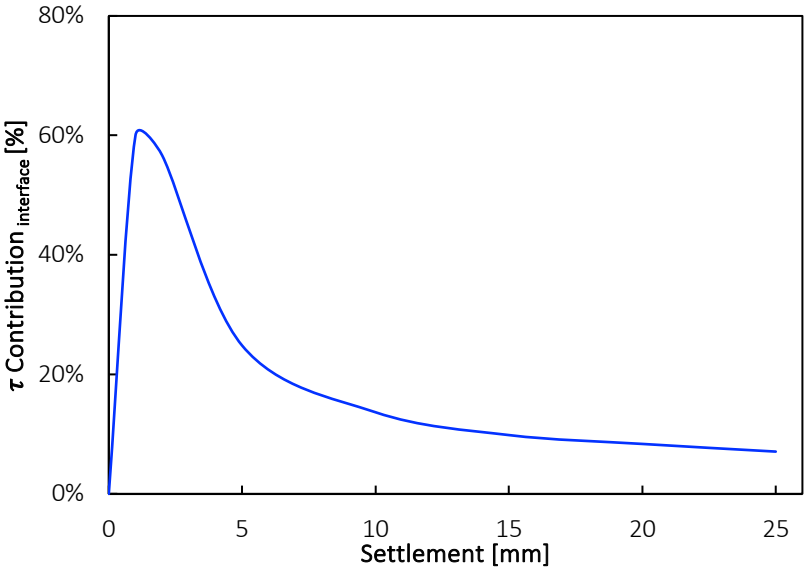

Figure 4.13.- Interface shear % contribution to load carrying model B-GEC-J34

The load transfer results highlight the importance of the interface shear strength between the GEC and the surrounding soft soil. However, it is also crucial to understand how the interface shear is distributed along the column profile. Discretizing the total interface shear provides valuable insights into local variations in interface shear.

To gain a more comprehensive understanding of the interface shear behavior, the total interface shear was discretized along the depth of the B-GEC-J34 baseline model column. **Figure 4.14** illustrates the vertical displacements and interface shear strength variations along the depth of the GEC model. **Figure 4.14a** presents a plot of the vertical encasement displacements at different depth sections of the GEC model for various top column settlements, with increments of 5 mm. The analysis reveals that the total settlement

does not accurately represent the non-uniform vertical displacement along the depth of the GEC. As the top settlement increases, the upper portion of the GEC model exhibits higher encasement vertical displacement, which gradually decreases with depth. The bottom part of the column experiences minimal settlement, while the top part closely follows the overall settlement value of the column. The decrease in vertical encasement displacement with depth follows a linear trend, with zero displacement at the bottom base of the column. This non-uniform vertical displacement along the depth of the column indicates that the interaction between the column and the surrounding soil varies at different depths. As the settlement increases, this encasement vertical displacement non-uniformity at the interface becomes more pronounced and has a more significant impact on the soil-column interaction.

Figure 4.14b illustrates the variation in the interface shear strength for the B-GEC-J34 baseline model. To determine the degree of interface shear strength, three encasement references at different depths (top, middle, and bottom) were tracked at five column settlement stages (5, 10, 15, 20, and 25 mm). The relative shear displacement was mapped onto a pullout test performed with the same geosynthetic encasement and laponite mix, since the main assumption of this analysis is that the interface shear from the pullout test is representative of the GEC model interface shear.

Initially, at low column settlements, the top, middle, and bottom encasement references exhibit similar interrace shear. However, as the settlement of the column increases, the displacement difference between these points becomes more pronounced. The top encasement references experience a vertical displacement range of 5 to 25 mm, rapidly approaching the residual interface shear. In contrast, the middle encasement

reference travels from 2 to 15 mm, and the bottom encasement reference only moves from 1 to 5 mm, all within the first 25 mm of column settlement of the GEC model.

As a result, the top portion of the column quickly mobilizes the peak interface shear and contributes the least to the overall interface shear at a given settlement stage. The middle section follows, while the bottom part of the column contributes the most to the interface shear. An exception occurs for settlements less than 1.5 mm, where the order is reversed, and the top part may briefly contribute more due to its pre-peak range. However, this narrow range is unlikely to be significant in prototype conditions, where large column settlements are expected.

Overall, **Figure 4.14** emphasizes the importance of the interface shear in understanding its load-carrying contribution, especially during the initial stages of the GEC system's performance. The contribution can be relevant if the soft soil exhibits higher shear strength behavior.

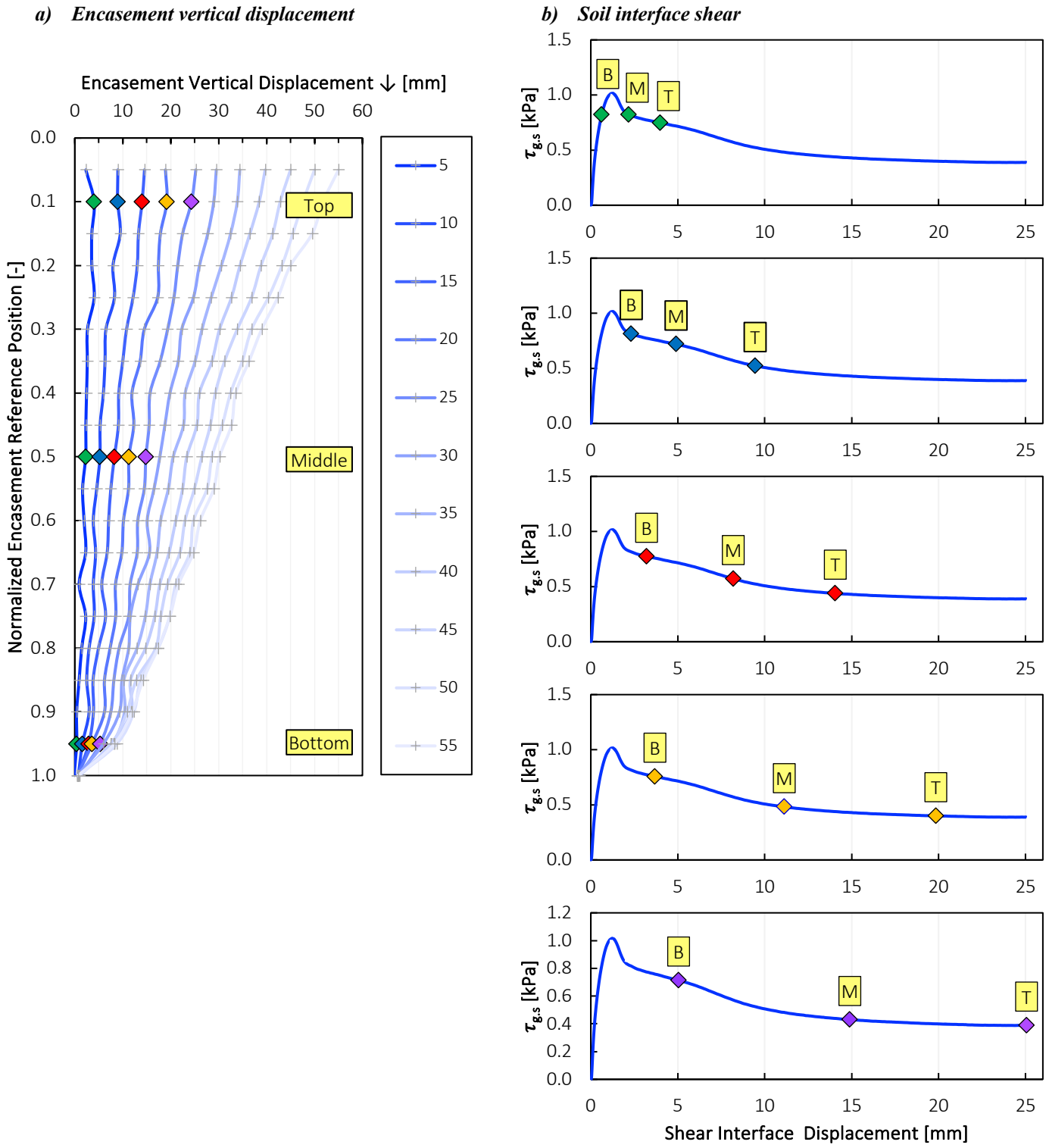

Figure 4.14.- Assumed Interface shear along the encasement column length and soil from baseline model B-GEC-J34

Figure 4.15 presents a comparison of the shear profiles obtained from the pullout test, the computed interface shear from the GEC model, and the vane shear test. The same approach as **Figure 4.14b** has been implemented, with the results superposed in terms of circumferential, frontal, and interface shear displacement, respectively. The plot focuses on the top encasement references over five different column settlement stages (5, 10, 15, 20, and 25 mm).

The three shear strength profiles for the same laponite mix exhibit highly synchronous behaviors, ultimately reaching the same residual value. This observation suggests that the shearing mechanisms and contribution of interface shear are consistent across the different testing methods. However, the vane shear test may present a higher peak strength compared to the pullout test and the GEC model. This difference can be attributed to the faster shearing rate in the vane shear test, while the pullout test and the GEC model were conducted at the same rate of 1 mm/min.

Notably, the accuracy of the pullout test and the computed interface shear from the GEC model is very similar. This finding indicates that the conditions of the pullout test were representative of the actual interface shear behavior within the GEC system. Consequently, the pullout test results can be used to anticipate the level of interface shear expected during the performance of other GEC models and prototypes.

The comparison of the shear strength profiles from different testing methods provides valuable insights into the reliability and applicability of each approach. The consistency between the pullout test and the GEC model interface shear computation validates the use of pullout tests as a practical and reliable method for assessing the interface shear behavior in GEC systems.

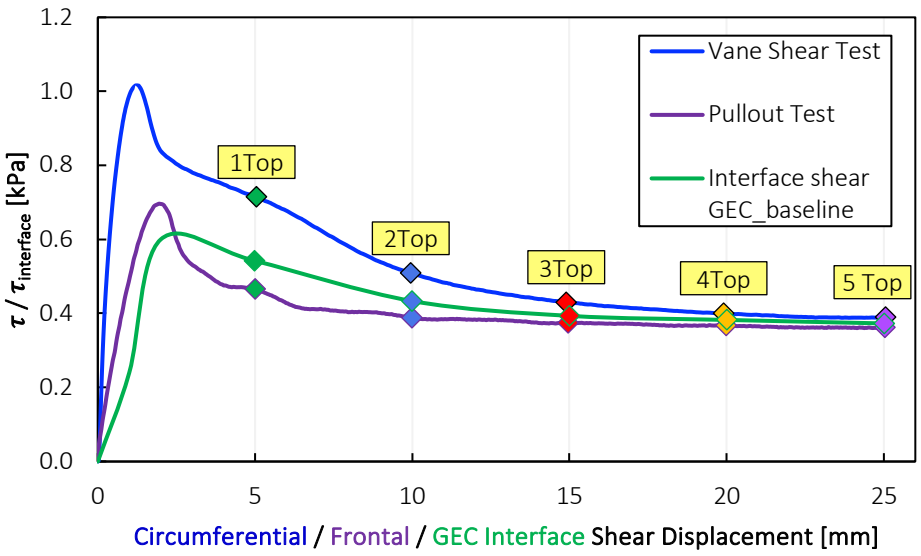

Figure 4.15.- Overlap of results from Vane shear test, Pullout test and B-GEC-J34 baseline model test, by using same laponite mix L10-S078 after 14 days aging and geotextile GTX34

4.5.3.- DIC SOIL SHEAR STRAIN RESULTS

The Digital Image Correlation (DIC) analysis presented below was conducted using the Ncorr software. The analysis focuses on two experimental setups: the pullout test and the baseline model B-GEC-J34. The primary objective is to visualize the soil displacement of the markers embedded in the plane of study and subsequently compute the shear strain field, evaluating the spatial influence of the shear bands developed along the interface between the geosynthetic encasement and the laponite, which serves as the surrounding soil.

Figure 4.16 illustrates the computation of shear strains (ε_{xy}) during the pullout test. The main observation from this analysis is the progressive increase in the thickness of the

shear band along the geosynthetic GTX34 used for the GEC encasement, parallel to the interface shear boundary. As the geosynthetic GTX34 is progressively pulled out, soil shear bands develop along the interface, reaching a peak at 3 mm of frontal displacement. Notably, the highest level of soil shear strain activation occurs within the first few millimeters of frontal displacement.

Beyond this point, the shear band reaches a peak influence and then decreases in both magnitude and thickness, from 20-25 mm to only 10-15 mm. The magnitude of the shear strains decreases, and the influence of the pullout process on the surrounding soil appears to diminish, particularly at higher displacements where the soil-geosynthetic interaction is reduced.

The interface shear under these conditions revealed that the softening behavior is not only observed in magnitude but also spatially. The shear bands along the interaction decrease as the interface softens. However, the thickness of the shear band does not significantly influence the surrounding soil, as the affected soil remains very close to the interface after reaching the peak. This phenomenon is expected due to the low stiffness of the soft soil, which results in minimal disturbance at a distance from the interface as the shearing progresses.

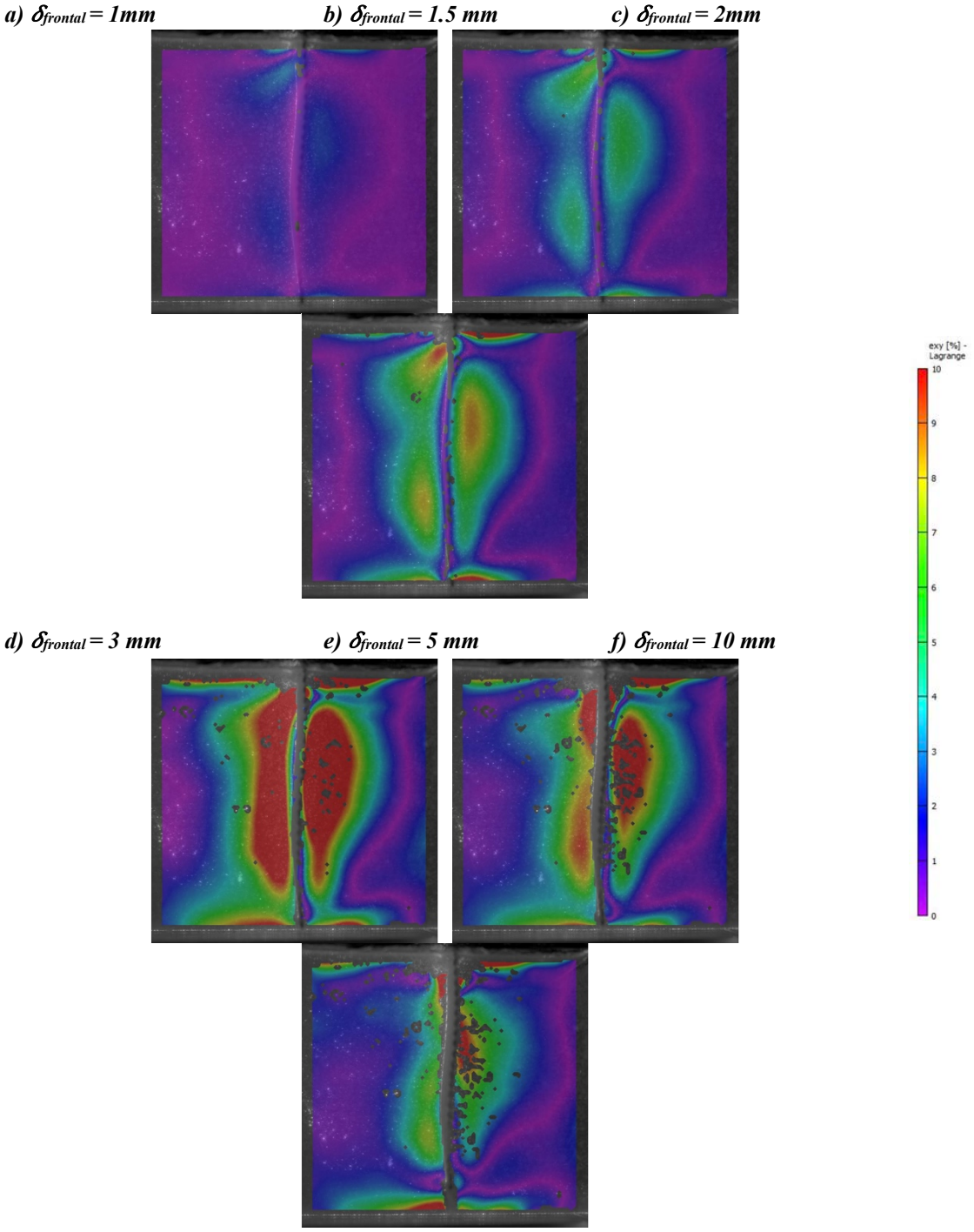

Figure 4.16.- DIC Shear Strain field results from Pullout test using laponite mix L10-S078 after 14 days aging and geotextile GTX34

For the DIC shear strain analysis of the two most representative models tested : B-GEC-J34 (baseline) and B-GEC-J70 are presented given the clear trend the evidenced and presented below.

Figure 4.17 presents the shear strain results of the B-GEC-J34 model (baseline) at different column axial strains (ε_a = 1, 2, 4, 6, 8, and 10%). The results reveal the development of longitudinal shear bands at the interface between the column and the soft soil. The thickness of the shear band varies from 30 mm at the top to 5 mm at the bottom of the column, with the band progressively increasing in the downward direction as the axial strain of the column increases but showing limited horizontal expansion.

The shear band development is initially more pronounced at the top of the column, consistent with the encasement vertical displacement trend observed in **Figure 4.14a**. However, after reaching the assumed interface shear peak at the top, the shear band exhibits a decreasing gradient from top to bottom at large column axial strains. This is because the bottom column interface has not yet settled as much as the top. As the column axial strain increases further, the shear band propagates in magnitude intensity from the top to the bottom, indicating a delayed propagation of the interface shear strength in the lower portion of the column.

At 10% column axial strain, the shear band becomes relatively uniform along the column length, suggesting that the overall vertical displacement in the column has surpassed the shear strain required to reach the post-peak shear strength. Notably, the shear band remains very close to the column, with no apparent additional widening beyond that reached at 4% axial column strain. The limited horizontal expansion of the shear band is

likely due to the significant stiffness contrast between the GEC model and the surrounding laponite soft soil.

It is important to note that these results are not affected by the disturbance caused by the upward movement of the ring overburden plate or the downward movement of the core column plate. The potential disturbance has been addressed and is not considered in this analysis. Furthermore, it is conventionally assumed in all columns embedded in soils that the first diameter is not considered in the analysis due to the multiple factors that may affect the interpretation of results.

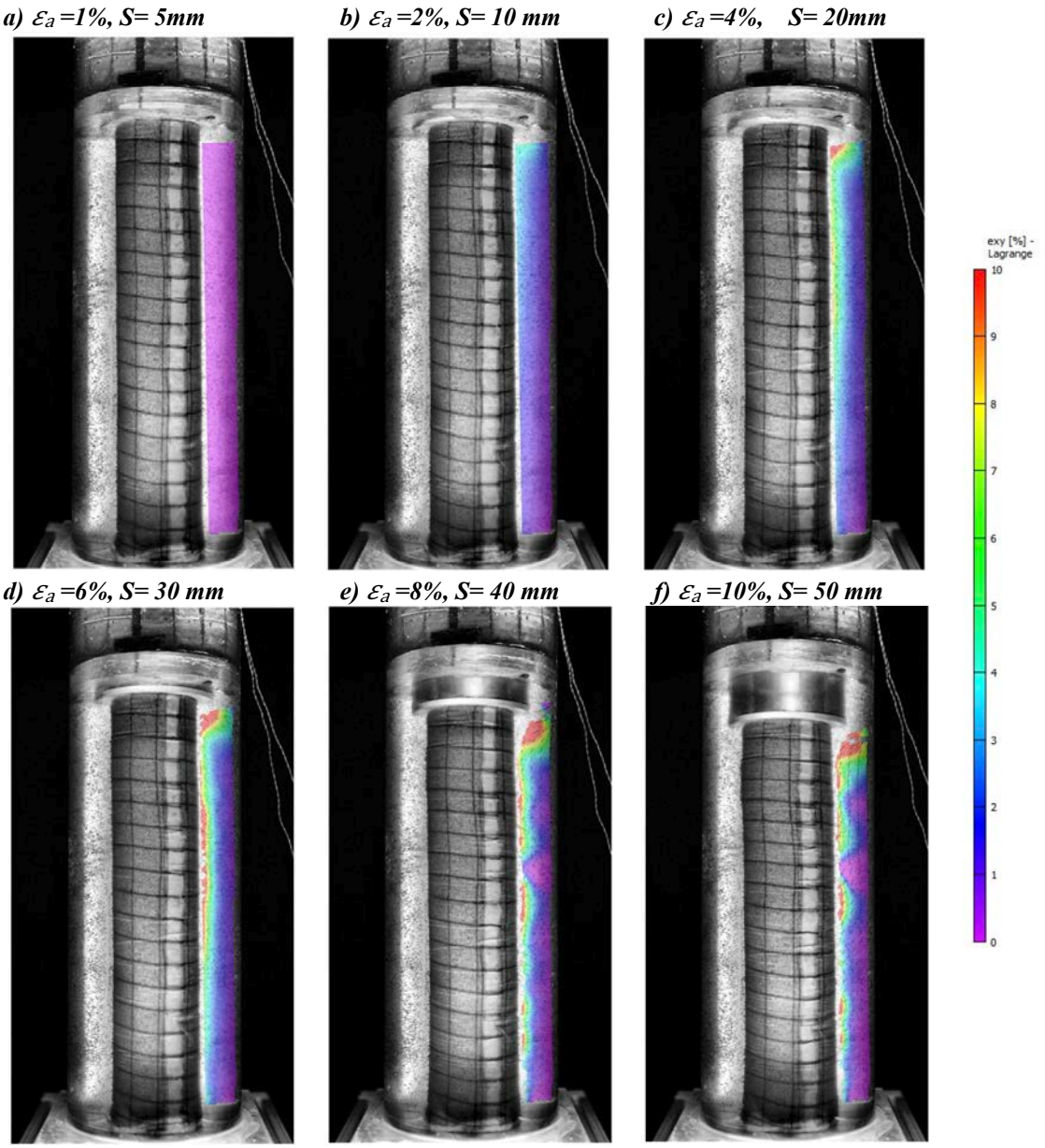

Figure 4.17.- DIC Soil shear strain field results from baseline model B-GEC-J34 at 1%, 2%, 4%, 6%, 8% and 10% of average column axial strain

Figure 4.18 presents the shear strain results from the B-GEC-J70 model at various column axial strains (ε_a = 1, 2, 3, 6, and 8%). Although the development of shear bands in this model follows a similar trend to the B-GEC-J34 baseline model, the higher stiffness encasement in the B-GEC-J70 model leads to notable differences. The longitudinal shear bands are narrower in the B-GEC-J70 model, which reduces the extent of soil-column interaction. Despite the column settling as much as the baseline model, the encasement radial strains are significantly lower, indicating that both encasement vertical displacement and encasement radial strain of the column impact the shear band shape.

The B-GEC-J70 model exhibits a significant reduction in shear strain magnitude compared to the baseline model, with the maximum ε_{xy} reaching only 5% instead of 10%. This decrease can be attributed to the more uniform encasement vertical settlements observed in the B-GEC-J70 model, which result from the higher relative stiffness. More uniform and lower column encasement vertical displacements limit the interaction between the column and the surrounding soil, leading to a more uniform distribution of loads and deformations along the column-soil interface. Although the interaction between the column and the surrounding soil in the B-GEC-J70 model is smaller in magnitude compared to the baseline model, it appears more consistent along the entire column length.

The spatial distribution and progression of shear strains are crucial factors to consider when evaluating the load transfer mechanisms and overall performance of geosynthetic encased column (GEC) systems in soft soil conditions. The results demonstrate that the stiffness of the geosynthetic encasement directly influences the uniformity of vertical settlements along the column profile. This uniformity, in turn, determines the level of interface shear displacement, which plays an important role in controlling shear band development and the magnitude of shear strain at the column-soil

interface. Additionally, encasement radial strains in the column significantly contribute to the system's performance and can only be reduced by increasing the encasement stiffness. These findings underscore the importance of carefully selecting the appropriate geosynthetic encasement properties to optimize the performance of GEC systems in soft soil environments.

When designing and analyzing GEC-reinforced soil structures, it is important to consider the variation in shear band thickness and the delayed activation of interface shear strength along the column length. The selection of an appropriate geosynthetic encasement stiffness is also crucial to optimize load transfer mechanisms within the system.

a) ε_a =1%, S= 5mm ***b) ε_a =2%, S= 10 mm*** ***c) ε_a =4%, S= 20mm***

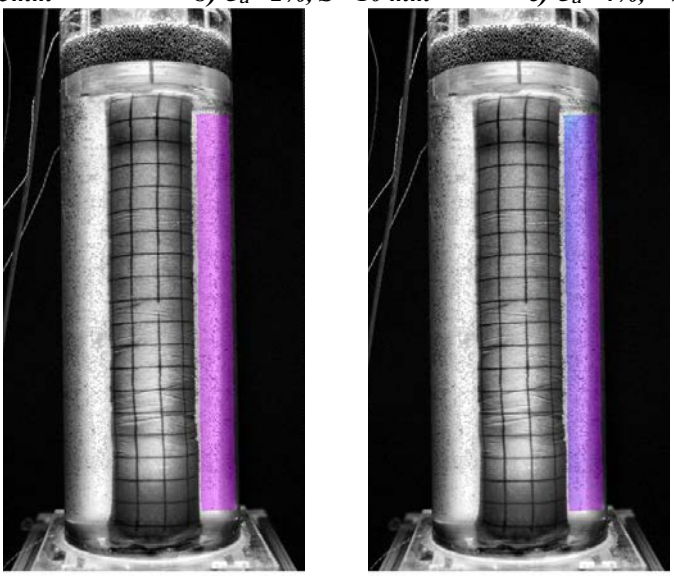

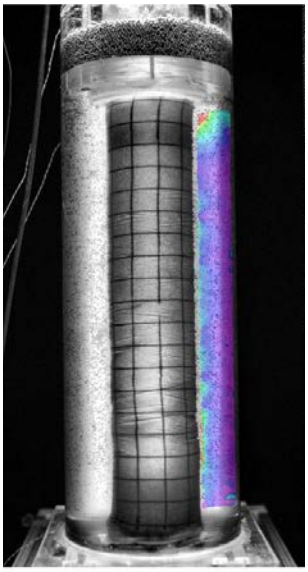

d) ε_a =6%, S= 30 mm ***e) ε_a =8%, S= 40 mm***

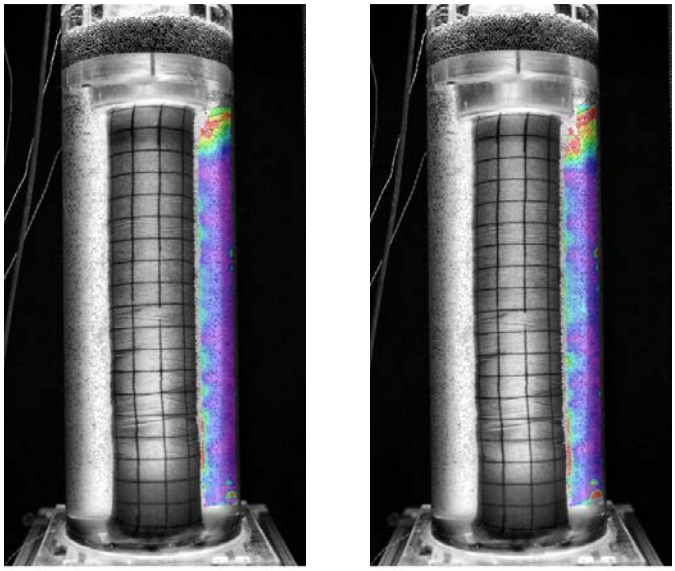

Figure 4.18.- DIC Soil shear strain field results from model B-GEC-J70 at 1%, 2%, 4%, 6%, 8% and 10% of average column axial strain

4.6.- CONCLUSIONS

Based on the comprehensive experimental study of interface shear behavior in geosynthetic encased columns (GECs), the following conclusions can be drawn:

- Interface shear stress between the GEC and the surrounding soft soil plays a relevant role in load transfer, especially at low column axial strains. The interface shear contribution rapidly increases, carrying up to 60% of the load at early stages of loading, before drastically dropping as other load transfer mechanisms activate.

- The interface shear stress varies along the GEC column profile. The top portion quickly reaches residual strength, while the middle and bottom sections contribute more to the overall shear stress at a given settlement stage. This non-uniform interface shear behavior should be considered in GEC design.

- Digital Image Correlation (DIC) analysis reveals the development of shear bands at the GEC-soil interface. The normalized shear band thickness varies from 0.5 column diameters at the top 0.1 of a column diameter at the bottom, progressively increasing downward as column axial strain increases, with limited horizontal expansion due to the stiffness contrast between GEC and soil.

- The geosynthetic encasement stiffness ($J_{5\%}$) significantly influences the vertical settlements of the GEC. Higher stiffness encasements lead to more uniform vertical displacement of the encasement along the column length.

- The pullout test and computed interface shear from the GEC model exhibit highly consistent behaviors, validating the use of pullout tests as a reliable method for assessing interface shear behavior in GEC systems.

- Spatial distribution and progression of interface shear stresses along the column length should be considered when designing and analyzing GEC-reinforced soil structures. Appropriate geosynthetic encasement stiffness selection is crucial for optimizing load transfer mechanisms.

In summary, this research provides valuable insights into the interface shear behavior and its contribution to load transfer in GEC systems. The findings emphasize the importance of considering non-uniform development of interface shear, the influence of geosynthetic encasement stiffness on the vertical settlements, and the reliability of pullout tests in assessing interface behavior.

4.7.- REFERENCES

Ads, A., Iskander, M., & Bless, S. (2020). Shear Strength of a Synthetic Transparent Soft Clay Using a Miniature Ball Penetrometer Test. *Geotechnical Testing Journal*, *43*(5), 20190020. https://doi.org/10.1520/GTJ20190020

Almikati, A., Pierozan, R. C., Sadek, S., & Zornberg, J. G. (2023). Geotechnical Characterization of Laponite as Transparent Clay Surrogate. *Geotechnical Testing Journal*, *46*(3), 20220106. https://doi.org/10.1520/GTJ20220106

Chini, C. M., Wallace, J. F., Rutherford, C. J., & Peschel, J. M. (2015). Shearing Failure Visualization via Particle Tracking in Soft Clay Using a Transparent Soil. *Geotechnical Testing Journal*, *38*(5), 20140210. https://doi.org/10.1520/GTJ20140210

Iskander, M. G. (2010). *Modelling with transparent soils: Visualizing soil structure interaction and multi phase flow, non-intrusively*. Springer.

Ng, K. S., & Tan, S. A. (2015). Stress Transfer Mechanism in 2D and 3D Unit Cell Models for Stone Column Improved Ground. *International Journal of Geosynthetics and Ground Engineering*, *1*(1), 3. https://doi.org/10.1007/s40891-014-0003-1

Tan, X., Feng, L., Hu, Z., & Abbas, S. M. (2021). The equivalent shear strength properties of the composite soil reinforced by stone columns: An FDM-DEM-coupled numerical evaluation. *Environmental Earth Sciences*, *80*(4), 125. https://doi.org/10.1007/s12665-021-09412-0

Tan, X., Feng, L., Hu, Z., & Zhao, M. (2021). Failure modes and ultimate bearing capacity of the isolated stone column in soft soil. *Bulletin of Engineering Geology and the Environment*, *80*(3), 2629–2642. https://doi.org/10.1007/s10064-020-02066-5

Tan, X., & Zhao, M. (2018). Deformation and Failure Behavior of the Isolated Single Stone Column with and Without Geosynthetic Encasement. In R. Chen, G. Zheng, & C. Ou (Eds.), *Proceedings of the 2nd International Symposium on Asia Urban GeoEngineering* (pp. 547–559). Springer Singapore. http://link.springer.com/10.1007/978-981-10-6632-0_42

Zhang, L., & Zhao, M. (2015). Deformation Analysis of Geotextile-Encased Stone Columns. *International Journal of Geomechanics*, *15*(3), 04014053. https://doi.org/10.1061/(ASCE)GM.1943-5622.0000389

Chapter 5: Conclusions

5.1.- SUMMARY

In summary, this dissertation utilized an innovative experimental approach with transparent laponite clay to investigate the behavior and performance of geosynthetic encased columns (GECs) in soft soils, yielding the following key conclusions from each chapter:

Chapter 2 demonstrated that laponite serves as an effective clay surrogate for visualizing the internal deformation of GECs and laponite, despite its low undrained shear strength of 1-2 kPa after 2 weeks of aging. The innovative experimental setup successfully measured column volume changes by monitoring displacements of the overburden loading plate and core column plate, attributing the total volume change to the column material and revealing a noteworthy dilative response of the GEC column under undrained loading. The model captures essential stages of the GEC settlement-clay consolidation process, providing valuable insights into the mechanical behavior of the surrogate clay under various conditions. Laponite's transparency allowed unique visualization of shear band formation and progression between the GEC and surrounding soil, while optimized DIC settings captured the evolution of localized shear planes within the column, offering an detailed perspective into GEC deformation mechanics. The testing methodology demonstrated substantial repeatability and reliability across key measurements of load, displacement, and various strains, validating the approach's capacity to produce uniform outcomes and supporting confidence in the data for analysis and modeling.

Chapter 3 showed that the experimental investigation demonstrated a significant increase in bearing capacity of GEC-reinforced samples compared to ordinary columns.

Encasement stiffness, column infill relative density, smaller diameters, and greater overburden pressure all contributed to bearing capacity increases. Dilation of dense sand column infill activated the encasement, allowing better confinement, while stiffer encasement, looser density, and higher overburden reduced dilation. Non-uniform axial and encasement radial strains developed along the column, with higher strains at bulging locations and the column base, and strain localization was more pronounced under higher loads. The predominant failure mode was encasement tensile breakage at 2-3 diameters depth, marked by large axial, encasement radial, and column infill volumetric strains, with high-density columns and low-stiffness encasement showing tensile rupture after bulging initiated. The encasement developed hoop stresses up to 10 times the surrounding soil, enabling full load transfer to the column base, and stress concentration ratios were 20-30 for GEC and 4-6 for ordinary columns.

Chapter 4 revealed that interface shear strength plays a crucial role in GEC load transfer, especially at low axial strains, with the interface contribution rapidly rising before dropping as other transfer mechanisms activate. Interface shear varies along the GEC profile, with the top reaching residual strength while the middle and bottom contribute more at a given settlement, and this non-uniformity should be considered in design. DIC reveals longitudinal shear bands at the GEC-soil interface that increase in thickness downward with limited expansion, and encasement stiffness significantly influences shear band development and magnitude. Pullout tests and computed GEC interface shear are highly consistent, validating pullout tests as reliable for assessing GEC interface behavior. Spatial shear distribution, shear strain progression, delayed activation of interface shear along the column, and encasement stiffness are important considerations for optimizing GEC load transfer and minimizing differential settlement.

Overall, this thesis provides valuable insights into the behavior and performance of geosynthetic encased columns in soft soils using an innovative transparent soil modeling approach with laponite clay. The experimental setup enabled visualization and quantification of column volume change, shear band evolution, and interface shear mechanisms.

5.2.- RECOMMENDATIONS FOR FUTURE STUDIES

The experimental approach and findings presented in this dissertation provide a strong foundation for further research into the behavior and performance of GECs in soft soils. The following recommendations are suggested for future studies:

- Conduct long-term studies: evaluate the long-term performance of GECs under sustained loading conditions to assess creep, consolidation, and aging effects on the soil-GEC system. This will provide valuable insights into the durability and serviceability of GECs over extended periods.

- Investigate group effects: study the interaction between multiple GECs in a group configuration to understand the load transfer mechanisms, stress distribution, and settlement behavior of GECs-reinforced foundations. This will help optimize the spacing and arrangement of GEC for maximum efficiency.

- Develop numerical models: utilize the experimental data to develop and validate numerical models that can simulate the complex behavior of GECs in soft soils. These models should incorporate the observed volume change, shear band evolution, and interface shear mechanisms to provide a comprehensive tool for GEC design and analysis.

- Conduct field-scale studies: validate the findings from laboratory-scale experiments through well-instrumented field-scale studies of GEC-reinforced projects. This will help bridge the gap between laboratory observations and real-world performance, allowing for refinement of design methods and construction practices.

- Investigate the effects of cyclic loading: assess the performance of GECs under cyclic loading conditions, such as those induced by earthquakes or traffic, to understand the dynamic response and potential for liquefaction mitigation in soft soils.

- Explore alternative encasement configurations: investigate the potential benefits of novel encasement configurations, such as multi-layered or composite systems, to optimize the load transfer and confinement effects of GECs in soft soils.

- By addressing these recommendations, future studies can build upon the findings of this dissertation and contribute to the development of more efficient, reliable, and cost-effective GEC-reinforced foundation systems for soft soil conditions.

Vita

Etienne González Domínguez is a Mexican citizen that was born in Montpellier, France in 1990. He attended Lycée Joffre in Montpellier where he graduated in 2008, returned to Mexico where he obtained his bachelor's degree in civil engineering with Honors from the Universidad Nacional Autónoma de México in 2013. Just after, he gained his first year of experience working for Soletanche Bachy Mexico as a contractor. In 2014, Etienne joined the Ecole Polytechnique Fédérale de Lausanne, Switzerland where the earned in 2016 his degree of Master of Sciences in Civil Engineering. After three years of professional experience as a contractor and consultant in Mexico and France, he started in 2019 his doctoral studies at the University of Texas at Austin. Etienne obtained his civil engineering Ph.D. in 2024 with a dissertation in geotechnical engineering focused on the application of geosynthetics, experimental modelling with transparent soils and digital image analysis.

Post-graduation, Etienne will join the industry to pursue his professional career as a consultant.

Permanent address : etienne.gonzalez@utexas.edu
This dissertation was typed by Etienne González Domínguez.